



This work is licensed under a [Creative Commons Attribution-NonCommercial-ShareAlike 4.0 International License](https://creativecommons.org/licenses/by-nc-sa/4.0/).

How to cite this thesis / dissertation (APA referencing method):

Surname, Initial(s). (Date). *Title of doctoral thesis* (Doctoral thesis). Retrieved from [http://scholar.ufs.ac.za/rest of thesis URL on KovsieScholar](http://scholar.ufs.ac.za/rest_of_thesis_URL_on_KovsieScholar)

Surname, Initial(s). (Date). *Title of master's dissertation* (Master's dissertation). Retrieved from [http://scholar.ufs.ac.za/rest of thesis URL on KovsieScholar](http://scholar.ufs.ac.za/rest_of_thesis_URL_on_KovsieScholar)

THE RELATIONSHIP BETWEEN THE
GEOHYDROLOGICAL, GEOPHYSICAL AND
PHYSICAL PARAMETERS OF THE VAALHARTS
AQUIFER

Schalk J Oberholzer

Submitted in fulfilment of the requirements for the degree

Magister Scientiae in Geohydrology

in the

Faculty of Natural and Agricultural Sciences

(Institute for Groundwater Studies)

at the

University of the Free State

Supervisor: Dr Francois Fourie

January 2018

DECLARATION

I, **Schalk Oberholzer**, hereby declare that the present dissertation, submitted to the Institute for Groundwater Studies in the Faculty of Natural and Agricultural Sciences at the University of the Free State, in fulfilment of the degree of Magister Scientiae, is my own work. It has not previously been submitted by me to any other institution of higher education. In addition, I declare that all sources cited have been acknowledged by means of a list of references.

I furthermore cede copyright of the dissertation and its contents in favour of the University of the Free State.

Schalk Oberholzer

26 January 2018

ACKNOWLEDGEMENTS

I would hereby like to express my sincere gratitude to all who have motivated and helped me in the completion of this thesis:

- Prof Danie Vermeulen, Head of IGS, who had the confidence to enrol a student of advanced age.
- Dr François Fourie, my project leader, whose trust in this project and advice I could not do without.
- Mr Eelco Lucas, WISH creator, whose patience was tested to the extreme.
- Ms Issie Oberholzer, my mother, for her caring trust, patience, and acting as farm manager in my absence.
- David Ebetseng, Ivan Mosienyane, Benjamin Makung and Paulina Motabogi, that shouldered responsibility on the farm during my studies providing me with much needed time.
- Ms Ena Theron, for the challenge set of personal growth.

TABLE OF CONTENTS

CHAPTER 1 : INTRODUCTION	8
1.1 INTRODUCTION	8
1.2 MOTIVATION FOR THE PROJECT	8
1.3 AIMS AND OBJECTIVES	10
1.4 RESEARCH METHODOLOGY	10
1.5 DISSERTATION STRUCTURE	10
CHAPTER 2 : LITERATURE REVIEW	12
2.1 INTRODUCTION	12
2.2 THE VAALHARTS AQUIFER	12
2.2.1 The Hydrological Parameters	12
2.2.2 Water Chemistry and Water and Salt Balances	13
2.2.3 The Influence of Soils and Geology	17
2.2.4 Conclusion	20
2.3 GEOPHYSICAL METHODS AND THE RELATIONSHIP BETWEEN PHYSICAL AND GEOHYDROLOGICAL PARAMETERS	21
2.3.1 Introduction	21
2.3.2 The Electrical Resistivity and Electromagnetic Methods	22
2.3.2.1 Electrical Resistivity Methods	23
2.3.2.1.1 <i>Basic principles</i>	23
2.3.2.1.2 <i>Electrode geometries</i>	27
2.3.2.1.3 <i>Electrical resistivity surveys</i>	29
2.3.2.1.4 <i>Data processing and interpretation</i>	30
2.3.2.1.5 <i>The influence of inhomogeneity and anisotropy on the interpretation of resistivity data</i>	32
2.3.2.2 Electromagnetic Methods	35
2.3.2.2.1 <i>Basic principles</i>	35
2.3.2.2.2 <i>Electromagnetic surveys</i>	36

2.3.2.3	The Application of Geophysical Methods in Agriculture	39
2.4	THE RELATIONSHIP BETWEEN PHYSICAL, GEOPHYSICAL AND GEOHYDROLOGICAL PROPERTIES OF THE EARTH	40
2.4.1	Physical and Geophysical Properties of the Earth and Archie's Law	40
2.4.1.1	Porosity	40
2.4.1.2	Soil texture	41
2.4.1.3	Water content and salinity	42
2.4.1.4	Temperature	44
2.4.2	Adaptations of Archie's Law to Unsaturated Conditions and Conductive Minerals	45
2.4.2.1	An application of Archie's Law on soils with clay content	45
2.4.3	A Modified Archie's Law for Two Conducting Phases (Glover <i>et al.</i> , 2000)	46
2.5	THE RELATIONSHIP BETWEEN GEOPHYSICAL AND HYDROGEOLOGICAL PARAMETERS	47
2.5.1	The Geohydrological Parameters and their Determination	47
2.5.1.1	The geohydrological parameters	47
2.5.1.2	Pumping tests	50
2.5.1.2.1	<i>The Step Test</i>	51
2.5.1.2.2	<i>The Constant Rate Pumping Test</i>	52
2.5.1.2.3	<i>The Recovery Test</i>	57
2.5.2	The Relationship of the Physical and Geohydrological Parameters to Geophysical Measurements	61
CHAPTER 3 : SITE DESCRIPTION		66
3.1	INTRODUCTION	66
3.2	REGIONAL SETTING	66
3.3	GEOLOGY	66
3.4	RAINFALL	69
3.5	SURFACE DRAINAGE	69
3.6	AQUIFER SYSTEM	70

CHAPTER 4 : FIELD INVESTIGATIONS	72
4.1 INTRODUCTION	72
4.2 GEOPHYSICAL SURVEY	72
4.2.1 Calibrating VES Survey	72
4.2.1.1 Results of VES survey	74
4.2.1.2 Correlation between geology and layer resistivities	75
4.2.2 ERT Profile	81
4.3 PUMPING TESTS	82
4.3.1 The pumping test method	82
4.3.2 Interpretation of the pumping tests	82
CHAPTER 5 : RELATIONSHIP BETWEEN THE GEOHYDROLOGICAL, GEOPHYSICAL AND PHYSICAL PARAMETERS	85
5.1 FORMATION FACTOR	86
5.2 REGRESSION RELATIONSHIPS WITH K AND T	87
5.3 NOTES ON THE CALCULATION OF POROSITY	90
5.4 NOTES ON THE EC, TDS AND DETECTION OF SALINATION USING GEOPHYSICAL METHODS.	91
5.5 SYNTHESIS OF THE RESULTS - THE CONCEPTUAL AQUIFER	91
CHAPTER 6 : CONCLUSIONS AND RECOMMENDATIONS	96
6.1 CONCLUSIONS	96
6.2 RECOMMENDATIONS	97
REFERENCES	98
ABSTRACT	101
APPENDICES	
APPENDIX A - VES Field Curves with inverse modelled layers	
APPENDIX B - Pumping test curves	
APPENDIX C - Table of VES data and modelled Dar Zarrouk parameters	

LIST OF FIGURES

Figure 2.2-1: Piper diagram of water samples in the Vaalharts area (after Ellington <i>et al.</i> , 2004) ..	14
Figure 2.2-2: The TDS -EC conversion factor calculated by Ellington (2004)	15
Figure 2.2-3: Conceptual geology after Temperley (1967)	18
Figure 2.2-4: The modelled geology of the Vaalharts Aquifer (after Ellington, 2003).....	19
Figure 2.2-5: Water levels and flow lines in the Vaalharts Area (Ellington, 2003)	20
Figure 2.3-1: Distribution of an electrical current in a homogeneous medium.....	24
Figure 2.3-2: Equipotential- and current lines for electrodes A and B in a homogeneous half space	25
Figure 2.3-3: Refraction of electrical current with change in resistivity	27
Figure 2.3-4: Refraction change distribution of electrical current	27
Figure 2.3-5: Common electrode geometries used in resistivity surveys and their geometric factors (k) (Loke, 1999).....	28
Figure 2.3-6: The procession of resistivity measurements along different profiles at different depths to obtain a 2D pseudo-section of the earth's resistivities.....	30
Figure 2.3-7: Algorithm for the inversion of apparent resistivity data	31
Figure 2.3-8: Example of the inversion of 2D ERT data	32
Figure 2.3-9: Example of conceptualisation of geology using ERT method	32
Figure 2.3-10: A modelled layered earth	34
Figure 2.3-11: The primary and secondary magnetic fields generated by a time varying electrical current	36
Figure 2.3-12: Relative response versus depth of horizontal and vertical co-planar orientations (after McNeill, 1980).....	37
Figure 2.3-13: Detection pattern over a thin conductive body).....	38
Figure 2.4-1: Water occurrence in soils (Meyboom, 1967)	43
Figure 2.4-2: Conceptual Bulk soil (EC_a) model taking into account solid and liquid conductivities (Rhoades <i>et al.</i> , 1976).....	46
Figure 2.5-1: Drawdown in an aquifer	50
Figure 2.5-2: The Step Test indicating drawdown versus pumping rate	51
Figure 2.5-3: The Hantusch-Bierschenk method to calculate B and C (ICRC,2000)	52

Figure 2.5-4: Thiem's method for analysing drawdown data.....	53
Figure 2.5-5: Constant Rate Pumping test - the drawdown plotted against time since pumping commenced (IGRG, 2000).....	54
Figure 2.5-6: Drawdown in an unconfined aquifer.....	55
Figure 2.5-7: Graphs indicating common deviations from a straight line of the Constant Rate pumping test.....	57
Figure 2.5-8: The drawdown graph versus the recovery graph.....	58
Figure 2.5-9: Theis Recovery curve.....	59
Figure 2.5-10: Recovery data deviating from a straight line.....	60
Figure 2.5-11: Layered model showing transverse and longitudinal current flow (Sinha <i>et al.</i> ,2009).	62
Figure 2.5-12: Relations between aquifer resistivity, matrix resistivity, and effective porosity (Worthington in Mazac ,1985)	63
Figure 2.5-13: Schematic diagram to show relations between hydraulic conductivity, porosity, and resistivity for different sediment types (Mazac <i>et al.</i> (1985).....	64
Figure 2.5-14: Characteristic shapes of K- and H-type resistivity curves Utom <i>et al.</i> (2012).....	64
Figure 3.2-1: Regional setting of the Vaalharts Irrigation scheme.....	66
Figure 3.3-1: The geology of the Vaalharts Irrigation Scheme and surround (De Bruyn, 2016)	68
Figure 3.4-1: Rainfall measured at Magogong.....	69
Figure 3.5-1: Hydrological drainage of the Vaalharts area.....	70
Figure 4.2-1: The positions of VES soundings and ERT profile in the study area	73
Figure 4.2-2: The VES curve of Borehole 1D7-1.....	74
Figure 4.2-3: The VES curve of Borehole 2E11-1	75
Figure 4.2-4: The VES curve of Borehole 13I5-1	75
Figure 4.2-5: The comparison of the geology with resistivity of Borehole 1B10-1	76
Figure 4.2-6: The comparison of the geology with resistivity of Borehole 2J5-1.....	76
Figure 4.2-7: The comparison of the geology with resistivity of Borehole 8H14-1	77
Figure 4.2-8: The comparison of the geology with resistivity of Borehole 5L7.....	78
Figure 4.2-9: Profile A; The continuation of geology and resistivity layers; Boreholes 1B10 to 1K10	79

Figure 4.2-10: Profile B; The continuation of the geology and resistivity layers; Boreholes 1K10 to 1N6 79

Figure 4.2-11: Profile C; The continuation of geological and resistivity layers; Boreholes 6L16 to 8L3 80

Figure 4.2-12: The ERT profile from east to west..... 81

Figure 4.3-1: This curve of recovery data 5L7..... 83

Figure 4.3-2: This curve of recovery data; 2K11 84

Figure 4.3-1: Flowchart showing the interconnection between the measured and estimated data of this study (after Kazakis *et al.*, 2016)..... 85

Figure 5.1-1: Formation Factor of the Vaalharts Aquifer..... 87

Figure 5.2-1: Correlation of Transmissivity with Transverse Resistance 87

Figure 5.2-2: Correlation of Transmissivity (pump tested) with Longitudinal Conductance 88

Figure 5.2-3: The correlation of transmissivity (calculated) with transmissivity (pumptested) 89

Figure 5.2-4: Correlation of hydraulic conductivity with longitudinal conductance 89

Figure 5.2-5: Correlation of Hydraulic Conductivity with Apparent Resistivity 90

Figure 5.4-1: Contour map of Transmissivity encountered in the Vaalharts Aquifer 93

Figure 5.4-2: Contour map of Hydraulic Conductivities encountered in the Vaalharts Aquifer 94

Figure 5.4-3: The modelled aquifer thickness in the Vaalharts Aquifer..... 95

LIST OF TABLES

Table 2.2-1: Hydrological parameters of the deeper Vaalharts Aquifer	13
Table 2.2-2: Vaalharts Water balance as calculated by Ellington <i>et al.</i> (2004).....	16
Table 2.2-3: Vaalharts water balance as calculated by Verwey (2009)	16
Table 2.2-4: The salt balances (tonnes per annum, t/a) of the Vaalharts Irrigation Scheme as calculated by Ellington <i>et al.</i> (2004).....	17
Table 2.3-1: The resistivity ranges of different rock types (Loke, 2000).....	23
Table 2.3-2: Characteristics of different resistivity array configuration types (Samouëlian <i>et al.</i> 2005)	29
Table 2.5-1: Definitions of hydraulic and electric layer parameters (after Mazac <i>et al.</i> , 1985).....	61
Table 4.3-1: Transmissivity and Hydraulic conductivity calculated from pumping test.....	84
Table 4.3-1: Compiled data set with actual and estimated values of K and T	86

CHAPTER 1: INTRODUCTION

1.1 INTRODUCTION

The proposal to irrigate the Harts River Valley by gravity-fed water from the Vaal River was made as early as 1875 by the then surveyor-general, Francis HS Orpen (Turton *et al.*, 2004). Investigations into the feasibility of such a scheme were interrupted by the Second Boer War, and then later by the First World War. The plan to develop the irrigation scheme gained momentum after the First World War, and finally came to a head when it became government policy to solve the widespread poverty that existed in the aftermath of the Great Depression. In 1933, a decision was made to continue with the development of the irrigation scheme, and the first farmer tenants were settled in the area in 1938 (Turton *et al.*, 2004; Van Vuuren, 2010). This marked the start of a major anthropogenic influence on the natural resources of the region.

In terms of irrigation, the balances in nature, relating to the salt and organic balances in the soils, the surface to groundwater interactions, and eventually the surface water quality through tail end runoff and drainage, are affected. The biggest changes usually manifest as a rise in the groundwater table, as well as a build-up of salts in the soils and groundwater. It was found that the water table rose from an average of 9 metres below ground level (mbgl) to 1.5 mbgl since the start of irrigation at Vaalharts. The TDS also rose from 1 005 mg/L to 1 350 mg/L during the period 1976 - 2004 (Ellington *et al.*, 2004), and still further to 1 476 mg/L in 2009 (Verwey, 2009). The impact of irrigation on the natural balances, however, can be controlled to a certain extent through farming and irrigation practices, but scientific methods for fast and efficient monitoring are sadly lacking.

1.2 MOTIVATION FOR THE PROJECT

Cash crops such as wheat, maize, lucerne, cotton, peas and peanuts, are cultivated within the Vaalharts Irrigation Scheme with double cropping the norm in order to maximize on the yield/return per hectare. Since the late 1970s, a tendency to establish more permanent crops such as citrus, deciduous fruit, and pecan nuts took momentum. With this change to permanent established crops, a change in irrigation and other farming practices also took place. With the change to permanent crops, in particular pecan nuts, the application and intensity of irrigation changed from the nearly even distribution throughout the year of the classical double cropping norm, to a more summer season irrigation norm. In addition, the water demands of the permanent crops exceed those of the cash crops. Irrigation methods changed from a primarily flood irrigation regime to overhead irrigation

through centre pivots, while the orchards and plantations lend themselves to sophisticated drip and micro-irrigation methods.

Through such methods, the leaching of salts, as well as the surface to groundwater interaction, can be controlled (Bear, 1979; Barnard, 2013). The results from previous investigations (Ellington *et al.*, 2004; Verwey, 2009) recommended more efficient irrigation practices to lessen the salt load in the soils added by the irrigation water. This was supported by Barnard (2013) who recommended an approach in which salt build-up would be allowed in the soil profiles, with occasional flushing through over-irrigation and periods of excessive rainfall. Although much of the salt load is flushed out through the subsurface drains, there still exists a surface to groundwater interaction, and the subsequent build-up of salt in the deeper aquifer cannot be ruled out. This has a direct impact on the cultivation of permanent crops, especially pecan nuts, which are not very salt tolerant.

The water allocation per hectare of the Vaalharts Irrigation Scheme considered leaving fallow fields in between the cash crops. With the establishment of permanent crops, however, the advantages of letting a field lie fallow are negated. No more time is allowed for the return of soil and water balances to normal, and no irrigation water is saved as the farms are planted to their full extent. As the water demands of the permanent crops exceed those of the cash crops, irrigation shortages frequently occur, both through evapo-transpiration and the spatial extent of the area planted. This impacts on the flushing of salts from the soil profile, evidenced by diminished subsurface drainage flow, as observed by several farmers. The irrigation shortages are somewhat reduced by the fact that the tap root system of the permanent crop interacts with the shallow groundwater table. This may exacerbate the salinization of the deeper aquifer as the plants selectively utilise the water and leave salts behind through the process of osmosis. The salinization of groundwater beneath wooded areas and plantations are a well-documented phenomenon (Nosetto *et al.*, 2013). The effect of the very elevated water table and the influence on regularity of irrigation, are recognised by the farmers where areas of high interaction are called “klimaatgronde” (climate soils). These areas are unfortunately also those that are prone to waterlogging and salinization.

Because of the irrigation shortages, farmers are starting to look at groundwater to augment surface water irrigation. Unfortunately, the groundwater is much more saline than the surface water due to the local geology that constitutes the aquifer (Rudolph and Hough, 2003), adding to the problem of salinization. Augmenting irrigation with groundwater, or water of poorer quality, may be feasible in the short term and under certain circumstances (Miyamoto *et al.*, 1995), but eventually it must impact on the broader hydrological system as it has a direct influence on the environmental balances that currently exist.

This project then seeks to quantify the relationship between the hydrological, geophysical and physical parameters of the Vaalharts Aquifer and soils. Once this relationship is established, it is hoped to be applied to detect the presence of salinization in the soils and aquifer in future. If

successful, the geophysical methods employed will provide fast, easy, and non-intrusive methods to investigate and manage groundwater in irrigated areas.

1.3 AIMS AND OBJECTIVES

As the Vaalharts Aquifer is classified as a non-stratified, unconfined aquifer (Ellington *et al.*, 2004) with a very shallow water table (1.5 mbgl), the influence of the aquifer on agricultural activities has to be considered. An investigation into the aquifer and its characteristics is therefore warranted.

The main aim of this study is to investigate the relationship between the geohydrological, geophysical and physical parameters of the Vaalharts Aquifer with a specific focus on the salinization of the aquifer. To address this aim, the following objectives are identified:

- To determine the extent of the Vaalharts aquifer in a specific area, both in depth, and laterally, using geophysical methods.
- To examine the lateral homogeneity/inhomogeneity in geology by means of geophysical methods.
- To investigate the relationship between the geohydrological, geophysical and physical parameters of the aquifer.

1.4 RESEARCH METHODOLOGY

This investigation entails a multidisciplinary approach, with geophysics, geology and water chemistry used in conjunction to describe the Vaalharts Aquifer. The methodology used during the investigations includes the following actions:

- i) A literature study of previous investigations of the study area, including the application of geophysical methods in agriculture.
- ii) A hydrocensus of the area, locating boreholes allowing measurement of groundwater levels, pump testing and water sampling.
- iii) The application of geophysical methods to determine the water level, depth of saturated zone and homogeneity of the aquifer.
- iv) The modelling of physical geology and geohydrological parameters to the geophysical parameters.

1.5 DISSERTATION STRUCTURE

This dissertation is structured in five chapters and the respective contents are discussed as follows:

Chapter 1 Chapter 1 contains the introduction and the motivation for this project. The aims and objectives are established, and the research methodology is presented.

Chapter 2 encompass the literature review and is divided in four parts. The first part is a study of previous work relating to this project was done and a conclusion to their relevance was reached. The second part of the literature review included the theory of electrical geophysical methods and their application. The discussion on the relationship between the geophysical and the physical- and geohydrological parameters constitutes the last two parts.

Chapter 3 presents the site description with the regional setting, geology and hydrological environment.

Chapter 4 describes the field investigations. That is the calibrating VES survey, ERT profile and pumping tests.

Chapter 5 presents the discussion and findings of the field investigations and concludes with recommendations for further work to be done

CHAPTER 2: LITERATURE REVIEW

2.1 INTRODUCTION

In this chapter a review of the literature pertaining to this investigation is given. The literature review is divided into three parts. Firstly, previous hydrological investigations in the Vaalharts area are considered. Then, the use of geophysical methods and the relationship between geophysical and hydrological parameters are discussed. Lastly, the effects of water quality on crops and their specific tolerances with regard to salt levels are described. It must be noted that a search of the available literature produced no record of previous geophysical investigations in the Vaalharts area.

2.2 THE VAALHARTS AQUIFER

Several authors have studied the Vaalharts aquifer to determine its characteristics and water and salt balances. Their findings will be discussed according to the hydrological parameters, the water and salt balances, and the influence of soil and geology. Unfortunately, none of the original datasets that the authors used are available, and information had to be gleaned from their written texts. In conclusion, their methods, findings, and applicability to this investigation will be assessed.

2.2.1 The Hydrological Parameters

During 1973 to 1975, boreholes were drilled to investigate the possible lowering of the groundwater table through dewatering to encounter water logging of soils (Gombar and Erasmus, 1976). Subsequent pump testing determined a hydraulic conductivity (K) value of 13.43 m/d, a specific storage (S) in the order of 10^{-1} , and a transmissivity (T) value of 70 m²/d.

In the study of Ellington (2004), 17 boreholes were drilled, and pump testing produced K -values between 0.1 m/d and 19 m/d, S -values in the order of 2.77×10^{-3} , and T -values ranging from 20 m²/d to 200 m²/d. An average porosity of 10% was calculated for the deeper aquifer. Ellington (2004) also conducted tracer tests where seepage velocities between 2 m/d and 220 m/d, and Darcy velocities between 1 m/d and 22 m/d were recorded. These velocities are driven by the pressure gradient provided by the topography. Pumping tests established a homogenic storage coefficient in the order of between 10^{-3} and 10^{-4} .

Rudolph (2003) investigated the vulnerability of the Vaalharts Aquifer to sewage pollution and evaluated K -values obtained from the Shephard Method (sieve analysis) against K -values obtained from the borehole method. He found a close correlation, and subsequently K -values from the

Vaalharts Agricultural Research Station were used in his investigations (De Bruyn, personal communication, 2016). These *K*-values were also obtained for the current investigation.

Verwey (2009) concentrated on the topmost 3 m layer of the aquifer (the surface to groundwater interaction) and the leaching of salts from the soil profile. His investigation revealed *K*-values between 0.013 m/d and 5.4 m/d. These parameters were mainly obtained through the bailing of piezometers and the measuring of the recovery rate of the 3 m soil profile.

It is clear that the investigators acquired data to their specific area of interest and thus the data can be divided into a parameter set of the deeper aquifer and a parameter set of the shallow subsurface (unsaturated zone). Hydrological parameters relating to this study of the deeper aquifer are presented in Table 2.2-1.

Table 2.2-1: Hydrological parameters of the deeper Vaalharts Aquifer

Source	Position	Transmissivity T	Hydraulic Conductivity K	Storage Coefficient S	Darcy Velocity	Seepage Velocity
Gombar & Erasmus in Verwey (2009)	Average A-E blocks		2,378 m/d			
	Average F-I blocks		13,437m/d			
Gombar & Erasmus in Ellington (2004)	Average	70 m ² /d				
Van Wyk in Ellington (2004)	Average			0,0057		
Ellington (2004)	1G14-1	43,3m ² /d	1,6m/d			
	1K10-1	31,6m ² /d	0,3m/d			
	6L16-1	4,2m ² /d	0,1m/d			
	6L16-2	4,5m ² /d	0,1m/d			
	1B10-1				2m/d	21m/d
	1D3-1	0,21m ² /d		0,01	1,5m/d	15m/d
	1D7-1	194m ² /d		0,022	3m/d	29m/d
	2J14Riv-3	58m ² /d		0,009		
	8H14-1	1,2m ² /d		0,01	22m/d	217m/d
	2J5-1	123m ² /d		0,026	1m/d	9m/d
	Other		0,045 - 6,25m/d	0,00277		
Verwey (2009)			0,013-5,4m/d			

2.2.2 Water Chemistry and Water and Salt Balances

The electrical conductivity (EC) of water depends on the total and relative concentration of ions in solution. Thus, the EC relates in direct proportion to the total dissolved solids (TDS) in the water. The relative concentrations of the respective ionic elements present, give an indication to the chemical balances and processes that prevail.

From historical water chemistry, Ellington *et al.* (2004) classified the water in the Vaalharts area as belonging to the Calcium-Sodium-Bicarbonate type (Figure 2.2-1). The majority of samples show no dominant cation in the chemical composition although they cluster slightly to the Ca-Na side. Dominant magnesium samples can be positively correlated to the Dwyka shale geology. Bicarbonate

is the dominant anion present. Higher sulphate levels were attributed mainly to the addition of the sulphate content of the irrigation water of the Vaal River. The overall chemical footprint correlates with those of the surface waters of the Vaal- and Harts Rivers, reinforcing the notion that irrigation-to-aquifer interaction is taking place.

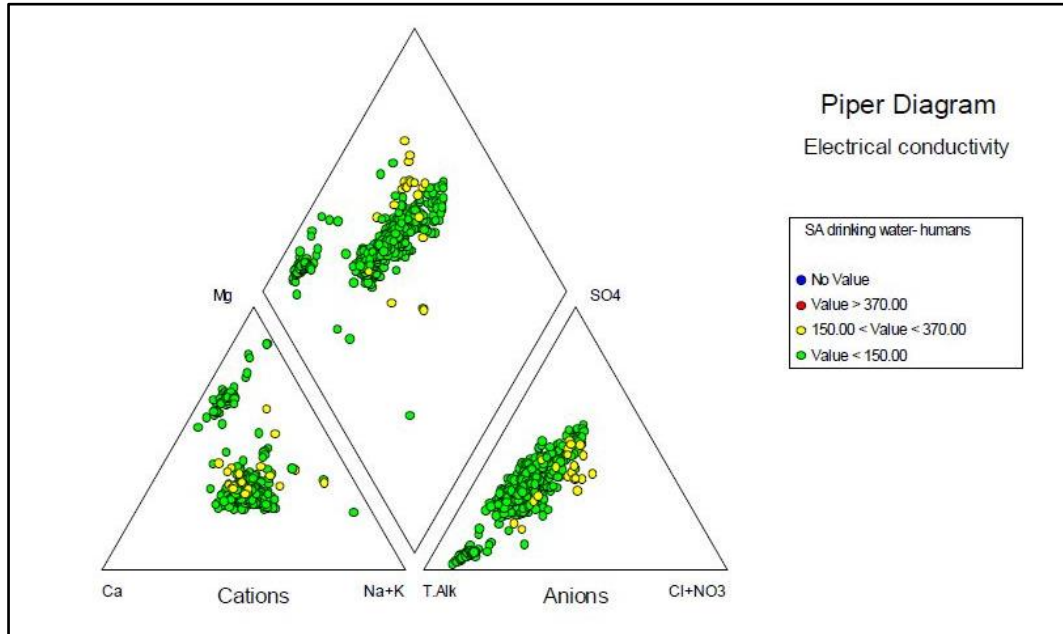


Figure 2.2-1: Piper diagram of water samples in the Vaalharts area (after Ellington *et al.*, 2004)

The water and salt balance calculated by Herold and Bailey (1996) in their study, revealed a salt deficit in water draining to the Harts River. The authors did not quantify, nor consider, the contribution of subsurface drains on the water balance. The influence of these drains was later investigated by Verwey and Vermeulen (2011). Herold and Bailey (1996) proposed the presence of a perched water table, where the deeper aquifer had not yet attained full salt saturation, acting as salt sink. A chloride load retention that was lower than the salt retention, was explained as salts precipitating in the soil profile. This was confirmed by the study of Simpson (1999) which found the precipitation of metal salts (in particular Manganese Sulphate) responsible for the clogging of subsurface drains. A potassium deficit in the soil water chemistry was also attributed to mineralization in the soil by Du Preez *et al.* (2000), especially in clay profiles.

The study of Du Preez *et al.* (2000) into the influence of irrigation on soils, determined a fluctuating trend in electrical conductivity (EC) values from year to year. However, first regression analysis calculated that the trend of salinization of the river water delivered to the irrigation scheme was increasing at a rate of 0.54 mS/m/a. The long-term average EC of the irrigation water based on historical data was calculated as 52 mS/m and the EC was expected to increase to approximately 74 (± 20) mS/m in the 20 years to 2020.

In the investigation of Ellington (2004), the existence of the salt sink postulated by Herold and Bailey (1996), which might pose an imminent environmental risk, was disputed. Hydrochemical profiling

and piezometer tests produced no evidence of stratification in the aquifer. EC values measured ranged from 100 mS/m to 270 mS/m and an average TDS of 1 350 ppm was observed. This TDS value represents a rise from 1 005 mg/L during the period 1976 to 2002; approximately 14 mg/L/a.

Adding to this investigation, Verwey (2009) found that accepting the non-stratification of water quality in the aquifer, and a constant net capacity of the aquifer, as supported by the subsurface drains, the TDS in the aquifer was still rising because of salts retained in the system. His findings entailed a non-return of the salts added by the subsurface water to the surface water at the Harts River. Subsurface drains that are not efficient, and not interspersed closely enough, were blamed for leading to a build-up of salt in the system through irrigation water inter-acting with the groundwater. Verwey (2009) also found that the average EC in the top 3 m horizon of the soil was 191 mS/m, representing a TDS of approximately 1 476 mg/L ($191 \times 7.699 + 5.4 = 1\,476$ mg/L). This indicated an increase of 96 mg/L since Ellington's 2004 investigation – an average increase of 19.25 mg/L/a. A continued rate of salinization of the aquifer was thus deduced. The TDS-EC conversion factor ($7.699x + 5.4$) is also very close to that determined by Ellington ($7.62x$; Figure 2.2-2). EC mapping from Verwey (2009) already suggested areas of soil salinity higher than crop tolerances, which could impact on crop yields.

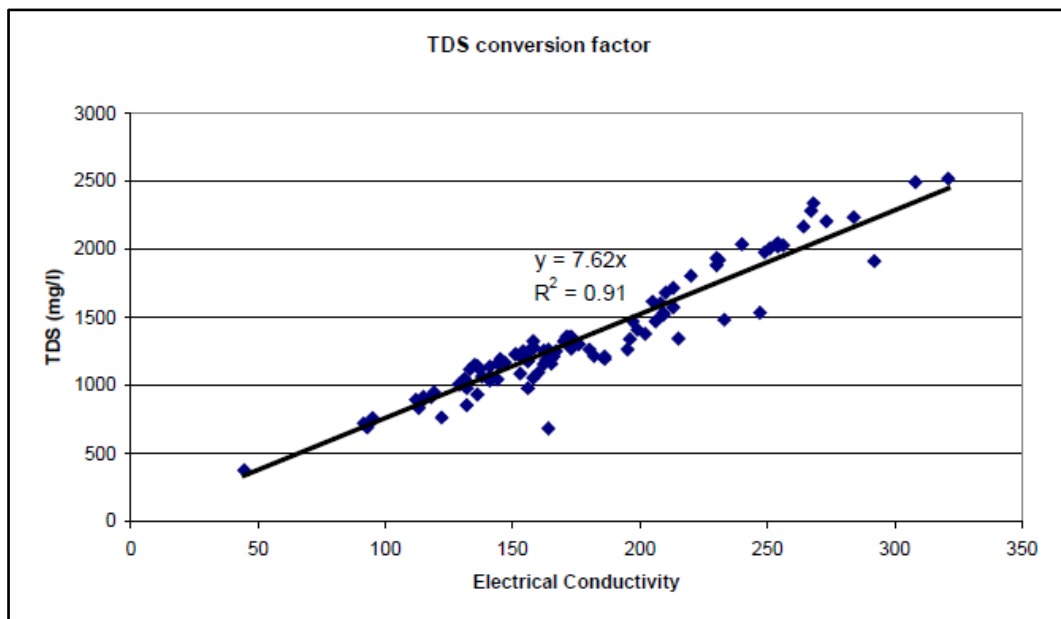


Figure 2.2-2: The TDS -EC conversion factor calculated by Ellington (2004)

Water and salt balances were calculated by several authors over the years to address the problems of water logging and salinization, the most recent those of being Ellington *et al.* (2004) (Table 2.2-2), and Verwey (2009) (Table 2.2-3). A glaring discrepancy between the two water balances is noted with Ellington *et al.* (2004) estimating the contribution of the rainfall at 309.6 Mm³/a, which corresponds to a water volume nearly twice as much as the average rainfall (431 mm/a) over the study area. Closer scrutiny revealed that the surface area of the Ellington project area was calculated as 72 000 ha, while the Vaalharts Irrigation Scheme has a surface area of only 36 950 ha (Haarbron,

2015). The bigger surface area used in the model of Ellington in all likelihood contributed to a dilution of salts in the salt balance calculation. In fact, one of the conclusions of their modelling indicates a dilution of the salt load away from the irrigated areas.

Table 2.2-2: Vaalharts Water balance as calculated by Ellington *et al* (2004)

Name	Incoming water (M m ³ /a)	Outgoing water (Mm ³ /a)
North Canal	272.01	
West Canal	42.97	
Rainfall	309.60	
Groundwater going to river		14.34
Canal Tailends		23.35
Recharge		28.38
Drainage		23.63
Runoff		4.10
Evapotranspiration		533.30
Totals	624.58	627.16
Difference (Inflow - Outflow)	-0.41%	

Table 2.2-3: Vaalharts water balance as calculated by Verwey (2009)

	Inflows (mm/a)	Outflows (mm/a)
Irrigation	980	
Rainfall	431	
Tailend		49
Recharge @ 5%		21
Drainage		?
Run-off		5.7
Evapotranspiration		774
Total	1411	849.7
Therefore drainage need (1411-849.7) / 365 = 1.54 mm/d = 562.1 mm/a		

Although Verwey (2009) referred to some of the parameters of Ellington *et al.* (2004) such as canal tail ends and runoff, he focused on the impact on irrigated land and the salt load delivered directly to the soils and aquifer. This might explain the high drainage calculated (562.1 mm/a) to maintain equilibrium in the water balance. This drainage is significant as it must be dealt with through subsurface drains and gravitational drainage in the aquifer to the Harts River.

When looking at the salt balance composed by Ellington *et al.* (2004) (Table 2.2-4), most of the salt contribution to the Vaalharts hydrological system is through the addition of irrigation water. It is much more than the amount of salts deposited through the application of fertilizer (11 2884 t through irrigation water to the 48 302 t from fertilizer). This salt balance distinguishes between salts removed by subsurface drainage and groundwater recharge to the Harts River. The recharge (84 287 t/a) mentioned in the table refers to salt added to the groundwater by leaching. Salinity levels in the aquifer are expected to increase due to increasing salinity of irrigation water and salt retention in the soils.

Table 2.2-4: The salt balances (tonnes per annum, t/a) of the Vaalharts Irrigation Scheme as calculated by Ellington *et al.* (2004)

Components	Option 1	Option 2
North Canal	112884	112884
West Canal	17832	17832
Groundwater going to river	15873	15873
Canal Tailends	17977	17977
Drainage	17979	17979
Recharge ^{1,2}	84287	111758
Salts taken up by crops ¹	25962	25962
Fertilizer addition ¹	48302	48302
Salts in soils ¹	1900	1500
Incoming salts	179018	179018
Outgoing salts	163979	191050
Incoming less outgoing	15039	-12032
Percentage difference	8.401%	-6.721%

¹Based on values obtained from du Preez *et al.*, 2000 and the numerical model
² Upper and lower values of calculated salt leaching used.

2.2.3 The Influence of Soils and Geology

The influence of the geology on the hydrological environment was recognised by all investigators. Temperley (1967) (in Ellington *et al.*, 2004) proposed a simplified conceptual geological sequence of Venterdorp Group lithology, overlain by sediments of the Dwyka Group, upon which Kalahari sands were deposited (Figure 2.2-3). Temperley (1967) also drew attention to the significance of the secondary calcrete horizon in the soil profiles. This calcrete horizon is probably a remnant of a historical water level, formed in the zone of capillary action of the water table. With the recent rise in the water table, this calcrete layer is now submerged and in a state of dissolution. Waterlogging experienced in the irrigated areas is attributed to the excessive application of irrigation water.

Salinization in the waterlogged areas is attributed to (Rudolph and Hough, 2003; Ellington *et al.*, 2004):

- The high mineral content of the Dwyka aquifer,
- The circulation of irrigation water with water of the aquifer, and,
- The high evaporation to rainfall ratio.

With subsequent investigations, the influences of the variations that exist in the geology came to light.

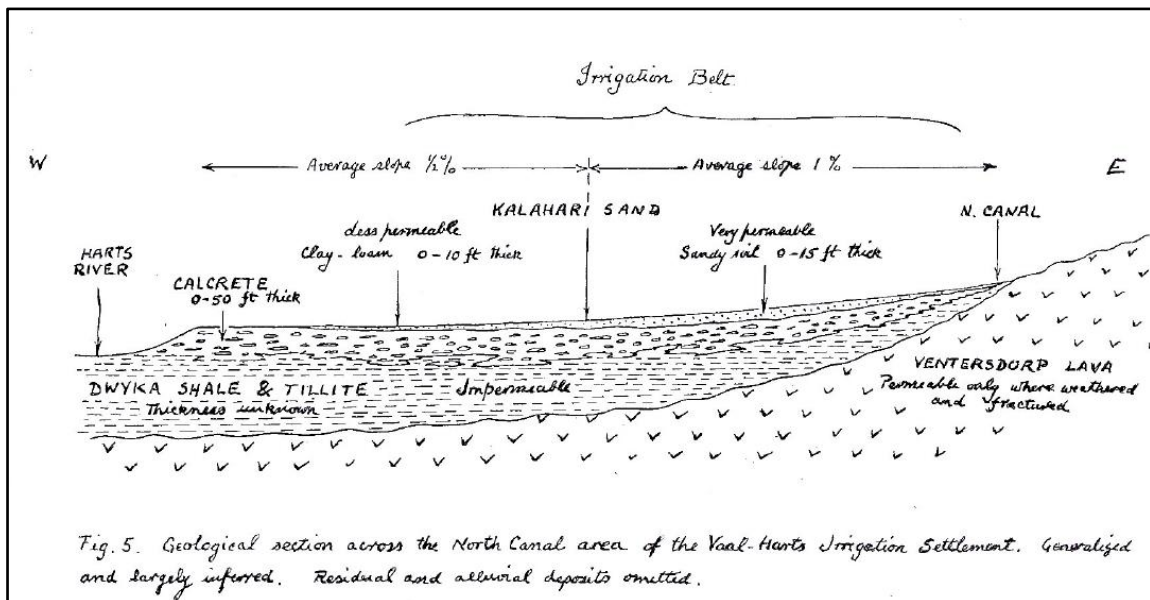


Figure 2.2-3: Conceptual geology after Temperley (1967)

With their investigation into the Vaalharts Aquifer, Gombar and Erasmus (1976) determined an aquifer composition of tillite, shale, weathered shale and calcrete, with the unweathered lavas of the Ventersdorp Group forming the bottom aquiclude of what is essentially an unconfined aquifer. Variation in the aquifer thickness as determined by the aquiclude was found to be directly responsible for waterlogging that occur in certain areas.

Herold and Bailey (1996) assumed the calcrete layer to be impermeable, posing this layer as an aquitard. The result of which is the presence of a perched water table. This, they postulated, may in part explain the deficit in their calculated saltwater balances, as the deeper aquifer had not yet reached full saturation point.

This was refuted by the investigation of Ellington *et al.* (2004), as no evidence of a stratified aquifer could be found in the groundwater chemistry and analyses of pumping tests. The important inference is, that the deeper aquifer does not behave independently from the topmost soil horizons. Ellington *et al.* (2004) also tried to construct a conceptual geological model to present variations in the geology encountered during his investigation (Figure 2.2-4). Water chemistry reported lower than expected nitrate values (2.2 mg/L), which the authors attributed to a lower than expected salt migration through the soil. Bayesian interpolation between water levels and topography yielded a correlation of 97%.

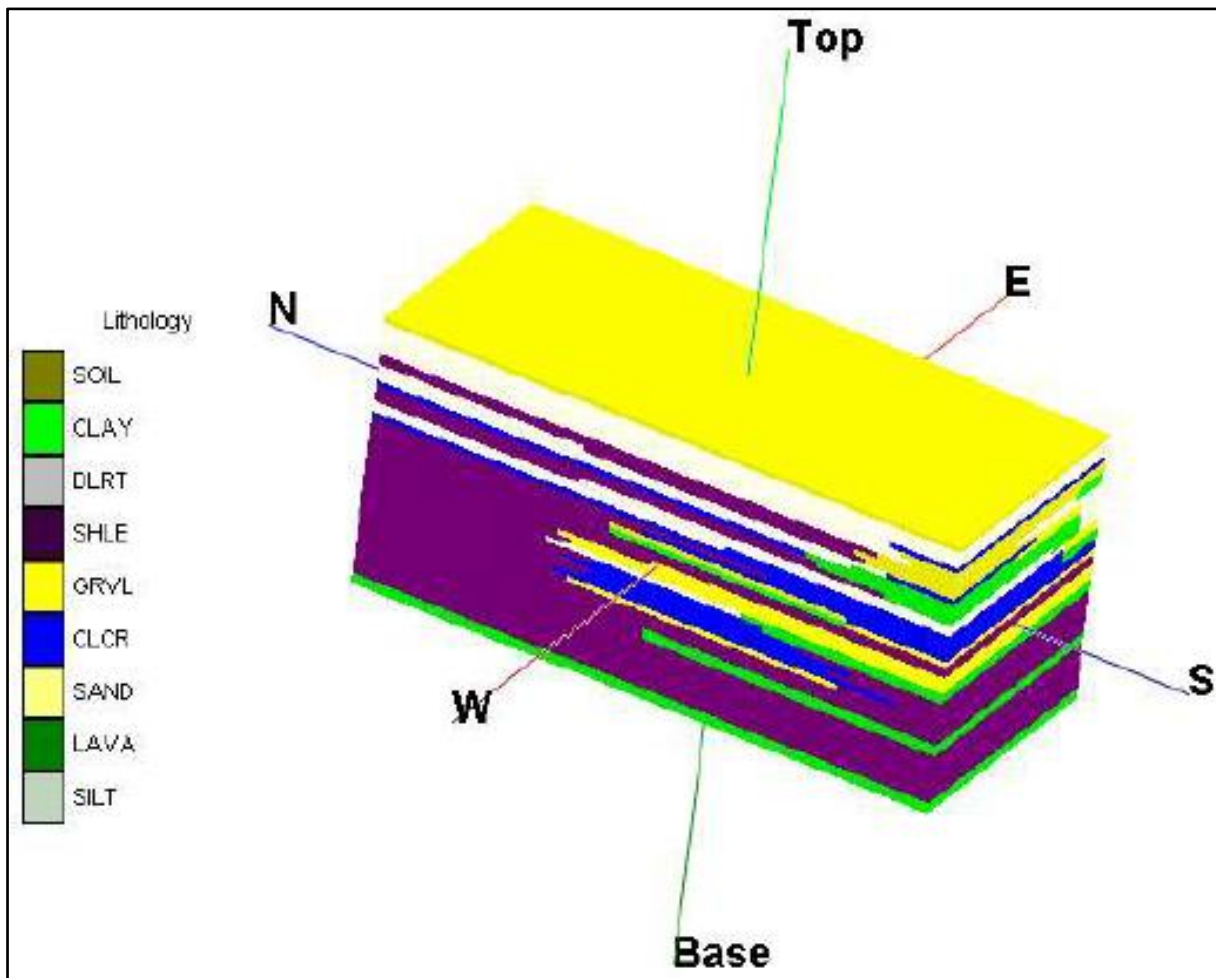


Figure 2.2-4: The modelled geology of the Vaalharts Aquifer (after Ellington, 2003)

The investigation of Verwey (2009) focused primarily on the top part of the Vaalharts aquifer, the soil properties, and their influence on the hydrological interaction between the soil and the deeper aquifer. Soil water constants were determined from soil analysis for sand, silt and clay fractions. No correlation between K -values and EC values was found, and only a vague correlation (not quantified) between EC values and clay content was mentioned. When interpreting the Cl concentrations of the chemical analyses, it was noted that at a specific point (s05) the rise in Cl concentration was accompanied by a rise in EC (Verwey, 2009). This point was in the middle of a pecan nut orchard. The presence of clay also gave rise to higher Cl concentrations in water analyses, probably due to a lower drainage capability. Special attention was given to the influence of subsurface drainage on the water and salt balances. Bayesian interpolation by Ellington (2003) and Verwey (2009) between measured water and topographical levels taken quarterly over a year, all showed a correlation of more than 99%, confirming the influence of the topography on the movement of the groundwater (Figure 2.2-5).

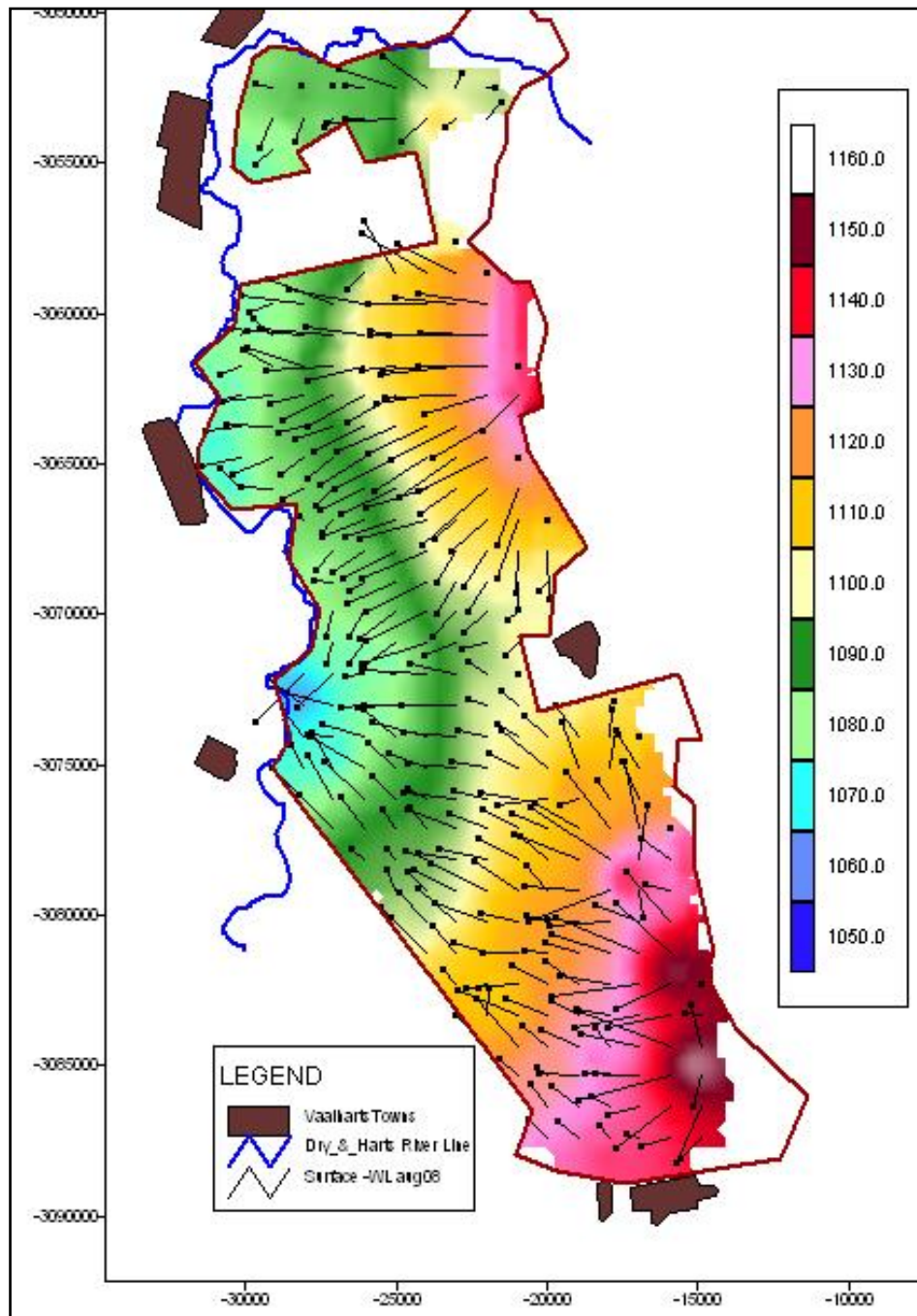


Figure 2.2-5: Water levels and flow lines in the Vaalharts Area (Ellington, 2003)

2.2.4 Conclusion

From the study of previous investigations, their methodologies and findings, the following conclusions can be drawn:

- a) By using a blanket approach, previous studies provided a generalised conceptual understanding of the behaviour of the Vaalharts Aquifer. Although hydrological parameters were determined by several authors through reliable methods, interpolation to other areas must consider variations in geological and soil variability.

- b) Drainage of the Vaalharts aquifer, is to the Harts River. This is supported by the topography, and the fact that the aquifer is an unconfined aquifer. It is also validated by water levels measured during studies by previous investigators (Ellington *et al.*, 2004);. See Figure 2.2-3.
- c) Water and salt balances seem not to be in equilibrium as found by Harold and Bailey (1996) and Verwey (2009). An explanation of the salt deficit might be found in mineralisation in the soils and the fact that the submerged calcrete horizon exists in a state of chemical imbalance (Du Preez *et al.*, 2000).
- d) The groundwater type classified by the chemical composition of the groundwater does not seem to have a marked influence on EC, although it affects the TDS conversion factor.
- e) In recent studies (Ellington *et al.*, 2004; Verwey, 2009), chemical parameters such as EC were directly compared to historical data and to each other to prove an increase of salinization. Such comparisons must be approached with care as sampling points do not correspond, and different horizons were sampled. A trend can only be established by long term monitoring of predetermined sample points to avoid yearly fluctuations, as reported (Du Preez *et al.*, 2000),
- f) From the expected increase in EC of the water of the Vaal River alone, as predicted by Du Preez *et al.* (2000), one can expect an increase in the salt load to the soils and the underlying aquifer.
- g) Correlation of chemical characteristics between surface (irrigation and runoff) water samples and subsurface water samples indicate a definite interaction between the application of irrigation water and the Vaalharts aquifer.
- h) By calculating the salt balance, it is evident that irrigation water is responsible for the bulk of the salt load added to the soils, and subsequently the underlying aquifer through the surface/groundwater interaction. (Gombar & Erasmus, 1976; Du Preez *et al.*, 2000; Ellington *et al.*, 2004)
- i) A regional water balance and salt transport model as composed by Ellington (2004) will only highlight the spread of salinity to the surrounding non-irrigated areas. A water and salt balance solely applied to irrigated areas will be more realistic of hydrological conditions.
- j) No geophysical studies have been done on the Vaalharts soils and aquifer.

2.3 GEOPHYSICAL METHODS AND THE RELATIONSHIP BETWEEN PHYSICAL AND GEOHYDROLOGICAL PARAMETERS

2.3.1 Introduction

The use of geophysical methods in geohydrology is mainly driven by the non-intrusive nature, speed, and consequent low cost of these investigations. The two methods most commonly used in shallow

earth applications, are the electrical resistivity (ER) method and the electromagnetic (EM) method. Information obtained through these methods, can be directly linked to the earth's physical characteristics through empirical equations such as Archie's Law. As the geohydrological parameters are in turn directly dependent on the physical characteristics, the relationship between these are of use to estimate one another if one can be measured. The implementation of Archie's Law is crucial to the interpretation of nearly all electrical geophysical methods.

The geohydrological parameters of the earth are parameters quantifying the ease with which a liquid can enter and move through the earth, and the holding capacity of such liquid within the earth. These parameters are usually obtained through laboratory testing of borehole core samples, or through pumping tests of boreholes. The geohydrological parameters are dependent on the physical properties of the earth such as the sizes and connectivity of the interstitial voids between minerals or grains, and the petrophysical and mineralogical composition of the earth.

This chapter then, deals with electrical geophysical methods and their application to investigate the relationship between electrical measurements, the earth's physical characteristics, and the geohydrological parameters.

2.3.2 The Electrical Resistivity and Electromagnetic Methods

Note must be taken of the differences between these two electrical geophysical methods. The electrical resistivity (ER) method applies a direct electrical current to the earth through electrodes, whereas the electromagnetic induction (EM) method relies on the induction of an electrical current in the earth through the indirect application of an electromagnetic field. The resistivity method measures the resistivity (ρ) while the electromagnetic method typically measures the conductivity (σ) of the subsurface. The resistivity is the reciprocal of the conductivity ($\rho = 1/\sigma$). Both methods may therefore be used to measure the electrical conductivity of the soil (Grandjean *et al.*, 2009), and thus resistivity and conductivity will be used interchangeably in their respective contexts in this investigation. The ER method has a variety of electrode arrays in its arsenal, each with its own pros and cons, as well as great flexibility regarding electrode spacing. The EM method is dependent on several variables in its geometry, and instruments are manufactured according to fixed specification settings to obtain direct measurements of the earth's apparent conductivity (McNeill, 1980a). Although a much faster method than ER, the EM method sacrifices some definition due to the fixed geometry settings.

The application of these methods rests on the premise that a resistivity contrasts exist between subsurface materials. Table 2.3-1 shows the typical ranges of resistivities for different rock types. It is seen that igneous and metamorphic rocks typically have a higher resistivity than sedimentary rocks, although the resistivities of sandstones can range from very low to very high. The resistivity of igneous and metamorphic rocks is greatly dependent on the degree of fracturing, and the percentage

of the fractures filled with groundwater. The reason for the lower resistivity values in sedimentary rocks is due to the fact that these rocks are usually more porous than igneous and metamorphic rocks which usually result in a higher water content. Since most electrical current flow through rock materials takes place through ionic conduction, higher water content generally leads to lower resistivity. Unconsolidated sediments generally have even lower resistivity values than sedimentary rocks, with values ranging from around 1 000 Ωm to less than 10 Ωm (McNeill, 1980a).

Table 2.3-1: The resistivity ranges of different rock types (Loke, 2000)

Material	Resistivity (Ω•m)	Conductivity (Siemen/m)
Igneous and Metamorphic Rocks		
Granite	$5 \times 10^3 - 10^6$	$10^{-6} - 2 \times 10^{-4}$
Basalt	$10^3 - 10^6$	$10^{-6} - 10^{-3}$
Slate	$6 \times 10^2 - 4 \times 10^7$	$2.5 \times 10^{-8} - 1.7 \times 10^{-3}$
Marble	$10^2 - 2.5 \times 10^8$	$4 \times 10^{-9} - 10^{-2}$
Quartzite	$10^2 - 2 \times 10^8$	$5 \times 10^{-9} - 10^{-2}$
Sedimentary Rocks		
Sandstone	$8 - 4 \times 10^3$	$2.5 \times 10^{-4} - 0.125$
Shale	$20 - 2 \times 10^3$	$5 \times 10^{-4} - 0.05$
Limestone	$50 - 4 \times 10^2$	$2.5 \times 10^{-3} - 0.02$
Soils and waters		
Clay	1 - 100	0.01 - 1
Alluvium	10 - 800	$1.25 \times 10^{-3} - 0.1$
Groundwater (fresh)	10 - 100	0.01 - 0.1
Sea water	0.2	5
Chemicals		
Iron	9.074×10^{-8}	1.102×10^7
0.01 M Potassium chloride	0.708	1.413
0.01 M Sodium chloride	0.843	1.185
0.01 M acetic acid	6.13	0.163
Xylene	6.998×10^{16}	1.429×10^{-17}

In-depth discussions on the principles of the ER and EM methods are given below to further explain the differences between these methods.

2.3.2.1 Electrical Resistivity Methods

The electrical resistivity method is used to study horizontal and vertical discontinuities in the electrical properties of the earth. It utilises direct currents or low frequency alternating currents applied directly to the earth by means of electrodes to determine the electrical properties of the subsurface (Keller & Frischknecht, 1996). Only the direct current method will be explained, as it is the most common method used and the one employed in this study.

2.3.2.1.1 Basic principles

Definition: electrical resistivity is the ability of a material to resist electrical current flow and is measured in ohm/m.

The electrical resistivity method is based on Ohm's Law which states that the electrical potential difference (V) needed to effect a given electrical current (I) through a homogeneous medium is directly proportional to the electrical resistance (R) of the medium (Herman, 2001):

$$V = IR \quad \text{Equation 2.3-1}$$

Consider an ideal cylinder of length L and cross-sectional area A of uniform composition with a voltage difference V applied across the length of the cylinder. For such a setup, the resistance may be expressed in terms of the material-specific resistivity (ρ) and the geometric parameters of the cylinder:

$$R = \rho \frac{L}{A} \quad \text{Equation 2.3-2}$$

The specific resistivity of the material through which current flow takes place may therefore be found from:

$$\rho = \frac{VA}{IL} \quad \text{Equation 2.3-3}$$

If an electrical point source is applied to a homogeneous earth (Figure 2.3-1), the current flows radially away from the source so that the current distribution is uniform over hemi-spherical shells situated over the point source. Lines of equal voltage (equipotential lines) intersect the lines of equal current at right angles.

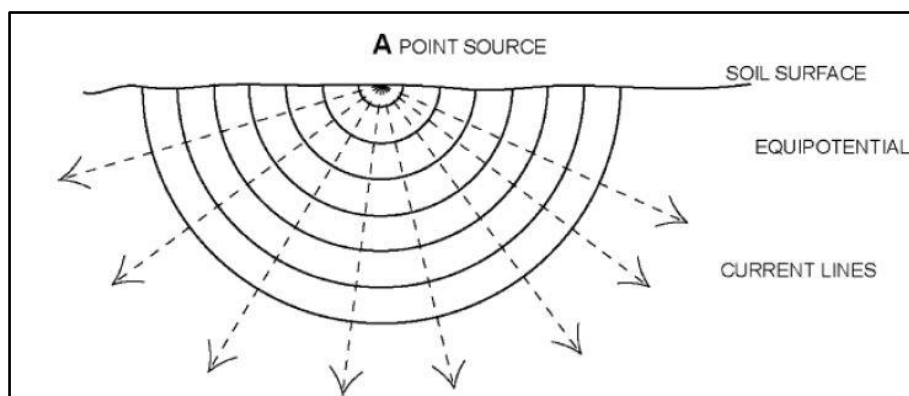


Figure 2.3-1: Distribution of an electrical current in a homogeneous medium

The potential at any point located a distance r away from the source can be calculated from:

$$V = \rho \frac{I}{2\pi r}$$

Equation 2.3-4

During resistivity surveys, the resistivity of the ground is measured by injecting electrical current into the subsurface and by measuring the resulting electrical potential difference at the surface of the earth (Figure 2.3-2). In the standard configuration, two pairs of electrodes are required, namely: two electrodes used for current injections (the *current electrodes*, normally denoted by A and B), and two electrodes for the measurement of the resulting potential difference (the *potential electrodes*, normally denoted by M and N) (Herman, 2001; Keller and Frischknecht, 1996).

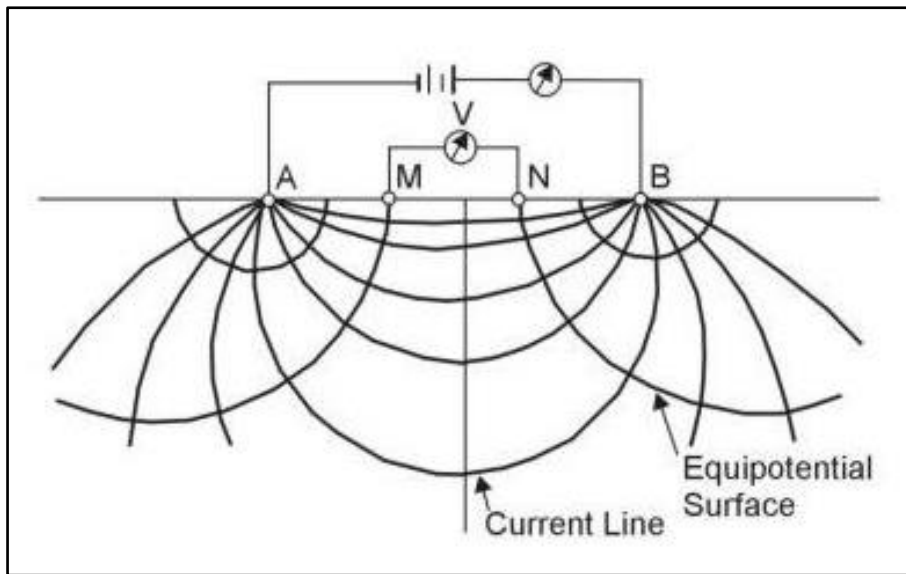


Figure 2.3-2: Equipotential- and current lines for electrodes A and B in a homogeneous half space

The electrical potential difference at any position in the subsurface can be calculated from:

$$V = \rho \frac{I}{2\pi r_A} + \rho \frac{-I}{2\pi r_B} = \rho \frac{I}{2\pi} \left[\frac{1}{r_A} - \frac{1}{r_B} \right]$$

Equation 2.3-5

where r_A and r_B are the distance from the subsurface position to electrodes A and B, respectively. The difference in electrical potential at the potential electrodes (M and N in Figure 2.3-2) can then be calculated from:

$$\Delta V = V_M - V_N = \rho \frac{I}{2\pi} \left[\frac{1}{AM} - \frac{1}{BM} + \frac{1}{BN} - \frac{1}{AN} \right]$$

Equation 2.3-6

Where AM is the distance between electrodes A and M, and so forth. The term in brackets is a function of the geometry of the array and allows Equation 2.3-6 to be written as:

$$\Delta V = \rho \frac{I}{2\pi K}$$

Equation 2.3-7

where K is the geometric factor or geometric coefficient. Equation 2.3-7 can then be solved for ρ and written as:

$$\rho = 2\pi K \frac{\Delta V}{I}$$

Equation 2.3-8

The resistivity from the earth (ρ) can thus be calculated by measurements of ΔV and I , and by calculating the geometric factor. In a homogeneous earth, the calculated resistivity will represent the true resistivity of the earth. In such a (idealised) case, the calculated resistivity will be independent of the electrode spacing and the surface location of electrodes. However, the earth is not homogeneous. Both lateral and vertical changes in geology, and hence resistivity, occur. During resistivity surveys on real earth materials, current flow in the subsurface is not restricted to a single pathway. Rather, the electrical current flows in three dimensions through the earth materials in the subsurface. It is therefore not possible to directly measure the resistivities of the subsurface materials. However, it is still possible to obtain information on the subsurface resistivity distribution.

For a standard four-electrode setup, such as shown in Figure 2.3-2, it is possible to calculate the apparent resistivity of the subsurface. The apparent resistivity is the resistivity that would have been recorded using such a setup on a homogeneous subsurface (Herman, 2001; Keller & Frischknecht, 1996; Parasnis, 1997). The apparent resistivity (ρ_a) may be calculated from the following equation:

$$\rho_a = 2\pi K \frac{\Delta V}{I}$$

Equation 2.3-9

When electrical current encounters boundaries between earth materials of different electrical resistivities, the current pathways are refracted at the boundaries. Figure 2.3-3 illustrates the behaviour of the electrical current in such a case. If a layer of higher resistivity is encountered, the current is refracted towards the normal, and away from the normal in the case of a layer of lesser resistivity.

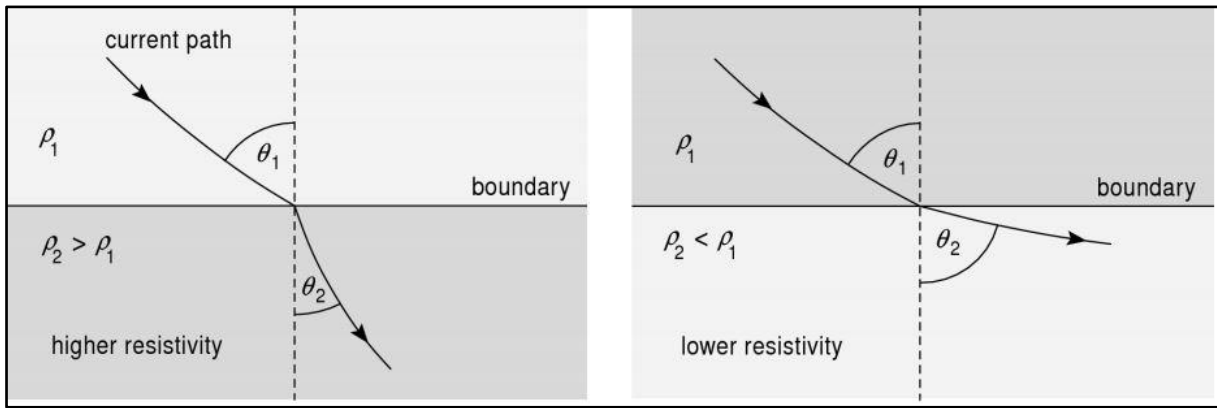


Figure 2.3-3: Refraction of electrical current with change in resistivity

The relationship between the angles of incidence and refraction is controlled by the resistivities of the two media in contact:

$$\rho_1 \tan \theta_1 = \rho_2 \tan \theta_2 \quad \text{Equation 2.3-10}$$

Figure 2.3-4 shows how current pathways in a layered earth differ from the pathways in a homogeneous (uniform) earth. Since the current pathways in a layered earth generally intersect media of different specific resistivities, an apparent resistivity may be calculated using Equation 2.3-9.

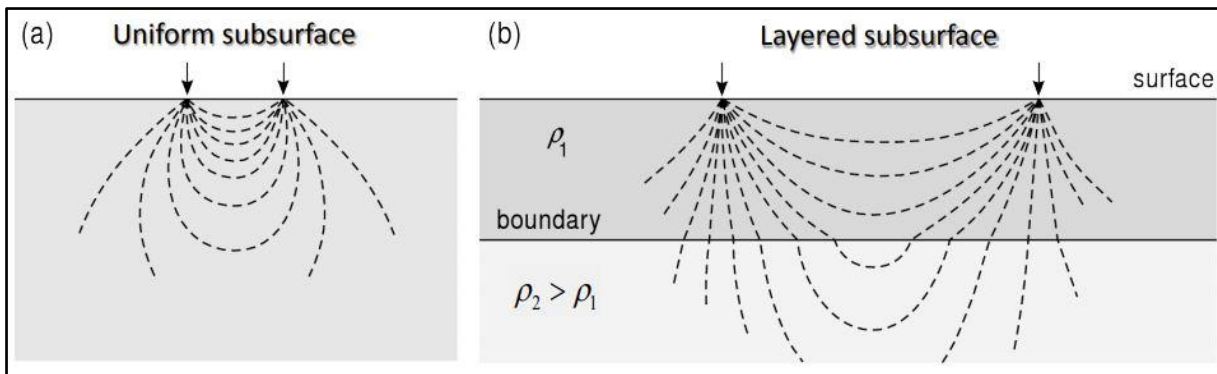


Figure 2.3-4: Refraction change distribution of electrical current

2.3.2.1.2 Electrode geometries

To ensure simplicity and practicality, linear geometries (arrays) are commonly used in electrical resistivity surveys. Each electrode geometry is characterised by advantages and disadvantages in terms of their abilities to resolve vertical and lateral changes in resistivities, their depths of exploration, their sensitivities to noise, and their coverage of the subsurface (Loke, 2000). The most commonly used electrode geometries are the Wenner, Schlumberger and Dipole-Dipole arrays. These geometries, as well as a few other common geometries, are shown in Figure 2.3-5.

When choosing which array to use in an electrical survey, the following factors (Loke, 2000) must be considered:

- The sensitivity of the array to vertical and horizontal changes in resistivity of the subsurface,
- The depth of the investigation,
- The horizontal data coverage, and,
- The signal strength produced by the array.

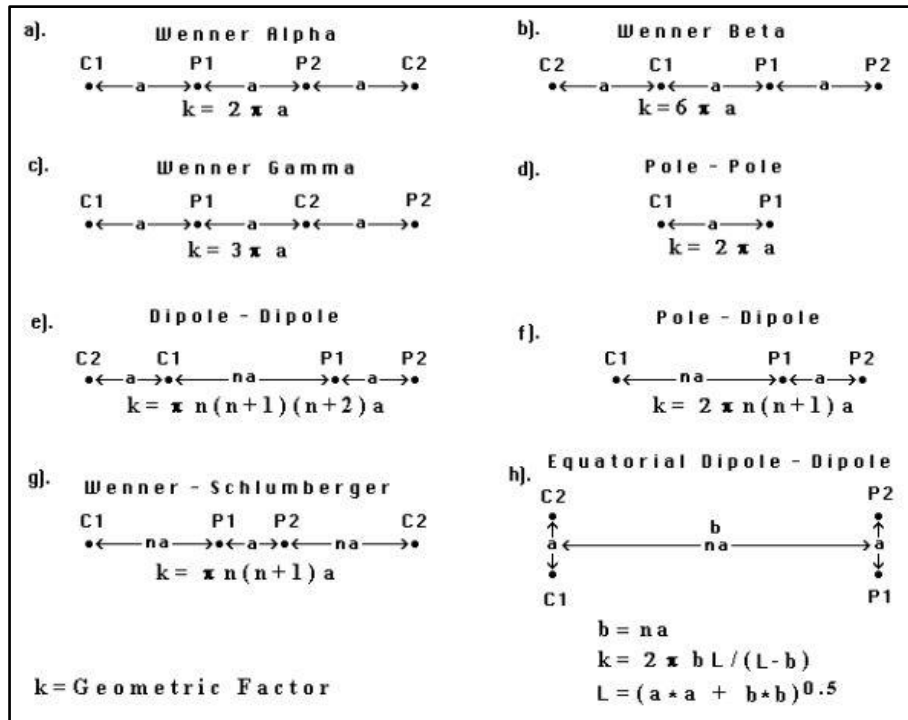


Figure 2.3-5: Common electrode geometries used in resistivity surveys and their geometric factors (k) (Loke, 1999)

The characteristics of a few common arrays are presented in Table 2.3-2 (Samouëlian *et al.*, 2005). It can be seen that the Wenner array is the most sensitive to horizontal structures, while its strong signal strength makes it suitable for surveys where background noise can be a problem. The Wenner array does not have a very deep sounding ability. By contrast, the dipole-dipole array is more suitable for finding vertical structures, and has a deep sounding ability, but is hampered by a very poor signal strength. The Wenner-Schlumberger array gives good horizontal as well as vertical resolution, while the Pole-Dipole array can be used if the number of electrodes is limited. If good horizontal coverage is needed with small electrode spacings, the Pole-Pole array can be used. Choosing which array to use will depend on the practical application thereof.

Table 2.3-2: Characteristics of different resistivity array configuration types (Samouëlian *et al.* 2005)

	Wenner	Wenner–Schlumberger	Dipole–dipole	Pole–pole	Pole–dipole
Sensitivity of the array horizontal structures	++++	++	+	++	++
Sensitivity of the array vertical structures	+	++	++++	++	+
Depth of investigation	+	++	+++	++++	+++
Horizontal data coverage	+	++	+++	++++	+++
Signal Strength	++++	+++	+	++++	++

The labels are classified from (+) to (++++), equivalent from poor sensitivity to high sensitivity for the different array configurations.

2.3.2.1.3 *Electrical resistivity surveys*

Electrical resistivity surveys can be used to explore the vertical changes in resistivity of a layered earth, or lateral changes in resistivity that might represent vertical structures such as faults, intrusions, cavities and lateral facies changes in geology.

Vertical electrical *sounding* (VES) investigates the vertical changes in the subsurface resistivities. During sounding, the centre point of the electrode array remains at a fixed position while the spacing between the current electrodes is incrementally increased to obtain information about deeper sections of the subsurface. *Profiling* is done by keeping the electrode spacing constant and moving the centre point of the array along a line to measure the apparent resistivity changes at a specific depth. Both sounding and profiling rely upon one-dimensional interpretations of the acquired apparent resistivity data. However, by doing repeated profiles using different electrode spacings, information on both lateral and vertical changes in the subsurface resistivity may be obtained (Samouëlian *et al.*, 2005). This is illustrated in Figure 2.3-6 where repeated profiles allow a two-dimensional (2D) section of the apparent resistivities to be recorded. This 2D section is referred to as a pseudo-section since only *apparent* (as opposed to *true*) resistivities are recorded and since the depths at which the recorded apparent resistivity data are plotted is chosen using some convention (typically half the distance between the current electrodes). The pseudo-sections may be displayed as contours to give a visual representation of the lateral and vertical changes in the apparent resistivities (Samouëlian *et al.*, 2005).

Two-dimensional (2D) electrical resistivity tomography (ERT) can be thought of as resistivity surveys during which both sounding and profiling data are recorded to provide information on the subsurface resistivities in 2D-sections underlying the survey lines. This technique allows rapid recording of resistivity data at different positions and depths along the survey line. ERT systems usually employ multi-core cables that connect to numerous electrodes at constant spacing (Loke, 2000). The system selects which electrodes should act as current electrodes and potential electrodes during a particular measurement of the subsurface resistivity.

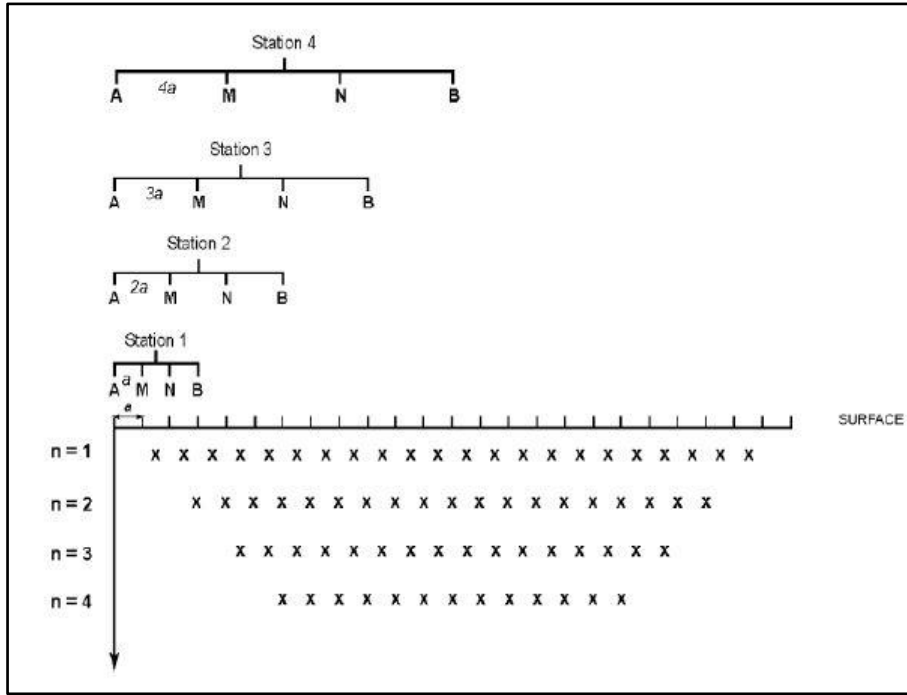


Figure 2.3-6: The procession of resistivity measurements along different profiles at different depths to obtain a 2D pseudo-section of the earth's resistivities

2.3.2.1.4 Data processing and interpretation

The aim of a resistivity survey is to gain information on the subsurface resistivity distribution, and to relate changes in the subsurface resistivities to the underground geological conditions. Interpretation of the resistivity data is therefore always done by considering the possible geological causes of the observed changes in resistivity.

Since only apparent resistivities are recorded during resistivity surveys, and since the resistivities are usually attributed to the subsurface conditions at some (pseudo-)depth conventionally chosen as some factor of the distance between the current electrodes, the recorded data need to be processed to yield a model of the true subsurface resistivity distribution. This is done through a mathematical process called *inversion*. During inversion, a model of the subsurface resistivity distribution is iteratively adjusted in such a way that the difference between the measured apparent resistivities and the calculated apparent resistivities corresponding to the model is minimised. The iterative adjustments are continued until the difference in the observed and modelled resistivity values attain an acceptable low value. The algorithm used during inversion is shown in Figure 2.3-7. The inverted resistivity models obtained from inverting the recorded apparent resistivity data are then used during the interpretation process (Fourie, 2010).

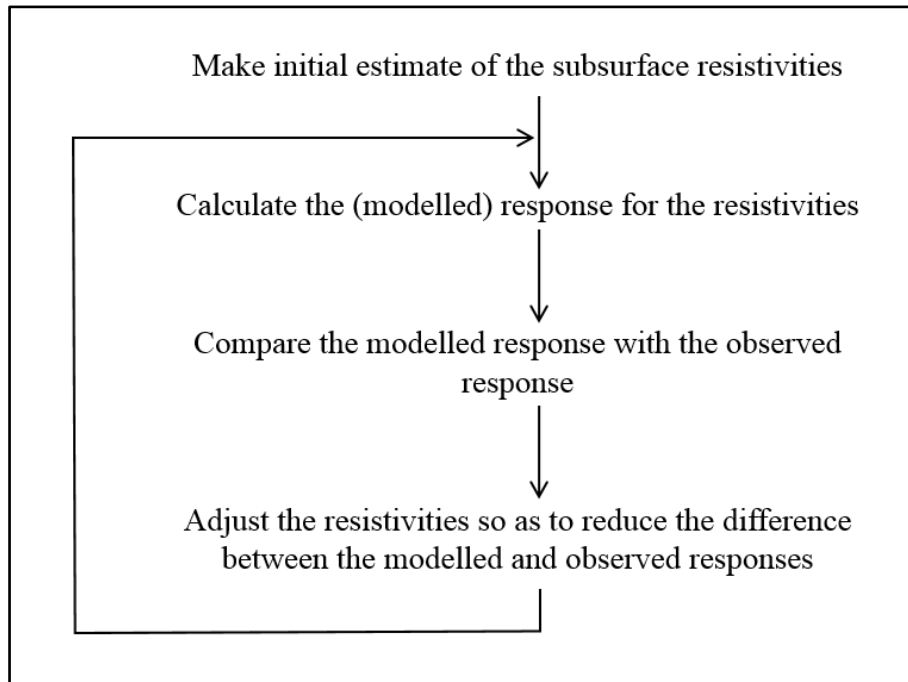


Figure 2.3-7: Algorithm for the inversion of apparent resistivity data

The number of iterations used to obtain a model depends on the quality of the data recorded. Data of good quality with a small error content can be modelled with a high number of iterations to obtain a well-defined inverse model. However, when using too many iterations on data of poor quality, the inversion algorithm will tend to model the errors in the data and will therefore introduce artefacts to the inverse model.

An example the inversion of 2D ERT data is shown in Figure 2.3-8. The topmost image represents the recorded pseudo-section of apparent resistivities, the middle image is the pseudo-section calculated for the modelled resistivity section shown as the bottom image. It is the modelled resistivity section that represents the changes in the subsurface resistivities and is used during interpretation. An example of such an interpretation is shown in Figure 2.3-9. Prominent changes in the modelled subsurface resistivities are related to possible geological or geohydrological causes of these changes.

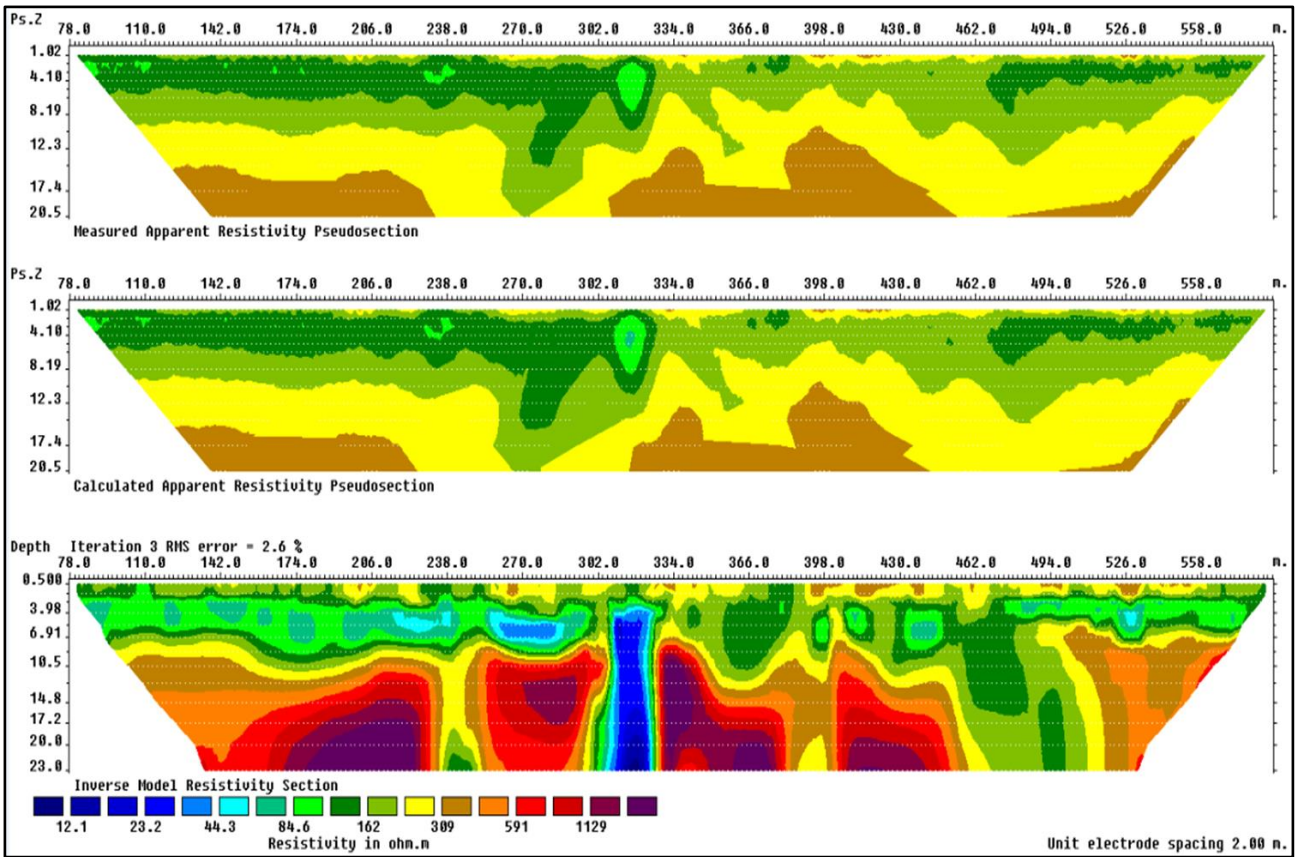


Figure 2.3-8: Example of the inversion of 2D ERT data

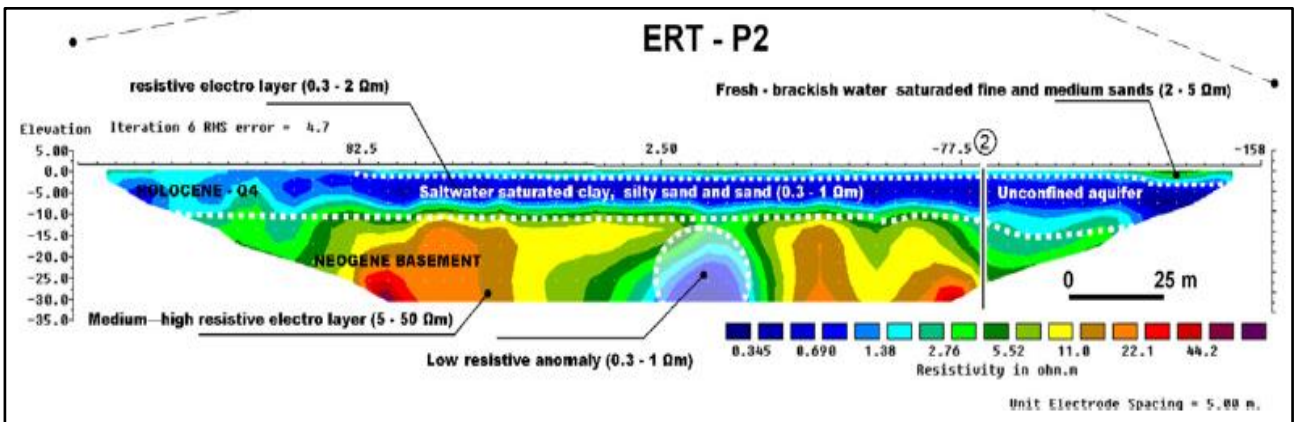


Figure 2.3-9: Example of conceptualisation of geology using ERT method

2.3.2.1.5 The influence of inhomogeneity and anisotropy on the interpretation of resistivity data

When interpreting resistivity data, the inhomogeneity and anisotropy of the earth must be taken into account. In such media the flow paths of electrical currents are distorted due the different subsurface resistivities encountered (Figure 2.3-3). To take such deviations into account, factors such as anisotropy, transverse and longitudinal components of electrical flow, and the possibility of unique solutions must be considered.

The Dar Zarrowk parameters

The Dar Zarrowk parameters (Maillet, 1947) are resistivity parameters that deal with layered anisotropic materials. Since the earth often resembles a layered medium (especially in sedimentary basins) it can often be approximated as consisting of a number of horizontal layers, each with its own thickness and resistivity. The goal of a resistivity surveys is to determine these thicknesses and resistivities.

Figure 2.3-10 shows a hypothetical cut through the earth intersecting layers of different thickness (h_i) and resistivities (ρ_i). With the application of an electrical current to the earth, one can see from the theoretical equipotential lines (Figure 2.3-1), that the current penetrates the layers from top to bottom (transversely), as well as along the layers (longitudinally). The flow of the electrical current then has a component that can be compared to flow through an electrical circuit of resistors in series (T), and a component that flow through the resistors in parallel (S) (Salem, 1999). In a series circuit, the current through each of the components is the same, and the voltage across the circuit is the sum of the voltages across each component. In a parallel circuit, the voltage across each of the components is the same, and the total current is the sum of the currents through each component. With this in mind, the transverse resistance of the layered column may be defined as:

$$T = \sum_{i=1} h_i \rho_i \quad [\Omega m^2] \quad \text{Equation 2.3-11}$$

while the longitudinal conductance may be defined as:

$$S = \sum_{i=1} h_i / \rho_i \quad [S] \quad \text{Equation 2.3-12}$$

T and S are known as the Dar Zarrowk parameters. The Dar Zarrowk parameters are of particular importance when succeeding layers have similar geo-electrical properties or are too thin to have a noticeable effect on the apparent resistivity measured. Multiple layers may manifest themselves as a single geo-electrical unit. The properties of these compound layers can be investigated through the Dar Zarrowk parameters (Zohdy, 1974).

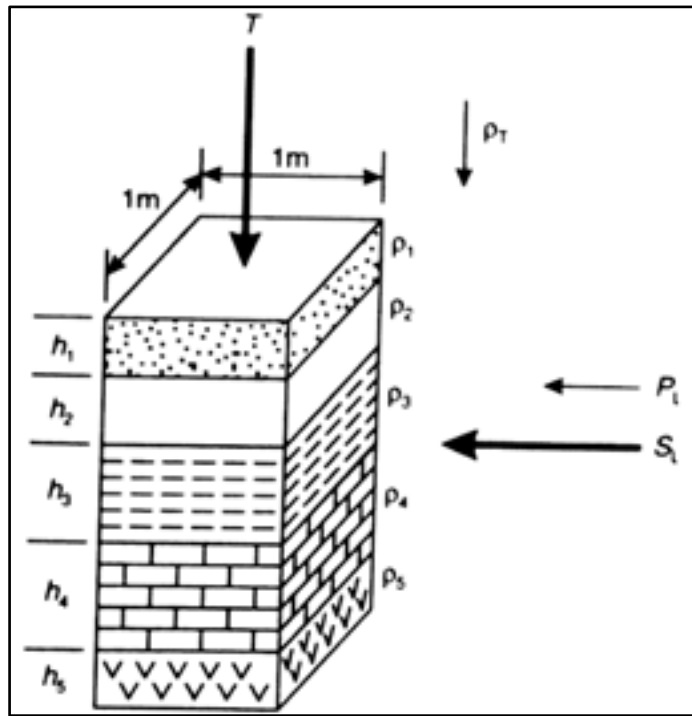


Figure 2.3-10: A modelled layered earth

Anisotropy

Anisotropy is described as the difference of resistivity in the transverse and longitudinal directions within a medium (Van Zijl, 1977). The coefficient of anisotropy (λ) may be defined as:

$$\lambda = \sqrt{\rho_t / \rho_l}$$

where ρ_t is the average transverse resistivity and ρ_l is the average longitudinal resistivity. The coefficient of anisotropy is always greater than unity, with unity representing completely isotropic conditions. In especially layered sediments, the resistivity perpendicular to the layering is usually greater than the resistivity parallel to the layering (Negi and Saraf, 1989; Keller and Frischknecht, 1996).

Equivalence and suppression

The apparent resistivity curve recorded during sounding can be interpreted by different resistivity models, using different pairs of thickness and resistivity. More than one model may give an acceptable fit to the data (Van Zijl, 1977). This gives rise to the principle of equivalence where the thickness and resistivity cannot be derived independently, but the Dar Zarrouk parameters can be determined accurately.

The principle of suppression is when three and more layers are present and their resistivities are descending or ascending in depth, the middle layer might not be identified, especially when it does not have enough contrast to the surrounding layers. Also, the thin layers of small contrast with respect

to background, will be suppressed and not be detected in an electrical sounding. While a thin layer of greater resistivity contrast might be detectable, the principle of equivalence prohibits the determination of a unique solution to boundary depths and resistivity.

2.3.2.2 Electromagnetic Methods

The electromagnetic induction method (EM), is an indirect electrical method that does not need to have direct contact with the ground. This lends itself to extend to even aerial applications. Instruments are designed with a fixed geometry, enabling surveys to be done with great speed. The instruments can measure apparent conductivity of the earth directly (Fitzpatrick *et al.*, 2003). The EM method includes both frequency (frequency-domain) and time (time-domain) based methods. The time-domain method measures the time decay of the induced electromagnetic field, while the frequency-domain depends on the alternating electromagnetic field created by a sinusoidal alternating current of a specific frequency. The frequency-domain method (in particular the Slingram array) is the preferred method in soil and shallow depth investigations (McNeill, 1980b), and the following discussion will focus on this method.

2.3.2.2.1 *Basic principles*

Definition: Electrical conductivity (measured in S/m) is the ease with which a current flow through a medium when an electrical potential difference is applied.

The EM method is based on two fundamental principles:

- a) Faraday's Law of magnetic induction which states that a changing magnetic field will give rise to a circulating electric field, and,
- b) Ampere's Law which states that the electrical current flow causes a circulating magnetic field.

These two equations were incorporated into the famous set of Maxwell equations which are fundamental to the understanding of the propagation of electromagnetic waves (Keller and Frischknecht, 1996). Consider the instrument geometry as in Figure 2.3-11 consisting of a small transmitter loop (T_x), carrying an alternating current (varying sinusoidally in time), and a receiver loop (R_x), both of wire coil construction. The alternating current from the transmitter produces a time-varying primary magnetic field (H_p). The primary magnetic field interacts with a conductive body and induces time-varying electrical eddy currents in this body which in turn produce a secondary magnetic field (H_s). The receiver senses the sum of the primary and the secondary magnetic fields. The secondary magnetic field is a function of the inter-coil spacing (s), the operating frequency ($\omega = 2\pi f$), and the conductivity of the conducting body (σ) (McNeill, 1980b).

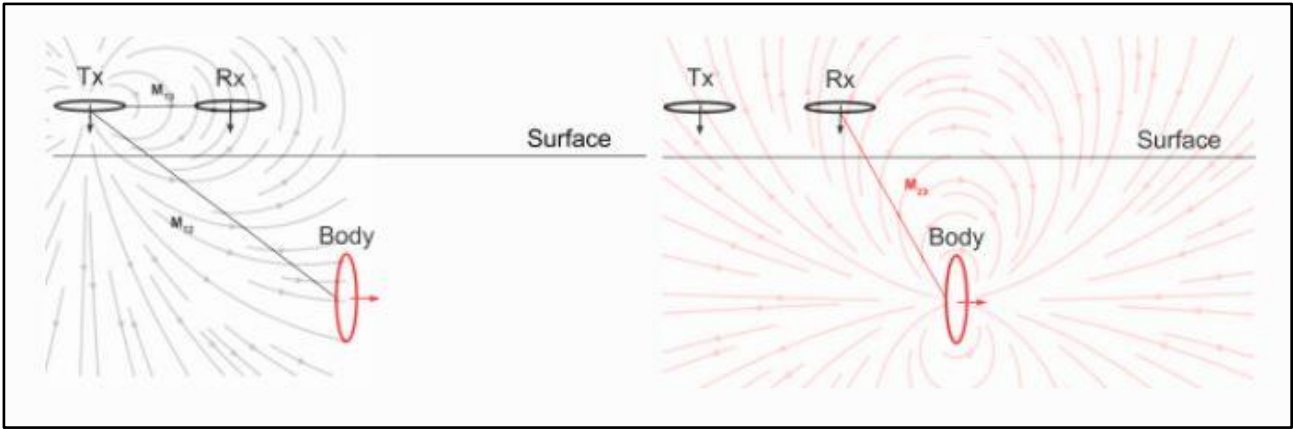


Figure 2.3-11: The primary and secondary magnetic fields generated by a time varying electrical current

A phase shift usually exists between the primary and secondary magnetic fields. The degree to which the secondary magnetic field is phase-shifted with respect to the primary field is dependent on the conductivity of the conductive body. Different frequency-domain EM systems use different methods to extract conductivity information from the measured phase shift between the primary and secondary magnetic fields.

The system generally used for shallow earth investigations (the Geonics EM34-3 system), operates at low induction numbers, that is, the inter-coil-separations used during surveying are much smaller than the skin depths of the electromagnetic waves employed by the system (McNeill, 1980b). The skin depth is a measure of how deep an electromagnetic wave can penetrate a conductive medium. When operating at low induction numbers, the ratio of the primary and secondary electromagnetic fields is related through factors expressed in the following equation:

$$\frac{H_s}{H_p} = \frac{i\omega\mu\sigma(s)^2}{4} \tag{Equation 2.3-13}$$

where μ is the permeability of free space, s is the inter-coil distance, and $i (= \sqrt{-1})$ is the imaginary number showing that the out-of-phase component of the secondary electromagnetic field is considered in Equation 2.3-13. Thus, the apparent ground conductivity (σ_a) can be calculated from the ratio of the secondary to the primary electromagnetic fields:

$$\sigma_a = \frac{4}{\omega\mu(s)^2} \frac{H_s}{H_p} \tag{Equation 2.3-14}$$

The geometry of the survey (one of the design constraints), is a major constraint on the depth of surveying. The claimed depth of penetration is approximately twice the inter-coil spacing (s) and this assumption is only valid when the coil separation is smaller than skin depth ($s \ll \delta$).

2.3.2.2.2 Electromagnetic surveys

Apart from the coil separation, the coil orientation also has an influence on the survey depth. If kept in mind that the electromagnetic fluxes produced are vectors with a specific orientation (Figure 2.3-11), the orientation of the respective dipoles will lead to different coupling of the primary magnetic fields with subsurface conductive bodies. The EM34-3 system uses both horizontal dipole and vertical dipole orientations during surveying. In the vertical dipole (horizontal co-planar) mode, the instruments are relatively sensitive to the inter-coil spacing, but less so in the horizontal dipole (vertical co-planar) mode (McNeill, 1980b).

Figure 2.3-12 shows the sensitivities of the different dipole modes as a function of the relative depth z (the depth divided by the inter-coil spacing). The vertical dipole configuration has the lowest sensitivity at the surface and increases with depth to maximum at about 0.4 inter-coil spacings, after which the sensitivity decreases with depth. The horizontal dipole configuration has the maximum sensitivity at the surface with decreasing sensitivity with depth. If the effective survey depth is taken at the depth at which 75% of the secondary electromagnetic signal is generated, the effective survey depth of the horizontal dipole configuration is about half that of the vertical configuration. This difference between the two modes can then be used to distinguish a layered earth by measuring and comparing the differences in apparent conductivities between different depths.

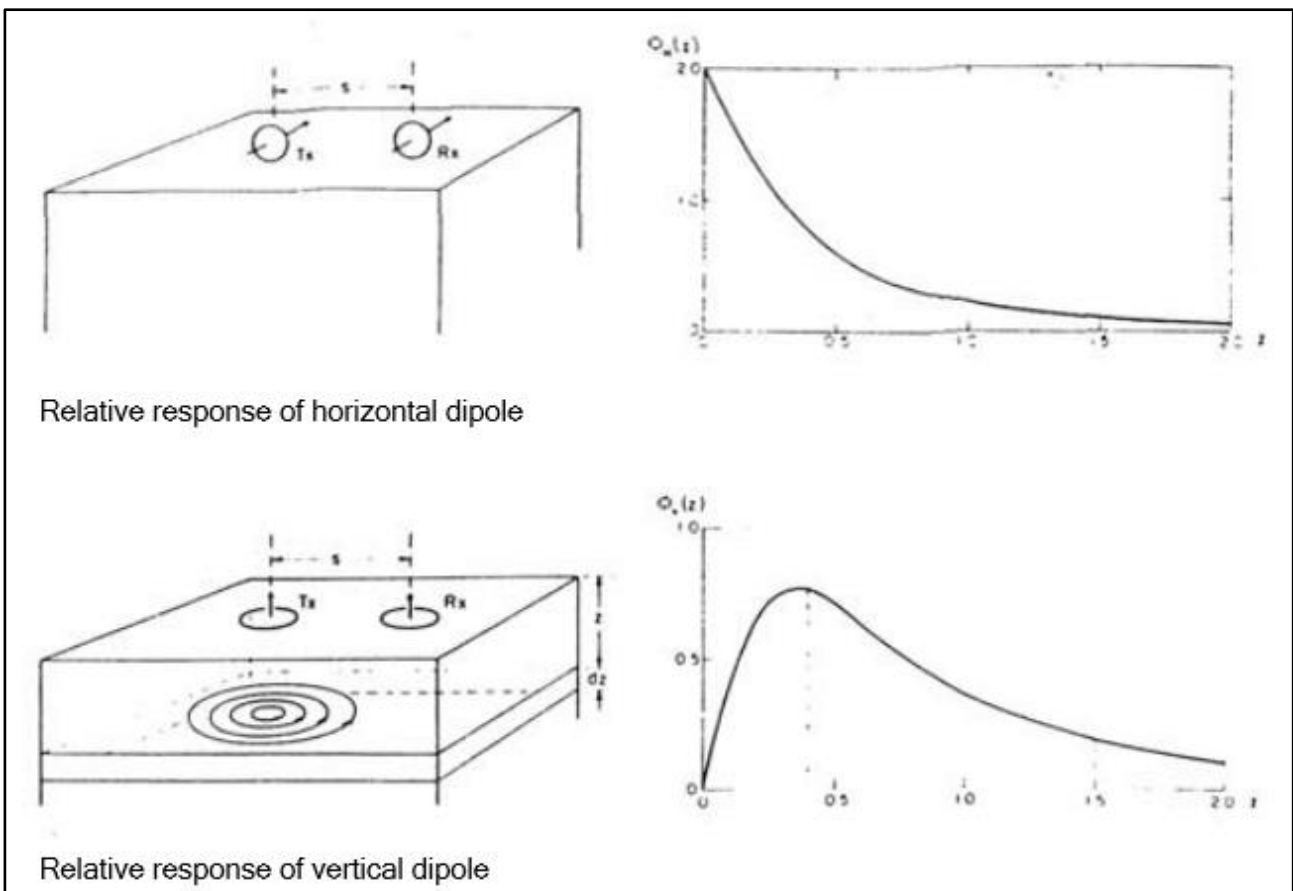


Figure 2.3-12: Relative response versus depth of horizontal and vertical co-planar orientations (after McNeill, 1980)

The detection pattern over a thin conductive body can be explained using the vertical dipole mode as example (Herman, 2001) (Figure 2.3-13). The survey direction is from left to right. At point A, the receiver is directly above the conductive body. The secondary field lines are orientated parallel to the receiver and very poor to no conductive coupling to the receiver coil is achieved. The apparent conductivity is zero.

At point B, the conductive body is halfway between the transmitter and receiver coils, and optimum coupling with the receiver coil is reached. Notice that the secondary field lines are opposite to the primary field lines, thus a negative signal is measured. When approaching or leaving the conductive body, the secondary field lines are complementary to the primary, thus a positive signal is measured. At point C the transmitter is directly above the conductive body, no primary field lines are crossing the conductive body, thus no secondary field is generated. The apparent conductivity measures zero again.

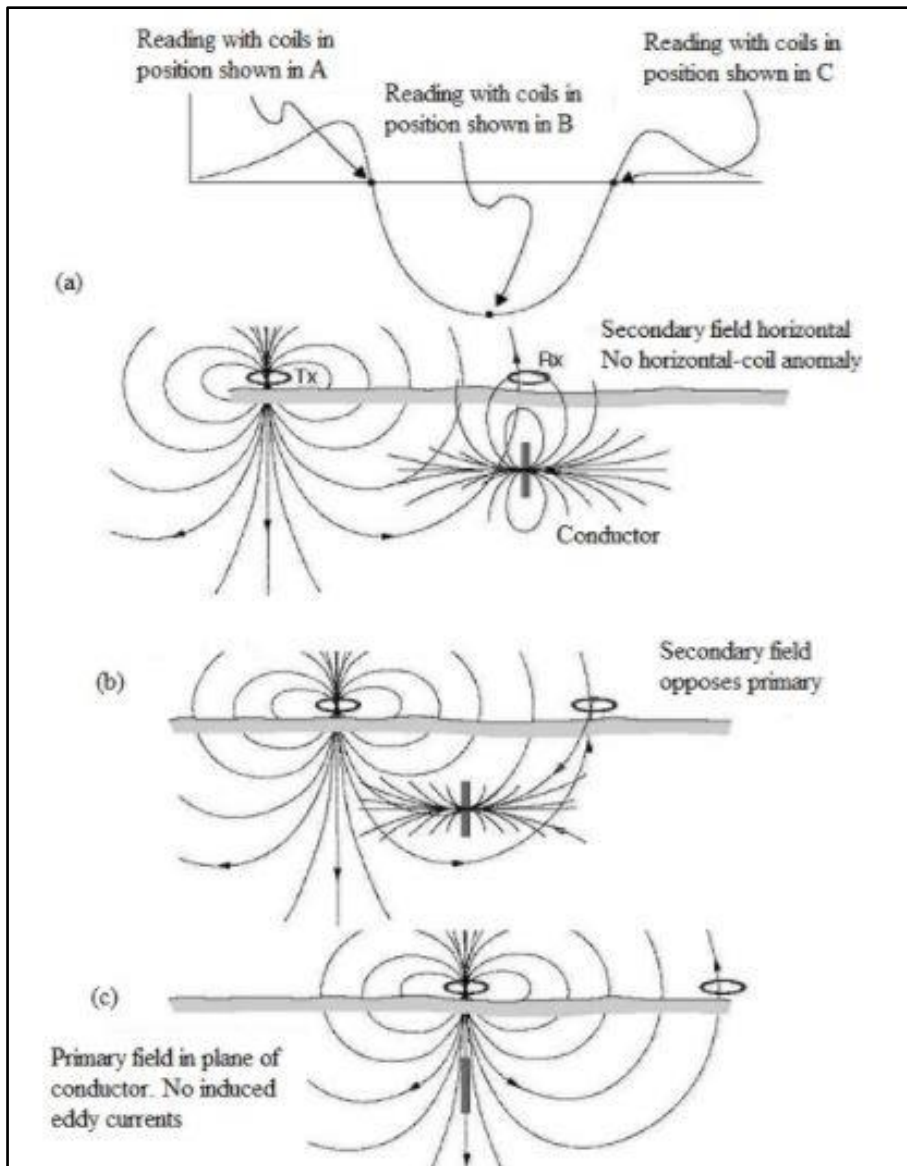


Figure 2.3-13: Detection pattern over a thin conductive body)

The EM method is mostly used in conductivity mapping in a profiling mode. This is most suitable for applications such as mapping groundwater contamination and soil and groundwater salinity. For detecting layering in the subsurface, the inter-coil spacing can be increased for progressive deeper detection, or the differences between the horizontal and vertical dipole penetration can be used. Because of the predetermined coil spacing configuration of the instruments, only a maximum of two layers can be detected with only the depth of the first layer calculated (McNeill, 1980b).

2.3.2.3 The Application of Geophysical Methods in Agriculture

The use of geophysical methods in agriculture was pioneered as early as the 1930s, where the moisture content of soils was investigated through the resistivity method. The apparent soil conductivity (EC_a) was measured, and temporal and spatial variations linked to changes in water content. During the 1960s to 70s, this method was also applied to determine salinity of soils, still measuring the EC_a . Ground penetrating radar (GPR) appeared in the 1970s and 80s, and is used to investigate soil structure and stratification. By the 1990s, spatial variations in soil properties were evaluated by EC_a mapping through geo-electric (resistivity, ER) and electromagnetic (EM) techniques. This discussion will concentrate on the application of the geo-electric and electromagnetic methods.

With the introduction of precision farming where the application of fertilizers, the plant density during planting, and eventually the yield of the crop were controlled and correlated with soil variability, the application of geophysical methods was refined to aid in the determination of spatial and temporal changes in soil parameters (Samouëlian *et al.*, 2005). The scale of these geophysical investigations may range from district-scale dimensions, down to field-scale dimensions, and even to sub-metre dimensions.

Agricultural geophysical methods are typically applied to:

- a) Soil suitability mapping,
- b) Soil water content mapping, including salinity mapping,
- c) Soil nutrient monitoring after fertilizer applications,
- d) Determination of changes in soil texture and structure such as clay-pan depths and compaction, and,
- e) Soil drainage class mapping

The use of bulk soil- or apparent electrical conductivity mapping in agriculture identifies soil spatial variability. This is used as a tool to identify sampling sites and compare results to similar soil characteristics within similar EC boundaries. It also characterises field soil variability in respect to different model soil parameters. In using EC_a in parameter map analyses, the nature (EC nature) of

soil variability can be inferred, but the cause (salinization, texture, structure, CEC, etc.) of such soil variability must be investigated further.

The causes of EC_a , such as salinity are directly related to EC_a of soil solution. In field surveys, EC measurements of soil solution extracts are time and labour intensive and not practical for characterisation of spatial variability of soil salinity at field extents and larger. Soil electrical resistivity (ER) or conductivity (EM) mapping is the simplest and most rapid methods of identifying the nature of soil variability (Rhoades *et al.*, 1976).

2.4 THE RELATIONSHIP BETWEEN PHYSICAL, GEOPHYSICAL AND GEOHYDROLOGICAL PROPERTIES OF THE EARTH

Electrical resistivity is influenced by many earth characteristics, including the texture (particle size, mineralogy), porosity (pore size, connectivity), the water content, electrical resistivity of the water (solute concentration) and temperature. These characteristics may also vary with depth (stratification) and lateral distribution, adding a third dimension to any earth survey (Grandjean *et al.*, 2009). Soil characteristics may be stable, such as texture and porosity, or might vary with time as in the case of water content, or the solute concentration of water, and temperature.

Archie's Law is the definitive work that describes the relationship between the electrical conductivity and the physical properties of porous earth materials. Archie's Law is constantly being adapted to accommodate more complicated relationships such as electrical conductive mineralogy.

In this section, the relationship between the physical and electrical characteristics will be discussed. Attention will also be given to adaptations of Archie's Law to accommodate unsaturated conditions and mineralogical conductivity. The geohydrological parameters are also directly linked to the physical characteristics through the property of porosity. The estimation of the geohydrological parameters using geoelectrical methods, will also be explained through relevant case studies.

2.4.1 Physical and Geophysical Properties of the Earth and Archie's Law

Archie's Law is empirically derived to describe ion flow through clean consolidated sands of varying intergranular porosity. Electrical conduction is assumed not to be present in the sand grains, only in the water. Porosity is the primary physical property of the earth that determine the ease of electrical conductivity (Archie (1942) in Coetsee, 1994)).

2.4.1.1 Porosity

With shallow geoelectrical investigations, it is assumed that the earth is porous, that the rock matrix is acting as an insulator, and that the electrical current is conducted through the water and moisture in the pores (Niwas *et al.*, 2011; Keller and Frischknecht, 1996). The relation between the porosity

and the electrical property is expressed by Archie's Law, which for a medium without clay, can be written as:

$$FF = \frac{\rho}{\rho_w} = a\phi^{-m} \quad \text{Equation 2.4-1}$$

Where FF (formation factor) is the ratio between the resistivity of the formation (ρ) and the resistivity of the pore water (ρ_w). The coefficient of saturation (a), and the cementation factor (m), are constants of the specific formation and ϕ is the porosity.

The cementation factor (m) describes the structure of the pore spaces in rocks. This has mainly to do with the tortuosity of the flow path and the interconnection of pores within the rock. For low values of m , the rock shows poor sorting and good bonding, while higher values of m , are associated with good sorting and poor bonding. If the porosity in a rock is represented only by cracks and joints, a minimum theoretical value of 1 (very effective connection of pores) can be assumed. All other forms of porosity are less effective and $m > 1$. Thus, the resistivity of a medium increases as the connectivity of the conductive phase decreases. Values of m for unconsolidated sands are about 1.3 and may rise to values of 2 for other sedimentary rocks (Doveton, 1986 in Niwas *et al.*, 2011; Kazakis *et al.*, 2016).

Factors affecting m , are (Ransom, 1984 in Coetsee, 1994):

- a) Geometry.
 - i) Ratio of the surface area to the volume of the grains.
 - ii) Sphericity of the grains.
 - iii) Degree of cementation.
 - iv) Packing of the grains.
 - i) Uniformity in the size of the grains (sorting).
- b) Anisotropy.
- c) The degree of electrical insulation through cementation or bonding.
- d) The prevalence of open joints.
- e) As it is not always practical to determine a and m , values of 1 and 2 may be assumed for an approximation in the normal porosity ranges of 10 - 30%. This is because the impact of the uncertainty of the values of a and m has less an effect than the value of the resistivity of the water in the pores (Keller and Frischknecht, 1996).

2.4.1.2 Soil texture

The texture of the soil affects the conductivity because of the surface area available to electrical charges. Thus, the electrical conductivity in soils with a high clay content will be much higher, than

those of a coarse-grained sandy soil (Samouëlian *et al.*, 2005). If the mineralogy of soils is taken into account, the silt and sandy fractions consist mainly of feldspar and quartz, but the clay fraction mainly of iron-manganese oxides and clay minerals such as smectites, illites, kaolinites and chlorites. The difference between the electrical resistivity of clay (2 Ohm.m to 100 Ohm.m) and sand (1 000 Ohm.m) is quite high (Samouëlian *et al.*, 2005). The geophysical parameters are therefore very strongly influenced by the clay fraction, making the clay fraction the most important characteristic of the soil texture (Grandjean *et al.*, 2009). The Waxman-Smits equation are commonly used to allow for the added conductance of clay in resistivity surveys (Waxman and Smits, 1968), especially where the clay conductivity over rides the pore water conductivity. The equation is:

$$FF = \frac{\rho}{\rho_w + \rho_\chi} \quad \text{Equation 2.4-2}$$

where χ = the resistivity added by the exchangeable cations. The coefficient of saturation (a) (also called the lithology constant or tortuosity coefficient) in Archie's Law, is meant to correct for variation in compaction, pore structure and grain size between different lithologies. Low values of a are representative of rocks with intergranular porosity, while high values of a might reflect the added advantage of cracks and joints adding to the porosity of the rocks. Typically values of a range between 0.6 to 2.3 (Keller and Frischknecht, 1996). Factors affecting a include:

- a) The surface conductivity and ionic mobility of the water that adheres to the matrix surface.
 - i) Cation exchange capacity (CEC)
 - ii) The amount of water adsorbed onto clay particles.
- b) The salt load of the water in the formation.
- c) The presence and distribution of electrically conductive minerals in the formation.
- d) The influence of texture and presence of clays on the resistivity measured, may be under certain circumstances negated by the water content and salt load (Rhoades *et al.*, 1990; Keller and Frischknecht, 1996; Niwas and de Lima, 2003).

2.4.1.3 Water content and salinity

The water contained in porous spaces is one of the main drivers of electrical conductivity in soils, as ions are displaced by the introduction of an electrical current. Thus, the electrical propagation depends on the saturation of the soil, as well as the concentration of dissolved ions and cations in the water (Grandjean *et al.*, 2009).

The distribution of the water content in the soil, also varies in depth till the level of full saturation is reached (Bear, 1979; McNeill, 1980a after Meyboom, 1967) described four stages of saturation (Figure 2.4-1):

- i) The first is the pendular zone. In this zone the water is attached by surface tension only, and does not form a continuous film around the grains. The pore spaces are mainly filled with water vapour. Resistivities measured are very high.
- ii) The funicular zone contains more water and the water starts to cover the grains. Although empty pore spaces still exist, a continuous moisture path in the soil starts to form. Because of the continuous conduit provided by the moisture film, resistivities begin to fall.
- iii) The capillary fringe, is where the water rise above the water table by means of adhesion. This action is entirely dependent on pore size and type. This zone may extend several metres, and the gradual transtion thereof makes it difficult to pinpoint the waterlevel of the saturated zone through electrical methods (Keller and Frischknecht, 1996)
- iv) The saturated zone is fully saturated by water under hydrostatic pressure and are defined by a static water level. Electrical resistivities measured are those mainly of the interstitial pore fluid.

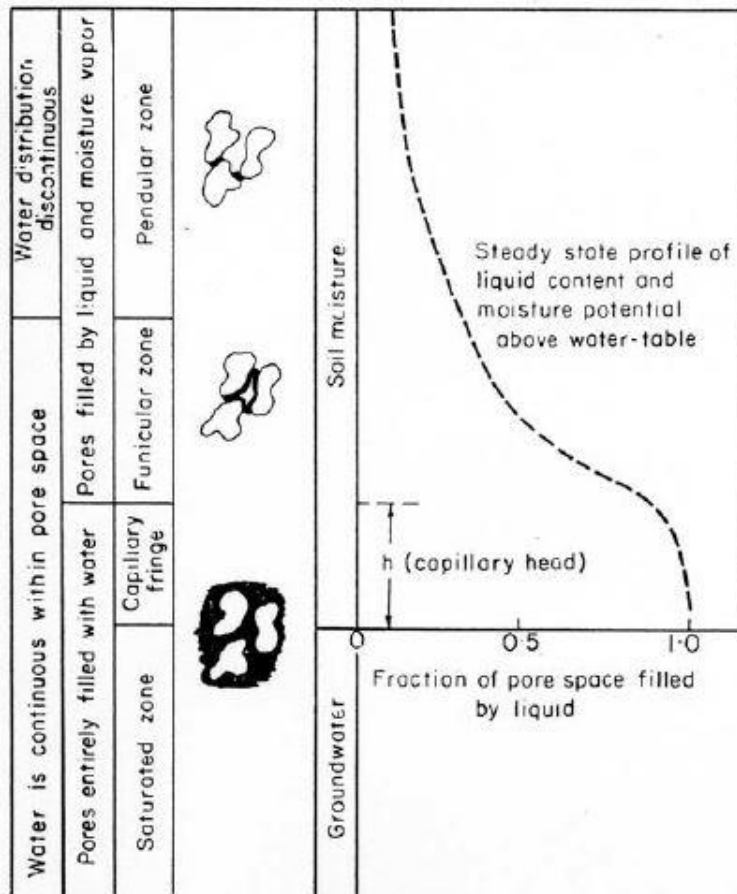


Figure 2.4-1: Water occurrence in soils (Meyboom, 1967)

When pores are partly filled with air or some other isolating medium such as petroleum, Archie's Law can still be applied. The water saturation (S) is expressed as a function of the formation factor (F), the resistivity of the formation (ρ), and the resistivity of the water (ρ_w) as follows:

$$S^n = F \frac{\rho_w}{\rho} \quad \text{Equation 2.4-3}$$

where n is a parameter related to the degree of saturation. When combined with Archie's Law (Equation 2.4-1), the direct relation with porosity is obtained (Samouëlian *et al.*, 2005):

$$S^n = \frac{a \rho_w}{\rho \phi^m} \quad \text{Equation 2.4-4}$$

The value of n was determined to approximately 2 by Archie. Equation 2.4-4 has been found to be representative of the water content of coarse-grained soils and rocks (Samouëlian *et al.*, 2005).

As the conductivity depends on the total concentration of ions and anions dissolved in the water, as well as their mobilities, the electrical conductivity of a solution can be calculated. Since a variety of salts is present (Section 2.2.2), it is easier to use the concept of equivalent salinity in calculating conductivity. Equivalent salinity is the salinity of a sodium chloride solution that equal the conductivity of a compound saline solution under investigation (Keller and Frischknecht, 1996). This has the advantage that calculations and comparisons can be simplified. The equation used is:

$$\sigma = [C_1 M_1 + C_2 M_2 + \dots]$$

where C_i is the number of gram equivalent weights of the i^{th} ion per 10^6cm^3 of water, M_i is the mobility of the i^{th} ion in meters per second per Volt per meter, and σ is the electrical conductivity (McNeill, 1980a).

2.4.1.4 Temperature

Although temperature is not a physical attribute of the earth, it has an influence on the viscosity of fluids, as well as on ion agitation. This temperature influence has a direct effect on the electrical conductivity of a fluid as resistivity decreases as temperature increases. Temperature varies with seasons, as well as during the day, but the biggest influences occur on a seasonal scale. The influence is quantified at around 2% per degree Celcius and are usually corrected to a standard of 25°C (Grandjean *et al.*, 2009). Temperature correction can however be neglected if surveys are done in the same season, at the same time of day and over a short period of time (Samouëlian *et al.*, 2005). However, it is recommended that temperature fluctuations be considered, and that data be corrected in accordance.

2.4.2 Adaptations of Archie's Law to Unsaturated Conditions and Conductive Minerals

2.4.2.1 An application of Archie's Law on soils with clay content

As the influence of clay on the conductance of an electrical current cannot be ignored, Rhoades *et al.* (1976) presented the following equation to describe the influence of the solid matrix on the bulk resistivity:

$$\frac{1}{\rho} = \frac{1}{\rho_w}(a\theta^2 + b\theta) + \frac{1}{\rho_s} \quad \text{Equation 2.4-5}$$

where ρ_s and ρ_w are the solid matrix and pore water resistivity, a and b are coefficients that depend on the solid phase characteristics representing texture and mineralogy, and θ is the volumetric water content (cm^3/cm^3). The degree of water saturation of the soil and the salinity of the water content interacts to influence the electrical conductivity of a soil. The higher the volumetric water content and the higher the ionic load of the soil water, the higher the electrical conductivity will be. To standardise the measurement of soil salinity, it is typically measured at soil water saturation point.

Soil conductivity and the different components that contribute are best presented in the soil EC model in Figure 2.4-2. In this model, electrical current flow may follow two distinct paths through a saturated porous medium, namely: a) the solid-liquid pathway where electrical current flows both through the solid grains and the pore fluid in contact with the grains, and b) the liquid pathway where electrical current flow is restricted to the fluid component (refer to Figure 2.4-2). An empirical relationship was established by (Rhoades *et al.*, 1976) to describe the bulk electrical conductivity (EC_a) in terms of the electrical conductivities of the fluid component (EC_w) and solid component (EC_s):

$$EC_a = \left[\frac{(\theta_s + 0.64\theta_w)^2 EC_w EC_s}{(0.64\theta_w) EC_s + (\theta_s) EC_w} \right] + (0.36\theta_w) EC_w \quad \text{Equation 2.4-6}$$

where θ_s and θ_w are the volumetric soil content and water content, respectively.

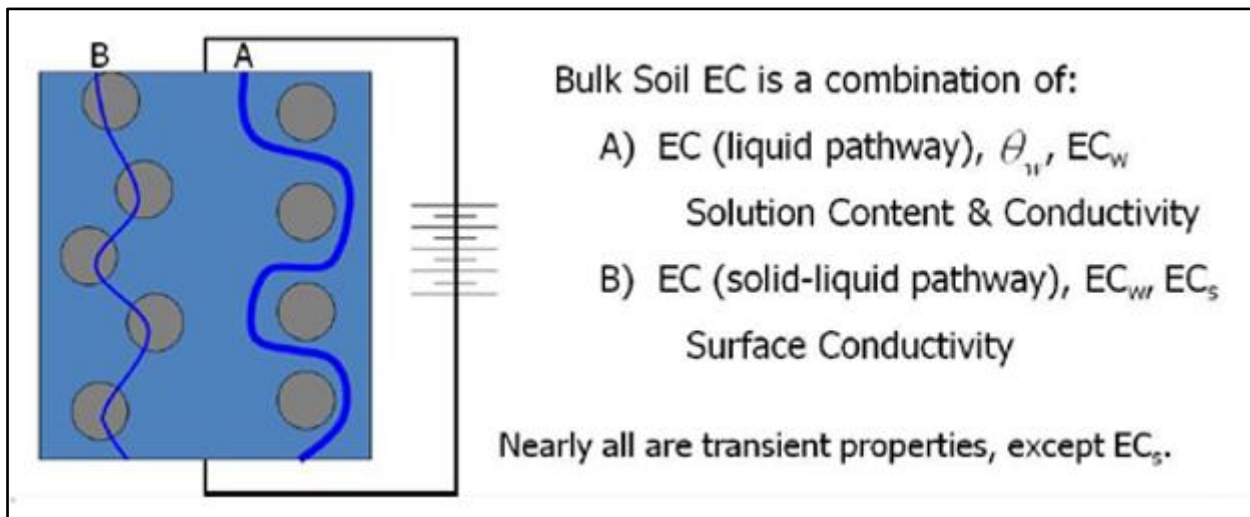


Figure 2.4-2: Conceptual Bulk soil (EC_a) model taking into account solid and liquid conductivities (Rhoades *et al.*, 1976)

2.4.3 A Modified Archie's Law for Two Conducting Phases (Glover *et al.*, 2000)

Archie's Law relies on the assumption that only one conductive phase exists in a non-conductive matrix. This assumption is only valid for the uppermost crust of the earth where low temperatures and pressures exist and for clean rock formations with low fractions of conductive clay minerals. As soon as a second conducting phase adds to the observed conductivity, this conductivity should be the sum of the respective conductive phases.

In terms of conductivity ($\sigma = \frac{1}{\rho}$), Archie's law can be expressed as:

$$\sigma_{eff} = C \sigma_2 \chi_2^m \quad \text{Equation 2.4-7}$$

where C is a constant relating to the medium, σ_2 is the conductivity of the conducting phase, χ_2 is the volume fraction of the conducting phase and m is the electrical connectivity of the conducting phase. The value of C can be taken as approximately unity because of a suspected close relationship with χ_2 (Glover *et al.*, 2000). Therefore, for two conducting phases with conductivities of σ_1 and σ_2 , and volume fractions of χ_1 and χ_2 respectively, the effective conductivity can be expressed as:

$$\sigma_{eff} = \sigma_1 \chi_1^p + \sigma_2 \chi_2^m \quad \text{Equation 2.4-8}$$

The exponents p and m represent the connectivity of the two phases. As the total volume fraction is the sum of the respective conductive fractions, we have:

$$1 = \chi_1^p + \chi_2^m \quad \text{Equation 2.4-9}$$

Solving for p we find:

$$p = \frac{\log(1 - \chi_2^m)}{\log(1 - \chi_2)} \quad \text{Equation 2.4-10}$$

Combining Equation 2.4-10 with Equation 2.4-8 yields:

$$\sigma_{eff} = \sigma_1(1 - \chi_2)^{\frac{\log(1 - \chi_2^m)}{\log(1 - \chi_2)}} + \sigma_2\chi_2^m \quad \text{Equation 2.4-11}$$

The conductivity of one of the two conducting phases can now be calculated if the volume fraction, apparent conductivity and conductivity of one phase is known.

2.5 THE RELATIONSHIP BETWEEN GEOPHYSICAL AND HYDROGEOLOGICAL PARAMETERS

This section will discuss the connection between Archie's Law, describing the electrical conductivity of a porous medium, and Darcy's Law, which describes the movement of a liquid through a porous medium.

2.5.1 The Geohydrological Parameters and their Determination

To investigate the relationship between the geophysical and geohydrological parameters, the geohydrological parameters first need to be defined. The geohydrological parameters of an aquifer are mainly determined from the analysis of pumping tests, and rests on the application of Darcy's Law.

2.5.1.1 The geohydrological parameters

The geohydrological parameters are: hydraulic conductivity, transmissivity, aquifer storativity, and specific yield. Other related concepts such as permeability and Darcy flux, will also be discussed.

Darcy's Law describes the flow of water through a porous medium and states that the movement of a volume of water through a porous media is proportional to the cross-sectional area and hydraulic gradient. In simplified form, Darcy's Law is written as:

$$Q = KAi \quad \text{Equation 2.5-1}$$

where Q is the rate of flow [L^3/T], K is the coefficient of proportionality relating to the physical attributes of the porous medium and liquid [L/T], A is the cross-sectional area [L^2], and i is the hydraulic gradient [-].

The hydrological parameters of an aquifer are defined below (Bear, 1979; Kruseman and De Ridder, 2000):

Aquifer Storativity (S) - The volume of water (V_w) that a permeable unit will absorb or expel from storage per unit surface area (A) for a unit change in head (dh):

$$S = V_w / (A \cdot dh) \quad \text{Equation 2.5-2}$$

Aquifer Specific storage (S_s) - The amount of water per unit volume of a saturated formation that is stored or expelled from storage due to the compressibility of the aquifer skeleton and pore water per unit change in head. ($S < 0.005$ for confined aquifers):

$$S_s = \rho_w g (\alpha + n\beta) \quad \text{Equation 2.5-3}$$

where ρ_w is the mass density of water [M/L^3], g is the gravitational acceleration [L/T^2], α is the compressibility of the aquifer skeleton [LT^2/M], β is the compressibility of water [LT^2/M], n is the porosity [-]. The specific storage has units of $1/L$. For a confined aquifer $S = bS_s$ where b is the aquifer thickness. This relates to conditions of a confined aquifer.

Specific yield (S_y) - The amount of water that can be drained from a unit volume of rock under the influence of gravity ($S_y = 0.02$ to 0.30). This relates to conditions of an unconfined aquifer. This is also called the drainable or effective porosity, but a film of water stays behind adsorbed to the surfaces of the rock (specific retention). The total porosity is thus the sum of the specific retention (S_r) and the specific yield:

$$n = S_y + S_r \quad \text{Equation 2.5-4}$$

Hydraulic conductivity (K) - The rate of flow (Q) under a unit hydraulic gradient ($i = (h_1 - h_2)$) through a unit cross-sectional area of aquifer. It is a measure of the rock's capacity to transmit a liquid and is dependent on both the physical properties of the liquid and the rock. It has the units of L/T :

$$K = \frac{Q}{Ai} \quad \text{Equation 2.5-5}$$

Transmissivity (T) - Is an aquifer parameter which is defined by the rate of flow per unit width through the entire thickness of an aquifer per unit hydraulic gradient. Expressed in units of L^2/T , it is calculated from:

$$T = \frac{Q}{Ai} h = Kh \quad \text{Equation 2.5-6}$$

where h the thickness of the aquifer.

Permeability (k) - a property of the porous media only, not the fluid. If the hydraulic conductivity value for a subsurface system is known, the permeability can be calculated:

$$k = K \frac{\mu}{\rho g} \quad \text{Equation 2.5-7}$$

where μ is the dynamic viscosity of the fluid [$M/(LT)$], and ρ is the mass density of the fluid [M/L^3]. In the case of clays, the ratio of the surface of the grains to the volume is very big. Although clay has a high porosity (45-55%), it has a low permeability because of the small interstitial openings.

Darcy flux (q) - the discharge volume per unit area:

$$q = \frac{Q}{A} = Ki \quad \text{Equation 2.5-8}$$

The Darcy flux is not the velocity (v) at which the fluid travels through the medium. The fluid velocity is related to the Darcy flux through the porosity (n) where:

$$v = \frac{q}{n} \quad \text{Equation 2.5-9}$$

The flux is divided with porosity to account that only a fraction of the area is available for flow. The fluid velocity would be the velocity experienced by a conservative tracer when carried by the fluid through the formation. The Reynolds number (R_e), is used to distinguish between laminar (low velocities) and turbulent flow (high velocities), and in porous media is directly related to grain size. Darcy's Law is only valid for laminar flow in porous media for Reynolds numbers between 1 and 10 (Bear, 1979).

2.5.1.2 Pumping tests

Pump testing of boreholes provide valuable information to understand the behaviour of groundwater and helping us to make informed decisions. Unlike laboratory testing that delivers exact measurable results, hydrogeology is not an exact science. The behaviour of the aquifer cannot be directly observed, and the scientist can only make derivations of its hydraulic properties by observing changes in water levels under controlled extraction during pumping tests. In addition, factors like the regional geology, hydrogeology and the environment must be accounted for when interpreting the data of a pumping test to arrive at the best possible result and decision.

Figure 2.5-1 illustrates the change in piezometric pressure that occurs in a confined aquifer when pumping from a borehole. The cone of depression relates to the changes in piezometric pressure away from the borehole in the confined aquifer. In an unconfined aquifer, the cone of depression relates to the area of dewatering around the borehole as the water level is physically lowered.

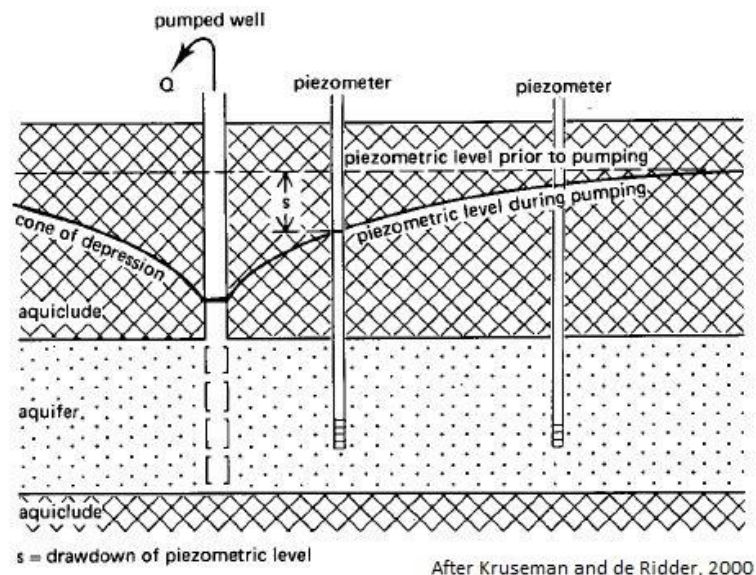


Figure 2.5-1: Drawdown in an aquifer

Pumping tests are executed to achieve various aims (ICRC, 2011). Some of these aims include:

- To determine the safe yield of a borehole.
- To determine how much water the borehole can deliver at a certain amount of drawdown.
- To derive the hydraulic properties, such as transmissivity and storage coefficient.
- To determine the influence of the drawdown in water on neighbouring boreholes.
- To determine what impact the exploitation on groundwater will have on the environment.
- To determine water quality and the possible salinization (ingress of seawater) or pollution of the aquifer

Pumping tests are designed to test different aspects such as the borehole construction, or hydraulic parameters. The main types of pumping tests that are used, are the step test, the constant rate pumping test, and the recovery test.

2.5.1.2.1 The Step Test

The Step Test is designed to provide information about the yield-drawdown relationship and reflect linear and non-linear losses. (Kruseman and De Ridder, 2000). This yield-drawdown relationship is also known as the “skin effect” that exists close to the borehole and is influenced natural phenomena as well as the drilling process and construction of the borehole. Through the step test the effectivity of the borehole is measured because the borehole losses are responsible for a greater drawdown inside the borehole than what will be measured in the aquifer or calculated using well flow equations.

The step test is performed by increasing the pumping rates for at least three consecutive periods or “steps”. The pumping rate is increased at set intervals, or after the water level of the previous step has stabilised. Figure 2.5-2 illustrates the drawdown during a pumping test at increased pumping rates.

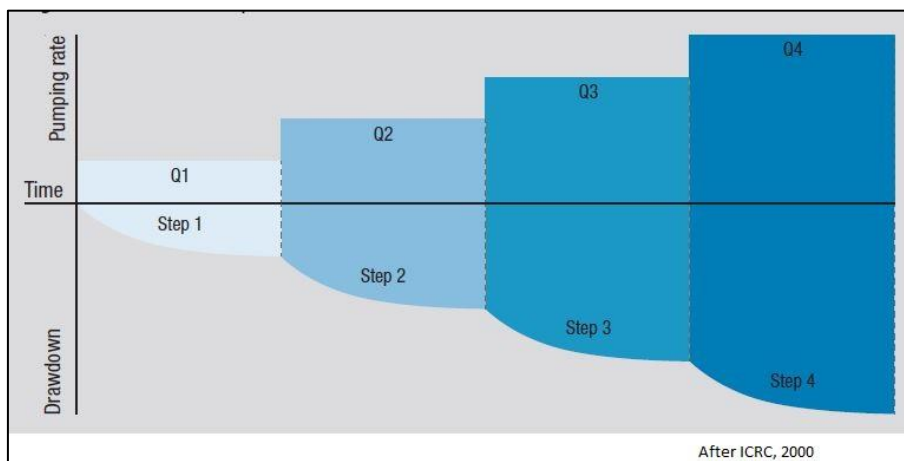


Figure 2.5-2: The Step Test indicating drawdown versus pumping rate

In analysing the data, Jacob’s equation (Kruseman and De Ridder, 2000), can be used. It is simplified by researchers to:

$$S_w = BQ + CQ^p \quad \text{Equation 2.5-10}$$

where:

S_w = Drawdown in the well (m)

B = Linear well loss coefficient

C = Non-linear well loss coefficient

Q = extraction rate(m³)

$P=$ values between 1.5 and 3.5 depending on the value of Q , but $P=2$ as suggested by Jacob is still widely used.

If B and C can be determined, the drawdown inside the well can be calculated for any discharge at a certain time. This information is used to decide on an optimum pumping rate for the borehole, or as indication of the efficiency of the borehole. Equation 2.5-10 can be developed by dividing by Q .

$$\frac{S}{Q} = B + CQ \quad \text{Equation 2.5-11}$$

The term S/Q , is referred to as the specific drawdown of the borehole and gives the relationship between drawdown and discharge. It is not a constant, it increases with time with constant Q , and increases with increase in Q . The inverse relations, Q/S , gives the specific capacity of the borehole.

Using the Hantusch-Bierschenk method (Kruseman & De Ridder, 2000), the specific drawdown (Q/S) for each step (Q) is plotted on semi log graph paper. If a straight line can be fitted through the points, and extended, the intersect with the y -axis will be B , and the slope represents CQ . This is illustrated in Equation 2.5-3.

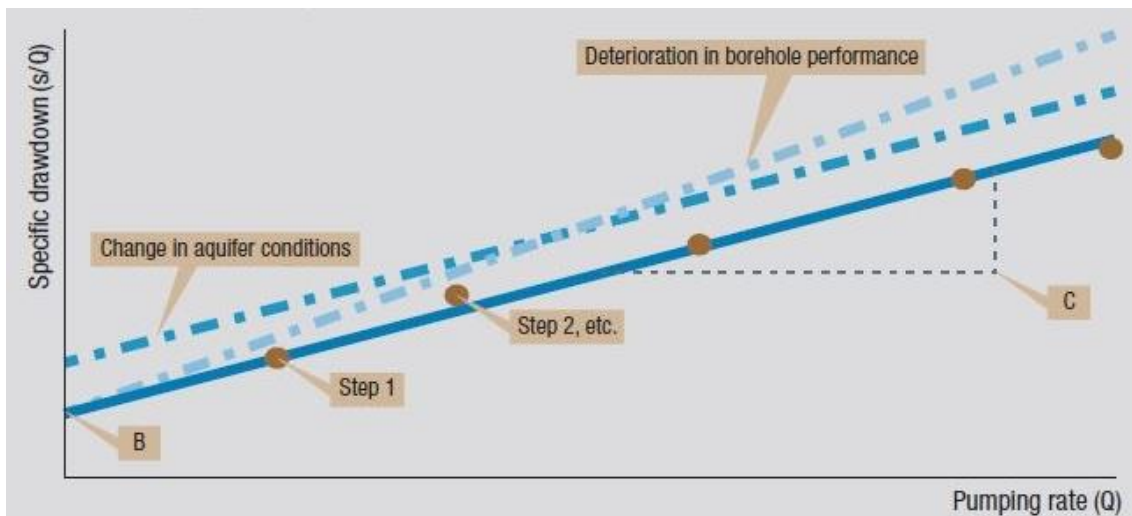


Figure 2.5-3: The Hantusch-Bierschenk method to calculate B and C (ICRC,2000)

By repeating the step test later in the borehole's life and comparing the results, deterioration and changes in aquifer conditions can be detected (refer to Figure 2.5-3).

2.5.1.2.2 The Constant Rate Pumping Test

With the constant rate pumping test, the borehole is pumped at a specific constant discharge rate for a certain period. This period can be hours, days, or even weeks. The minimum pumping time will depend on the physical structure of the aquifer as different parts of the aquifer system (fractures and matrix storage) are tested during the pumping period. The pumping time however must be long

enough to ensure that all contributing systems are tested. The longer the borehole is pumped, the more confidence can be had in the behaviour of the aquifer and the calculation of the hydraulic parameters. The transmissivity (T), can be calculated from the drawdown of the pumped borehole. If data from an observation borehole is available, the storage coefficient (S_s) (confined aquifer) or the specific yield (S_y) (unconfined aquifer), can be calculated.

Confined aquifer

Using piezometer data, Thiem expressed the discharge from a borehole in a confined aquifer as (Kruseman and De Ridder, 2000):

$$Q = \frac{2\pi KD(s_{m1} - s_{m2})}{2.3 \log\left(\frac{r_2}{r_1}\right)} \tag{Equation 2.5-12}$$

where:

Q = discharge in m^3/d

KD = transmissivity in m^2/d

r_1 and r_2 = piezometer distances from borehole in m

s_{m1} and s_{m2} = steady state drawdown in piezometers.

If the steady state drawdowns (s_m) of the respective piezometers and the borehole are plotted against the distances (r) on semi log paper, a straight line can be fitted (Figure 2.5-4).

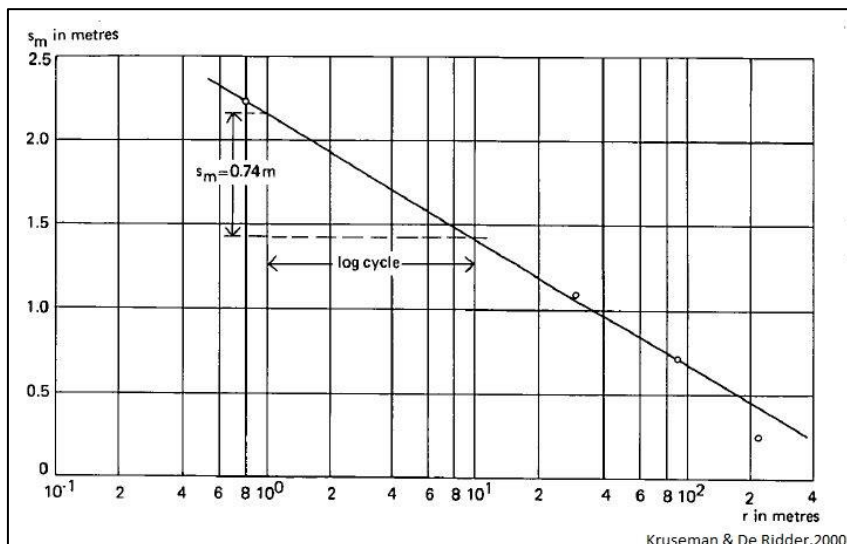


Figure 2.5-4: Thiem's method for analysing drawdown data

The slope of this line is the difference in drawdown (Δs_m) per change in r . Measuring the difference in drawdown per log cycle ($\log r_2/r_1 = 1$) reduces Thiem's equation to:

$$Q = \frac{2\pi KD}{2.30} \Delta s_m \tag{Equation 2.5-13}$$

Solving for KD :

$$KD = \frac{2.30Q}{2\pi \Delta s_m} \tag{Equation 2.5-14}$$

The main assumptions to which Thiem's method must conform are laminar flow and steady state conditions. For unsteady state flow conditions, Theis took into account the time factor and the storativity (S) (Kruseman and De Ridder, 2000). Jacob and Cooper refined the Theis equation to:

$$s = \frac{2.30Q}{4\pi KD} \log \frac{2.25KDt}{Sr^2} \tag{Equation 2.5-15}$$

where S , KD , and Q are the constants and s and t are the variables.

Thus, if the drawdown (s) is plotted against the logarithm of t , a straight line can be fitted (Figure 2.5-5).

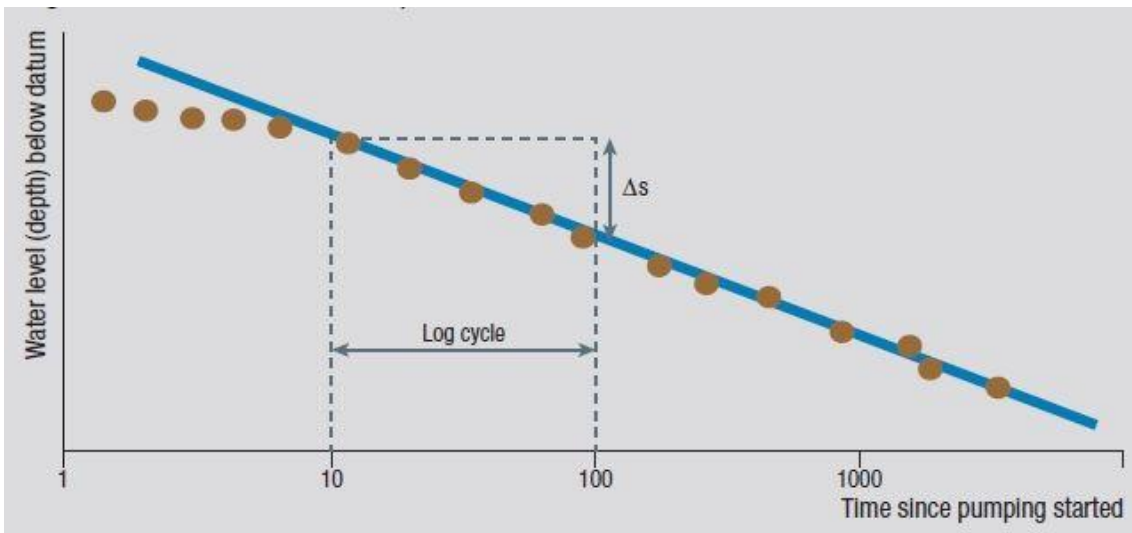


Figure 2.5-5: Constant Rate Pumping test - the drawdown plotted against time since pumping commenced (IGRG, 2000)

The extension of this straight line intersects the time axis of the graph where $s=0$ and $t = t_0$. Equation 2.5-15 can then be written as:

$$0 = \frac{2.30Q}{4\pi KD} \log \frac{2.25KDt_0}{Sr^2} \quad \text{Equation 2.5-16}$$

Because $\frac{2.30Q}{4\pi KD}$ is not zero, it follows that $\log \frac{2.25KDt_0}{Sr^2}$ must be equal to zero. Measured over log cycles, the slope of the fitted straight line is given by:

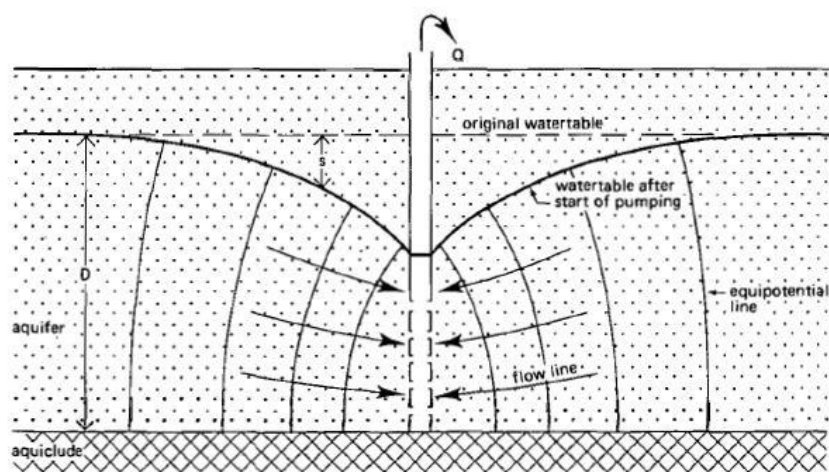
$$\Delta s = \frac{2.30Q}{4\pi KD} \quad \text{Equation 2.5-17}$$

The transmissivity can then be calculated from: $T = KD = \frac{2.30Q}{4\pi \Delta s}$.

The storativity can also be calculated from: $S = \frac{2.25KDt_0}{r^2}$ (if an observation borehole is present).

Unconfined aquifer

When applying the Theis equation to the pump testing of an unconfined aquifer, differences from a confined aquifer environment must be taken into account.



After Kruseman & De Ridder, 2000

Figure 2.5-6: Drawdown in an unconfined aquifer

The assumption that the water flow towards the extraction point is perpendicular, is no longer valid. Because of the drop in water level, the equipotential lines vary along the cone of dewatering and the flow occurs perpendicular along these lines. (See Figure 2.5-6). This has the effect that the drawdown as predicted by the Theis equation, is not realised. Time drawdown curves produced on log-log paper no longer follows a straight line, but exhibit an s-curve. This lag in the water table response, is referred to as *delayed yield* or *delayed water table response*. Three distinct time lapses can be distinguished in the s-curve; early time, intermediate time and late time.

- At **early time**, immediately after the start of pumping, the waterflow is released from storage toward the borehole. The cone of dewatering is still shallow, and water flows toward the borehole at approximately a horizontal level. The Theis equation is valid for this period.
- At **intermediate time** the drawdown slows down. This is because of the effect of dewatering that accompanies the lowering of the water table. The water flow towards the borehole occurs at an increasing angle and is not horizontal nor perpendicular to the borehole. The effect of dewatering can be compared to those of a leaking aquifer. This is because water is flowing across a greater cross-sectional area to the borehole. Because of this, the assumptions made for the Theis equation is not in effect and cannot be applied to this time frame.
- At **late time** , that is after a considerable time of pumping, the cone of dewatering extends far away from the borehole. Water flow towards the borehole occurs at a very shallow angle and the Theis equation is valid again for this period of time.

Therefore, in applying the Theis equation to an unconfined aquifer, only the early and late time data can be taken in consideration for interpretation of the hydraulic parameters.

When using the method of Jacob and Cooper, not all pumping tests will exhibit a straight line. There are several reasons for this and it is important to identify such deviations and compensate for it when interpreting the data. Keeping in mind that the main assumptions for this method is a confined aquifer with a fully penetrating borehole, will aid in the interpretation of such deviations. Macdonald *et al.* (2005), briefly discussed common deviations. This is graphically presented in Figure 2.5-7.

Referring to Figure 2.5-7, the following explanations are given:

- i) Perfect drawdown - This graph gives an example of a straight drawdown curve where the slope of the line will be dictated by the transmissivity.
- ii) Sudden changes in pumping rate - Drawdown in a borehole also decreases the pumping rate as the pump must lift the water to a higher head. Adjustments to the pumping rate may over compensate and exacerbate fluctuations.
- iii) Gradual decrease in drawdown - Recharge from outside of the aquifer is taking place. This can be from either leakage from other aquifer layers, or surface recharge from rivers or lakes, or from the bottom of a non-penetrating borehole.
- iv) Gradual increase in drawdown - The geohydrological parameters is changing away from the borehole. This is commonly observed in alluvial deposits where the depositional environment varies.

- v) Sudden increase in drawdown - The cone of dewatering is encountering a hydraulic barrier. In fractured formations, dewatering of a fracture may also lead to a sudden increase in drawdown.

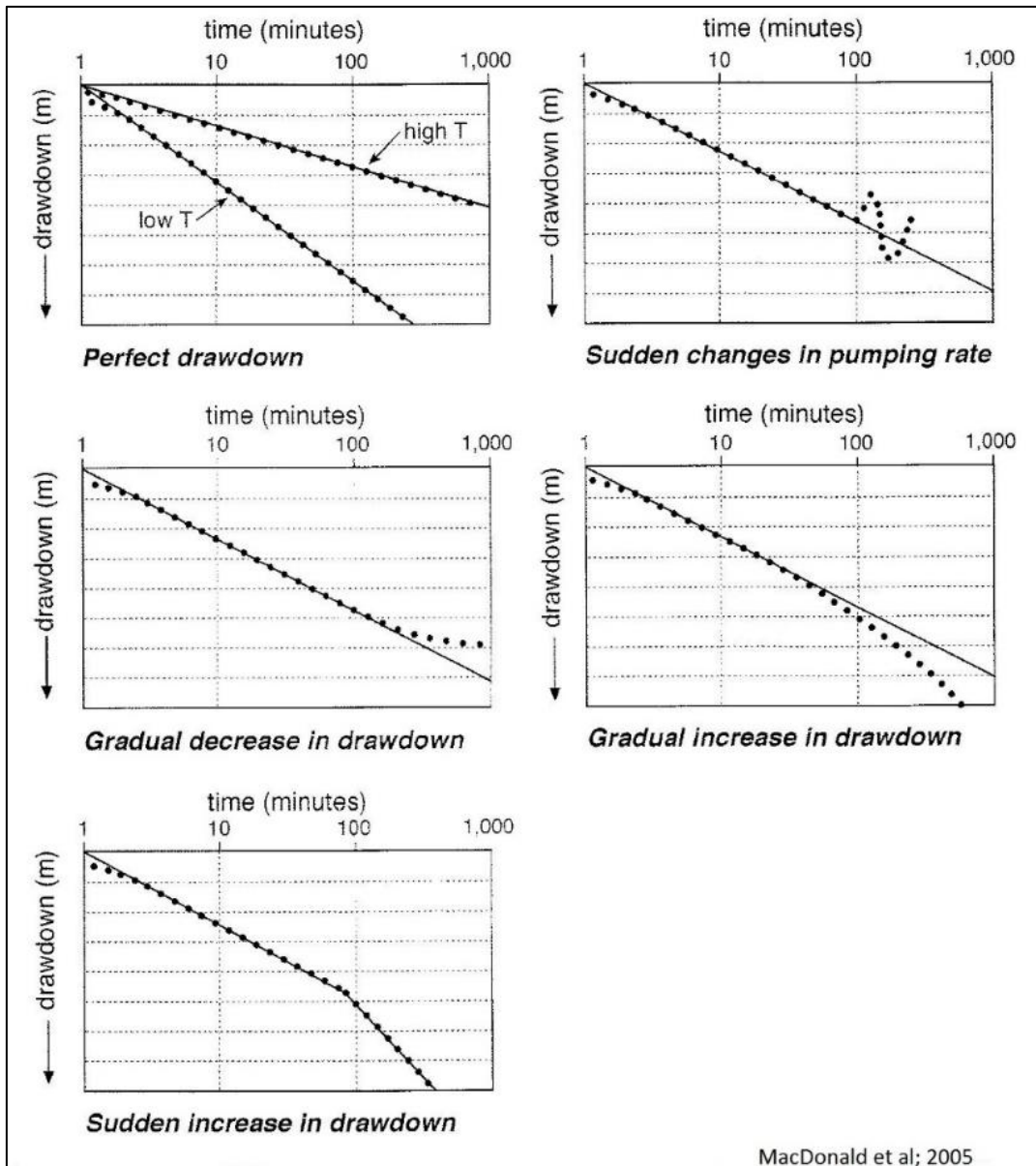


Figure 2.5-7: Graphs indicating common deviations from a straight line of the Constant Rate pumping test

If leakage, recharge, or hydraulic barriers are encountered, the methods of other researchers must be applied in the interpretation of the borehole data (Kruseman and De Ridder, 2000).

2.5.1.2.3 The Recovery Test

The recovery test is the measuring of the recovering water levels and can be done after any drawdown pumping test or cessation of pumping of a production borehole. A mirror image of a constant rate pumping test can be expected - at least in theory (Figure 2.5-8).

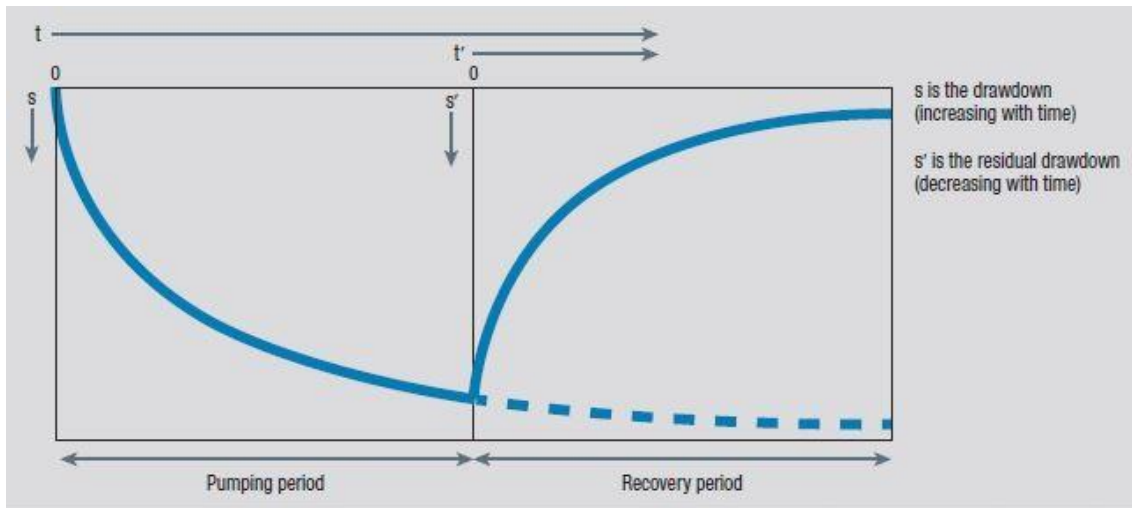


Figure 2.5-8: The drawdown graph versus the recovery graph

Recovery tests have several advantages over drawdown pumping tests. The most obvious are:

- A recovery test can be done after prolonged pumping of a production borehole or drawdown test at no extra cost.
- Recharge to the borehole takes place at a constant rate, where as a drawdown test may experience fluctuation in discharge.
- No borehole losses from turbulent flow is present, as is experienced during pumping.
- Water levels can be measured more accurately because less turbulence is present in the borehole.

Interpretation of the recovery data, can be done using the Theis equation (Kruseman and De Ridder, 2000). Although applied to confined aquifer conditions, this equation is also applicable to unconfined aquifers as mentioned by Kruseman and De Ridder (2000) on the work of Neuman (1975). Applied to unconfined aquifer conditions, the Theis method is only valid to late time data after the effect of elastic storage have dissipated.

The Theis equation uses a borehole function ($W(u)$) to compensate for any borehole losses. If these losses are sufficiently small (see advantages of recovery tests), The Theis equation can be simplified to:

$$s' = \frac{Q}{4\pi KD} \left(\ln \frac{4KDt}{Sr^2} - \ln \frac{4KDt'}{S'r^2} \right) \quad \text{Equation 2.5-18}$$

where:

s' = residual drawdown (m)

r = distance from borehole to piezometer (m)

KD = transmissivity (m^2/d)

S' = storativity during recovery

S = storativity during drawdown

t = time since start of pumping (d)

t' = time since cessation of pumping (d)

Q = rate of discharge (m^3/d)

Thus, for $S' = S$ and KD staying the same, Equation 2.5-18 can be written as:

$$s' = \frac{2.30Q}{4\pi KD} \log \frac{t}{t'} \quad \text{Equation 2.5-19}$$

If this equation is graphically presented with s' plotted against $\log \frac{t}{t'}$ on semi-log paper, a straight line is found (Figure 2.5-9). The slope of this line per log cycle ($\log \frac{t}{t'} = 1$) is:

$$\Delta s = \frac{2.30Q}{4\pi KD} \quad \text{Equation 2.5-20}$$

This equation can be solved to calculate the transmissivity (KD).

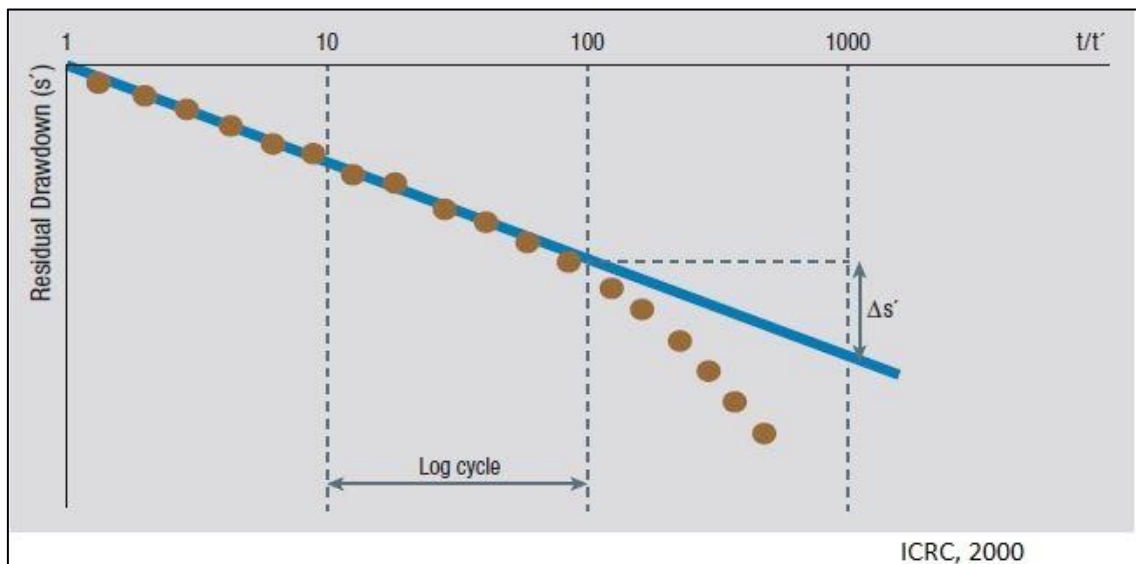


Figure 2.5-9: This Recovery curve

The recovery curve may not always exhibit a straight line due to various reasons. MacDonald *et al* (2005), discussed common reasons for deviations from a straight line. These are graphically presented in Figure 2.5-10.

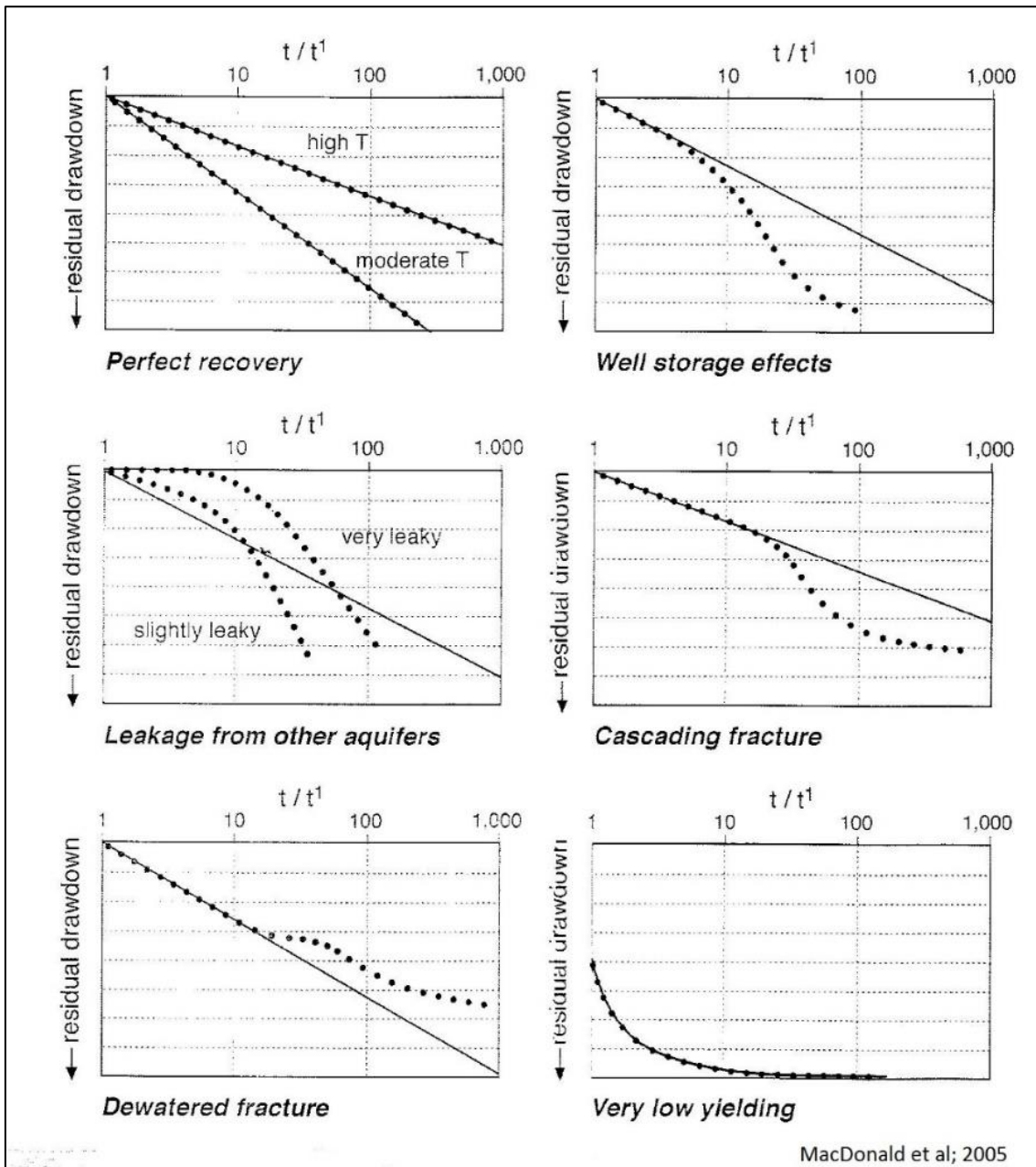


Figure 2.5-10: Recovery data deviating from a straight line

The reasons for deviations are explained as follows:

- i) **Perfect recovery** - All data falls on a straight line. The slope of the line is dependent on the transmissivity of the aquifer.
- ii) **Borehole storage effects** - Borehole storage will affect the recovery curve when the need to fill the borehole volume is dominating the recharge to the borehole.
- iii) **Leakage from other sources** - The aquifer is receiving recharge from another source.
- iv) **Cascading fracture** - A fracture above the pumped level is filling up the borehole volume, before the representative recovery of the aquifer can be observed.

- v) **Dewatered fracture** - The recovery of the water level in the borehole is slowed down by the recovery of a dewatered fracture
- vi) **Very low yielding** - The recovery of the water level is very slow and is dominated by the need to fill the borehole volume.

2.5.2 The Relationship of the Physical and Geohydrological Parameters to Geophysical Measurements

Earlier in this chapter, the concepts of Ohm’s Law and the flow of electrical current through a porous medium (Archie’s Law), and hydraulic flow through a porous medium (Darcy’s Law), were explained. When electrical flow and hydraulic flow are dependent on the same characteristics of the porous medium, it stands to reason that an inter-relationship will exist (Keller and Frischknecht, 1996; Mazac *et al.*, 1985; Niwas and de Lima, 2003). This relationship is sought in laboratories (sample scale) as well as in the field (aquifer scale). The aquifer parameters of yield, hydraulic conductivity, and transmissivity are the main hydraulic parameters commonly estimated from electrical characteristics.

At sample as well as aquifer level, the resistivity (ρ), transverse resistance (T), and longitudinal conductance (S), as measured by surface resistivity and EM soundings, are compared to average longitudinal and transverse hydraulic conductivities (K_l and K_t), transmissivity (T_h), and leakance (L_h). These relationships are defined in Table 2.5-1.

Table 2.5-1: Definitions of hydraulic and electric layer parameters (after Mazac *et al.*, 1985)

Electrical	Hydraulic
Transverse resistance: $T = \sum h_i \rho_i = H \rho_l$	Transmissivity: $T_h = \sum h_i k_i = K_l H$
Longitudinal conductance: $S = \sum h_i / \rho_i = H / \rho_l$	Leakance: $L_h = \sum k_i / h_i = K_t / H$
Average aquifer resistivities: ρ_l, ρ_t	Average hydraulic conductivities: K_l, K_t

The similarity between the flow of electrical current and that of groundwater is stated from the writing of Maillet (1947), and are explained by Sinha *et al.* (2009), as well as Batayneh (2009). This analogous model is presented in Figure 2.5-11.

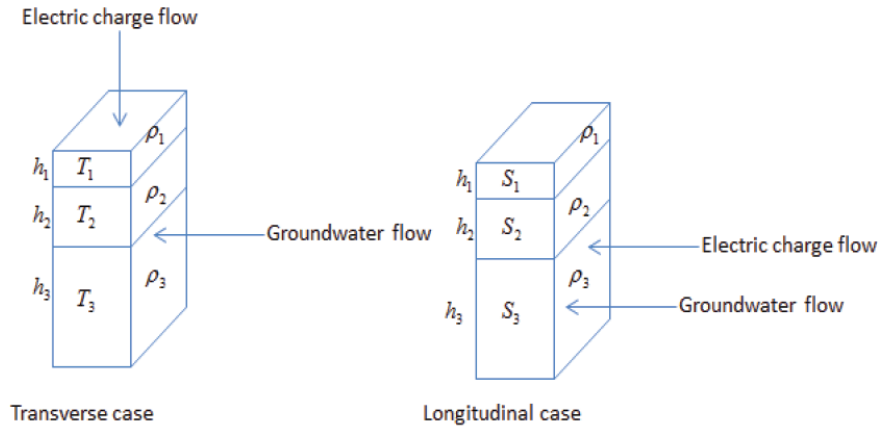


Figure 2.5-11: Layered model showing transverse and longitudinal current flow (Sinha *et al.*,2009).

The hydraulic conductivity of groundwater flow parallel to the layering throughout the profile will be the sum of the hydraulic conductivities of the respective layers, with the average hydraulic conductivity the sum thereof divided by the total thickness:

$$K_h = \frac{\sum_i^n K_i h_i}{\sum_i^n h_i} \tag{Equation 2.5-21}$$

Longitudinal resistivity (ρ_l), will then be expressed as:

$$\rho_l = \frac{\sum_i^n h_i}{\sum_i^n \frac{h_i}{\rho_i}} \tag{Equation 2.5-22}$$

And the transverse resistivity (ρ_t) will be determined from the layer parameters as:

$$\rho_t = \frac{\sum_i^n \rho_i h_i}{\sum_i^n h_i} \tag{Equation 2.5-23}$$

The work of various authors that reported relations between hydraulic conductivity and aquifer formation factor, and transmissivity and transverse resistance, were discussed by Mazac *et al.* (1985). Because it gives a compilation of insights in the field of hydrogeophysical application, it will be heavily relied upon in this section.

Mazac concluded that for homogeneous sediments where hydraulic conductivity is dependent on effective porosity, an inverse correlation between formation factor and hydraulic conductivity is exists. If hydraulic conductivity increases with decreasing porosity, a direct correlation with formation factor will be found. If resistivity changes are controlled by the presence of clay, a direct correlation with hydraulic conductivity will also be shown. Thus, both direct and inverse correlations should be accommodated depending on the type of aquifer.

To make sense of the electrical/hydraulic relationship of an aquifer, a general hydrogeophysical model relating to the aquifer conditions should be constructed (Mazac *et al.*, 1985; Niwas and de Lima, 2003). This model should account for the following:

- a) That any correlation that exist be fundamentally explained. Sand and gravel aquifers, aquifers where the clay is dispersed in sandy matrix, and aquifers where clay occur in layers, will show different correlations.
- b) That hydraulic conductivity correlates with grain size and effective porosity in clay free sediments, and with clay content in clayey sediments.
- c) That the parameter of electrical resistivity is determined by porosity in clay free sediments, and of clay content plus porosity in clayey sediments.
- d) That resistivity at aquifer scale will reflect the sample scale relationships. That the mean resistivity, the transverse resistivity, and the longitudinal resistivity will be the same in a homogeneous sandy aquifer and a where clay occurs in a sandy matrix. That in an anisotropic aquifer, the three resistivities will differ, but that the mean resistivity be approximately equal to the average longitudinal resistivity.
- e) That the inverse or direct relationship the most important feature is to explain the hydrogeophysical relationships. This is explained in the following graphs:

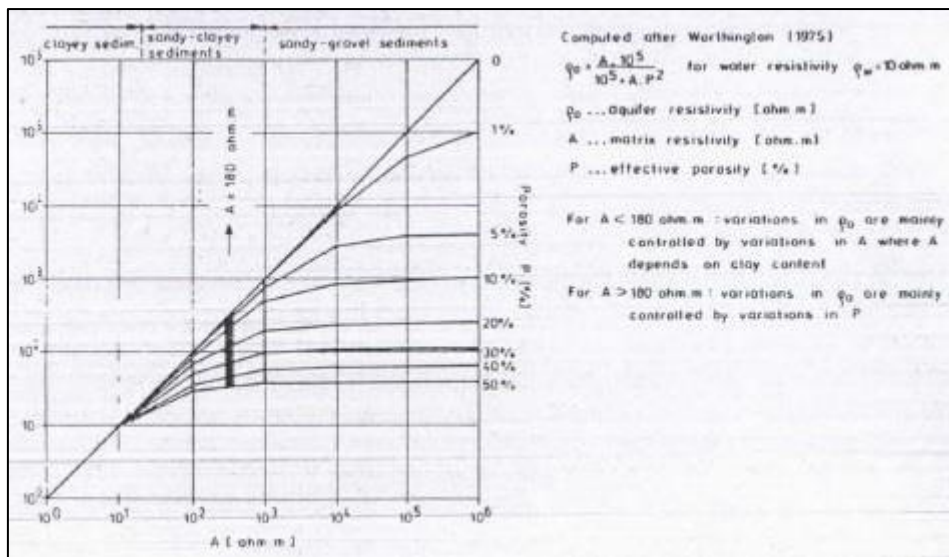


Figure 2.5-12: Relations between aquifer resistivity, matrix resistivity, and effective porosity (Worthington in Mazac ,1985)

From Figure 2.5-12 it can be concluded that for matrix resistivity $A < 180 \text{ohm.m}^{-1}$ and associated hydraulic conductivity, are controlled by clay content. For a matrix resistivity $A > 180 \text{ Ohm.m}^{-1}$, the hydraulic conductivity and resistivity for more sandy aquifers are determined by porosity.

The hydraulic conductivity and porosity relationship can also be presented as in Figure 2.5-13. Variation in hydraulic conductivity within a layer defined by a certain grain size

(lithology unit such as clay), will reflect differences in porosity, and will exhibit a direct relationship. However, variation in hydraulic conductivity between lithological units (clay to gravel), will exhibit an indirect relationship. The same direct-indirect relationship exists between hydraulic conductivity and resistivity.

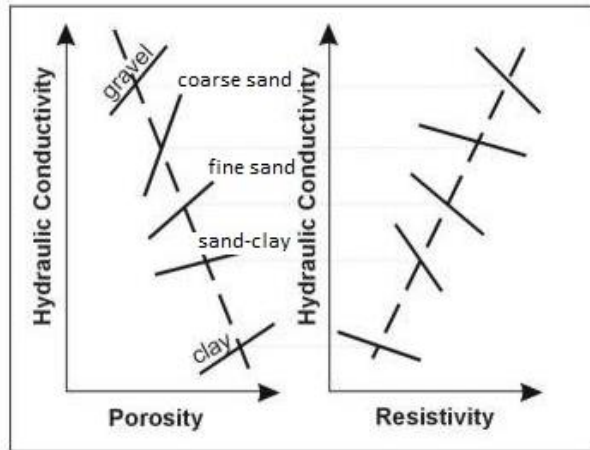


Figure 2.5-13: Schematic diagram to show relations between hydraulic conductivity, porosity, and resistivity for different sediment types (Mazac *et al* (1985).

- f) Resistivity from a sounding curve must first be determined, before an estimate of hydraulic conductivity of an aquifer can be made. If the influence of equivalence is present, and only *T* for K and Q -type curves or *S* for H and A-type curves, can be determined, then it is only possible to estimate transmissivity. This is explained in detail by Niwas *et al.* (2011).

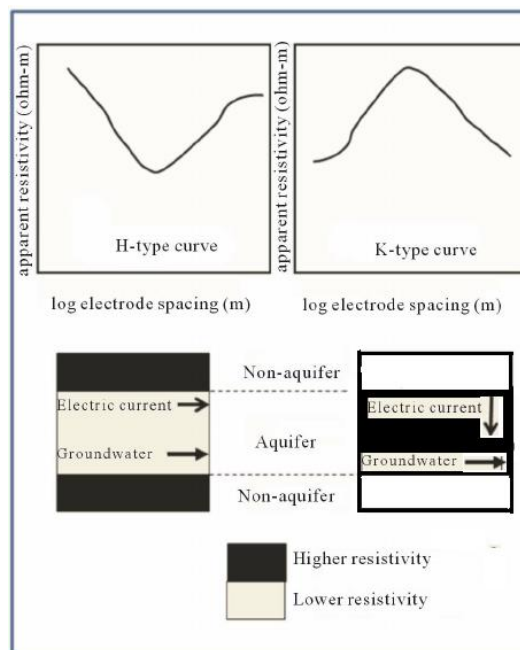


Figure 2.5-14: Characteristic shapes of K- and H-type resistivity curves Utom *et al.* (2012)

It is graphically presented in Figure 2.5-14. If the aquifer is underlain by a resistive basement (H-type), the dominant electrical flow is parallel to the layers, and the longitudinal conductance (S) will be measured. If underlain by a conductive layer, the electrical current flow will tend to avoid the resistive aquifer layer, and the transverse resistivity (T) will be measured. (Also see Figure 2.3-3 and Figure 2.5-11).

This is theoretically explained by two analytical equations derived from Ohm's Law and Darcy's law by Niwas and Singal (1981, 1985) and validated at the Krauthausen test site in Germany (Niwas *et al.*, 2011). These equations for transverse resistance and longitudinal conductance solve the inverse and direct relationship between electrical resistivity and hydraulic conductivity:

$$T = \alpha S; \quad \alpha = K\rho \quad \text{Equation 2.5-24}$$

and:

$$T = \beta R; \quad \beta = K/\rho \quad \text{Equation 2.5-25}$$

Where T is the hydraulic transmissivity (m^2/s), R ($d\rho$) the transverse resistance (Ohm), S (d/ρ) the longitudinal conductance (S) d - the thickness of the aquifer and α, β - a constant of proportionality. The value of these equations is that only one value of hydraulic conductivity is needed to compute the values of α or β .

- g) In anisotropic aquifers where layers of sand and layers of clay alternate, the most appropriate geoelectrical parameter that correlate with hydraulic conductivity, depends on the flow direction relative to the layering (see Table 2.5-1 and Figure 2.5-11). If the electric flow is normal to the bedding, the correlation will be between hydraulic conductivity and transverse resistivity, and if parallel to the bedding, between longitudinal conductance and leakage. The choice of which parameter to use, will depend on the hydrogeophysical conditions of the aquifer and the adjacent layers as discussed in (f). Frohlich and Kelly (1985) concluded that for complicated aquifers, the transverse resistance (or longitudinal as the case may be) is a more reliable electrical parameter than layer resistivity.

CHAPTER 3: SITE DESCRIPTION

3.1 INTRODUCTION

The Harts-/Dry Harts River Valley was formed approximately 280 Ma ago, carved by glaciers of the Permian ice age. The valley runs in a north-south direction, and closely follow the formational boundary between the Griqualand West Supergroup and the Ventersdorp Supergroup (Temperley, 1967; in Ellington *et al.*, 2004). This glacier valley enabled the deposition and preservation of Dwyka lithologies of the Karoo Supergroup. Both Ventersdorp, Griqualand West and Karoo lithologies are covered by wind-blown sands of the Kalahari Group of Quaternary age. It is this unique topographical and geological setting that enabled the development of the Vaalharts Irrigation Scheme.

3.2 REGIONAL SETTING

The Vaalharts Irrigation Scheme (Figure 3.2-1), lies approximately halfway between the towns of Kimberley and Vryburg. It is situated on the border of the Northern Cape Province and the North-West Province. It is well served by logistical infrastructure such as tarred roads and a railway line.



Figure 3.2-1: Regional setting of the Vaalharts Irrigation scheme

3.3 GEOLOGY

Formations of the Ventersdorp- and Griqualand West Supergroups, form the bedrock of the Harts River Valley. The Taung and Hartswater Group of the Ventersdorp Supergroup are present on the eastern flank of the valley, while the Schmidtsdrift and Ghaap Plateau Dolomite Formation of the

Griqualand West Supergroup occur on the western flank. The stratigraphy and geology are presented as follows in Kent and De Grys (1980) and mapped by the South African Council of Geoscience (Figure 3.3-1).

The Taung- and Hartswater Groups mainly consist of a granite-pebble conglomerate at the base that is overlain by an alternating succession of tuffaceous sediments, arkose and chert in which lenses of stromatolitic limestone are locally developed. Towards the town of Hartswater, volcanic and sedimentary material alternates. This comprises of tuff and tuffaceous shale with layers and lenses of andesitic lava and chert. The dip of the sedimentary layers points mainly to northerly direction. In the study area the contact (which is unconformable in nature), between the Ventersdorp and the Griqualand West lithologies are yet to be confirmed due to the extensive overburden of Dwyka and Quarternary deposits.

The Griqualand West sequence adjacent to the study area consists of the basal Vryburg Siltstone Formation, followed by the Schmidtsdrift and Ghaap Plateu Dolomite Formations. The Schmidtsdrift Formation may be considered as a transitional zone of interbedded shale, quartzite, dolomite and chert. The Ghaap Plateu Dolomite Formation, consists mainly of dolomite, limestone and chert. The average dip of this sequence is in a westerly direction.

The tillites and shales of the Dwyka formation lies unconformably on both the above formations. These lithologies outcrop poorly in the study area, and the extent and areas of facies change from tillite to shale, are largely obscured by the overlying alluvium. Tillites can be observed on the eastern flank near the Lemoenkop Orange Warehouse and shales exposed in the Harts River. The tillites consists of mainly a granite/gneiss agglomerate in a very fine-grained matrix. The shales reach their maximum thickness at the bottom of the valley. The rocks of the Dwyka formation was found not to be deeply weathered (Temperley ,1967) and drilling (Ellington, 2003), confirmed a very shallow weathered horizon between the Dwyka and the overlying alluvium. A pocket of weathered tillite situated on the extreme eastern slope is quarried and used as road and construction filling. Near the Harts River, shale is quarried by a brickyard for the use in brickmaking.

Extensive Quarternary sedimentary deposits consists both of massive calcrete and windblown sands. The calcrete deposits dominates the western flank of the Harts River Valley, while the windblown sands of the Kalahari dominate the eastern flank. The calcrete deposits on the western flank must not be confused with the calcrete deposits within the soil horizon of the eastern flank. They do not share the same origin as the Harts River acts as a divide between different geochemical environments. The western flank is situated beneath the escarp of the Ghaap Plateu Dolomite

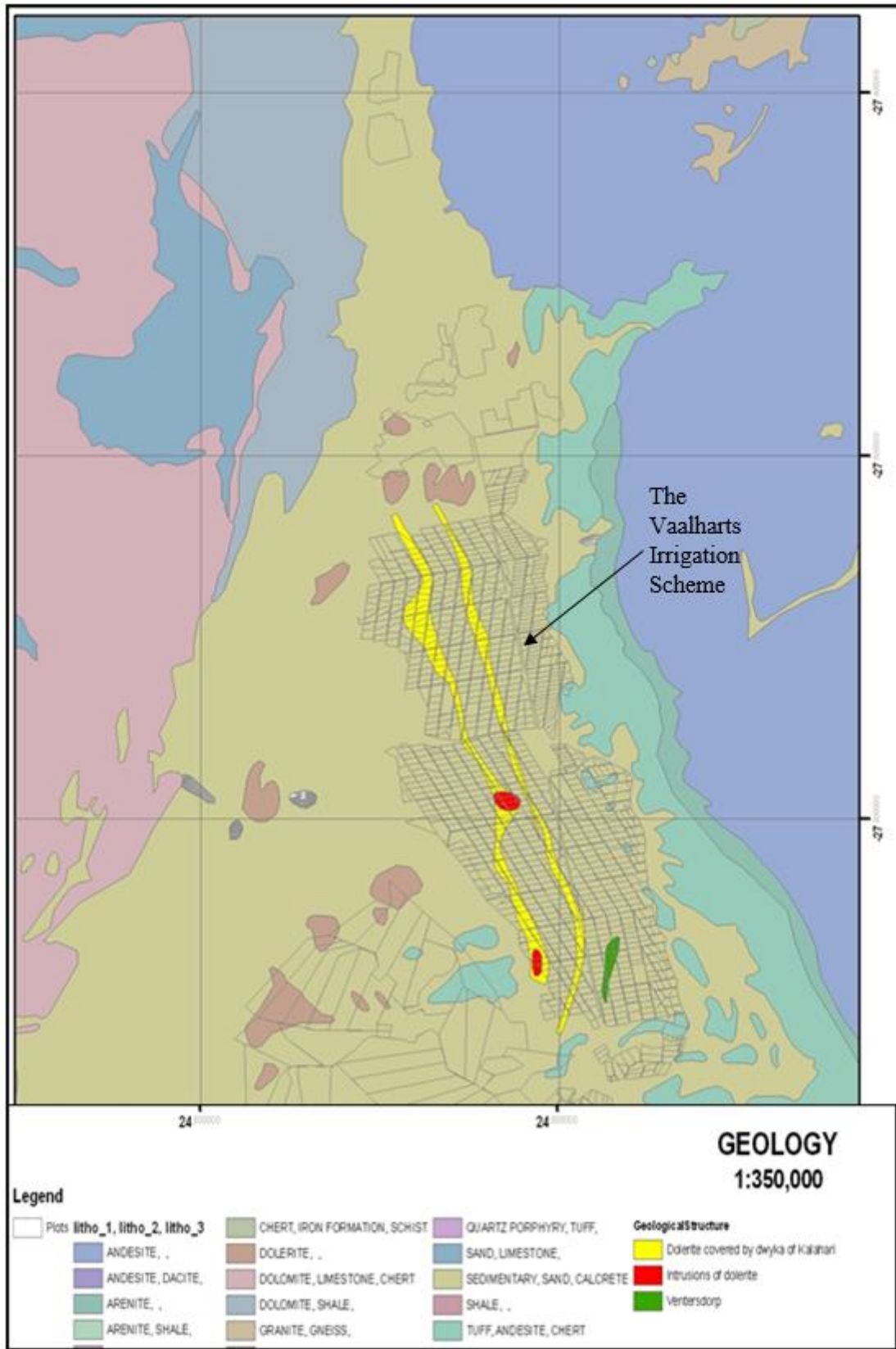


Figure 3.3-1: The geology of the Vaalharts Irrigation Scheme and surround (De Bruyn, 2016)

Formation, and weathering and leaching of the dolomite is responsible for the extensive calcrete deposits in this area. These deposits were once mined for agricultural and industrial uses.

Sands of the Kalahari group, dominates the eastern flank of the Harts River Valley. Massive calcrete layers may occur, especially in the low-lying areas, but these calcrete formations are mostly associated with weathering of the Ventersdorp lithologies. A soft calcrete layer situated within the soil horizon is speculated to be the product of groundwater/evapotranspiration interaction in the capillary zone above the groundwater level (Temperley ,1967 in Ellington, 2003).

3.4 RAINFALL

The long term mean annual rainfall in the Vaalharts area is approximately 450 mm/a (De Bruyn, 2016). Personal records from the past 16 years however, measured the mean annual rainfall as 485 mm (Figure 3.4-1). Of note is the exceptional below average rainfall that occurred during the timespan (2015 - 2016) of this investigation.

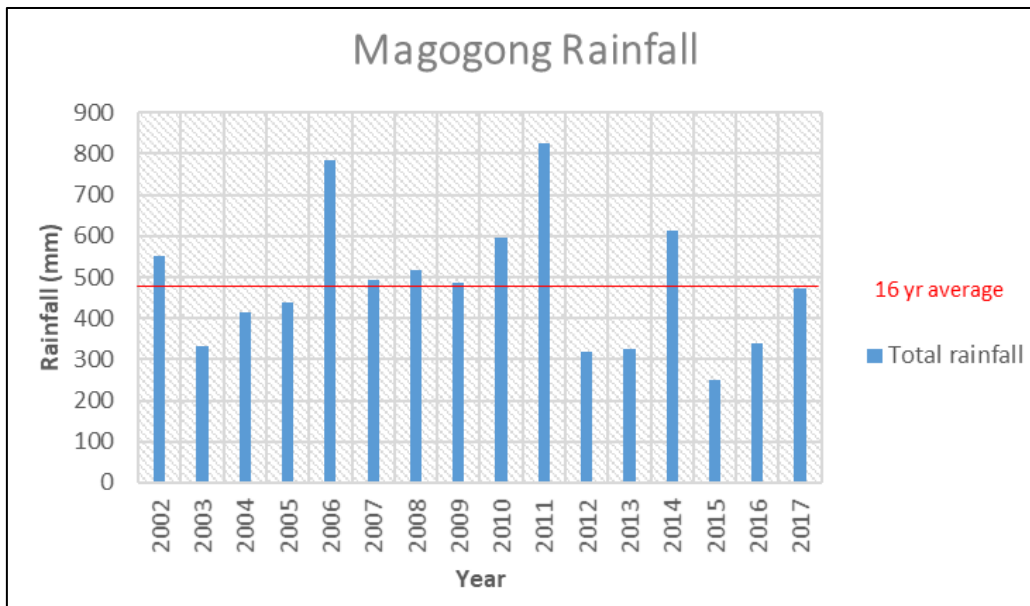


Figure 3.4-1: Rainfall measured at Magogong

The western slope of the Harts River, is a separate hydrological entity, and apart from contributing to the base flow of the Harts River, do not have any influence on the eastern half.

3.5 SURFACE DRAINAGE

The Vaalharts Irrigation Scheme is situated next to the Vaal River, a perennial river. Irrigation water is channelled from the Vaal River through an extensive canal system to the farms. As the irrigation scheme is situated on the slopes of the Harts River valley, the natural drainage of the area is towards the Harts River. The Harts River is a seasonal river, but irrigation drainage and tailends induce a continuous flow in the river downstream of the irrigation scheme. This excess is collected in the Spitskop Dam and is also used for irrigation purposes. The location of the Vaalharts Irrigation Scheme relative to the natural river drainage is shown in Figure 3.5-1.



Figure 3.5-1: Hydrological drainage of the Vaalharts area

The irrigation allocation adds 980mm (or about 314.98M m³/a in Table 2.2-1) of water to the irrigated areas. Tailends, drainage and runoff add an estimated 51M m³/a to the Harts River.

Runoff from rainfall from the hills on the eastern slope of the Harts River valley, occurs as flash floods. These are directed with cement lined drainage canals through the irrigation area and thus is expected to have little or no effect on the groundwater recharge in the irrigation area. This runoff is dumped directly into the Harts River.

3.6 AQUIFER SYSTEM

The Vaalharts aquifer is considered an unconfined aquifer situated in the alluvium above the impervious lithologies of the Dwyka Formation (Rudolph and Hough, 2003; Temperley in Ellington *et al.*, 2004; Verwey, 2009). Although considered to be impervious, pump testing in some deeper boreholes produced higher *K*-values and this was attributed to fracturing that exists in the shale horizon Ellington *et al.*, 2004). Because of the riverine/glacial depositional environment of the Dwyka lithologies in a relatively small area, one can expect much variation within the succession. On top of this, the meandering stream of the Harts River and minor tributaries also left a legacy of paleo streambeds of gravel and sediment on the unconformable contact with the Dwyka, as well as within the sandy alluvium horizon (Figure 2.2-4). This is confirmed by drilling logs and productive boreholes that intersects shallow gravel horizons above the shale beds. The unconformable contact zone between the Ventersdorp and Dwyka is also a known water strike.

Water levels in the Vaalharts Irrigation Scheme varies between 7 m to less than 1.5 m below ground level. Because of the proximity of the water level to the soil horizon and surface, the hydrological parameters measured in the soil horizon, are expected to be the same and may be extrapolated to the deeper aquifer where similar lithological composition exists, and vice versa.

The aquifer drains towards the Harts River and contributes approximately 14.34 M m³/a (Table 2.2-2) to the baseflow of the river.

CHAPTER 4: FIELD INVESTIGATIONS

4.1 INTRODUCTION

The borehole positions of Ellington, (2003) were located and relevant information such as waterlevels, EC, pH and temperature were collected. Vertical electrical soundings (VES) at each position were taken using the Wenner array. These soundings were modelled to obtain the layer resistivities and these were correlated with the known geology, water levels and aquifer depths. New boreholes were pumping tested to obtain hydraulic parameters.

Correlation between hydraulic parameters (K and T) (compiled data from the literature study and present), and geoelectric properties was done. Relations between longitudinal conductance (C) and transverse resistivity (R) with both K and T were obtained.

An ERT traverse was done in a region of the deepest alluvium cover to profile the variation of the alluvium and the geology from the eastern flank of the Harts River valley down to the lowest point - the river itself. A variation in the thickness of the alluvium can be equated to a variation in thickness of the aquifer.

4.2 GEOPHYSICAL SURVEY

Because of the higher depth and resolution that can be obtained through the use of the resistivity method, it was the method chosen for this investigation. In a sedimentary geological environment, the Wenner array is used because of its sensitivity to horizontal layers (Table 2.3-2). The methods used in this investigation is also applicable to the EM method, taking into account the instrument configurations and limits.

4.2.1 Calibrating VES Survey

Wenner VES soundings were done at borehole positions where the geological succession is determined through drilling. These boreholes were drilled during the study of Ellington (2003), and are properly capped to preserve the borehole for future investigations. Three of the original boreholes could not be located and are presumed destroyed. In addition to these boreholes, five new boreholes drilled in the study area were geologically logged, the relevant hydrological and chemical data collected, and were included in the geophysical investigation. The positions of the boreholes are shown in Figure 4.2-1.

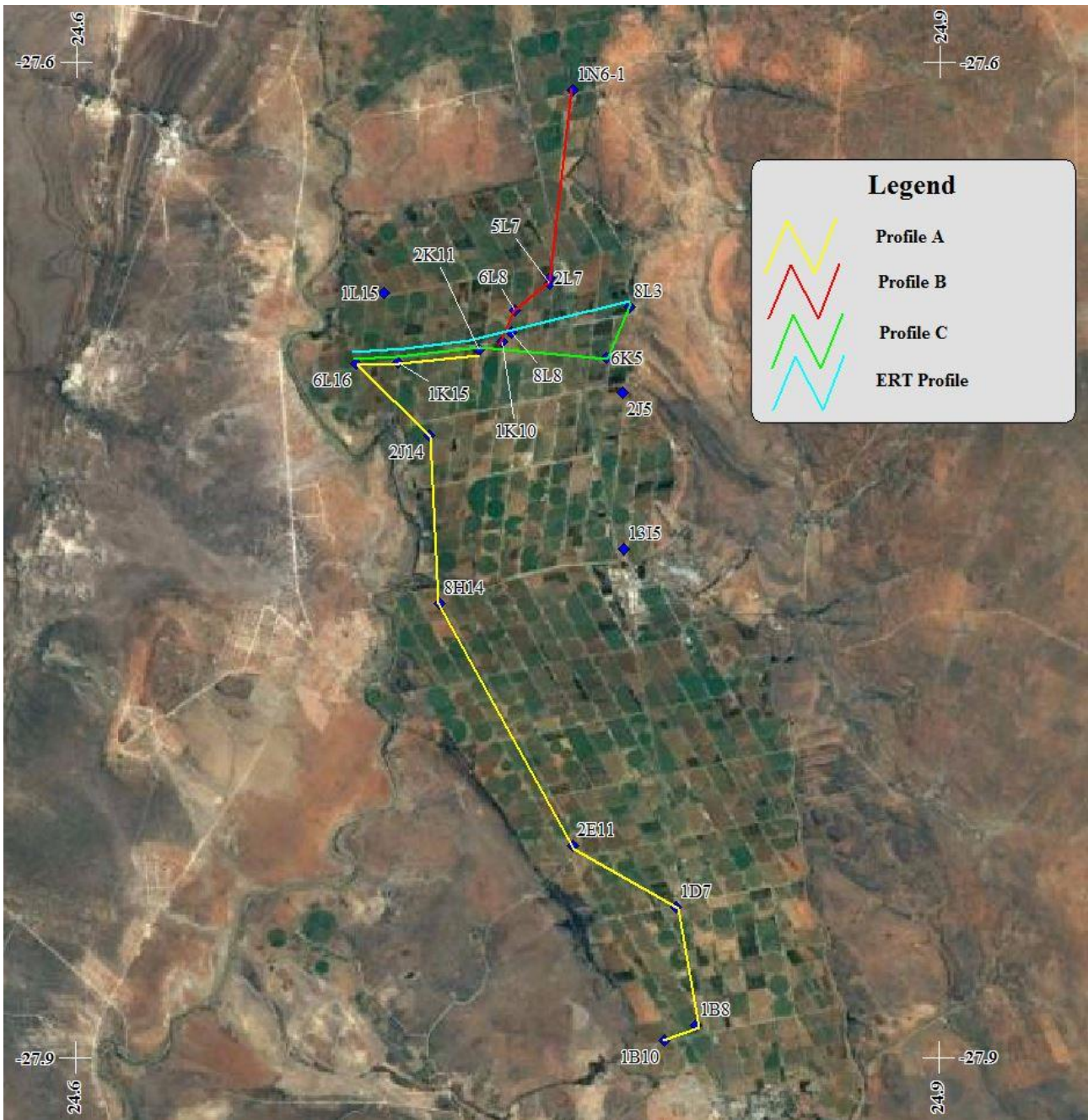


Figure 4.2-1: The positions of VES soundings and ERT profile in the study area

Because of the sedimentary nature of the aquifer geology, the layout of the VES array was to follow the strike of the sedimentary layers. This is in order to diminish the influence of longitudinal variation in geology within the array dimension. No physical measurement of such strike direction is available, but using the morphology of the Harts River Valley, the deduction can be made that it will be parallel to the direction of the valley, which is a North-South direction. The layout of the infrastructure in the Vaalharts Irrigation Scheme, follow a North-North-westerly direction south of Hartswater, and North-North-easterly direction north of Hartswater. On a practical approach, the VES layouts were to follow these directions.

The Wenner array used in this investigation spanned a maximum 200 m (*length AB*). This gives an estimated depth of investigation of 66 m ($AB/3$) in homogeneous conditions. This would be more than sufficient to cover the depth of the alluvial aquifer. Array spacing started with increments of 1 m up to AA=10, increased to increments of 2 m up to AA=30 m, and 4 m up to AA=66 m. This is in order to obtain a high level of resolution, especially in the top 10 m of the soil horizon.

4.2.1.1 Results of VES survey

The VES soundings were inversely modelled using the IPI2WIN program. No restrictions were placed on the model as its accuracy to determine water levels and depth of aquifer and geological succession, must be determined.

The results of the VES survey is presented in Appendix A. The inversely modelled layer resistivities with their respective depths and thicknesses are tabled with each figure. Very good fits of the modelled curves with the apparent resistivity curves were obtained with Root Mean Square (RMS) errors of about 2- 4% and one or two cases at about 8-14%.

Three broad groups of VES curves can be distinguished according to the shape of the curves:

Boreholes where the solid Venterdorp bedrock was intersected, all show an H-type curve (Figure 2.5-14). This is inherent of conditions where a layer of low resistivity is sandwiched between layers of high resistivity. The layer of low resistivity being the aquifer, and the layers of high resistivity those of the unsaturated top soil and bedrock. This simple situation is reflected in the VES curve of Borehole 1D7-1 (Figure 4.2-2).

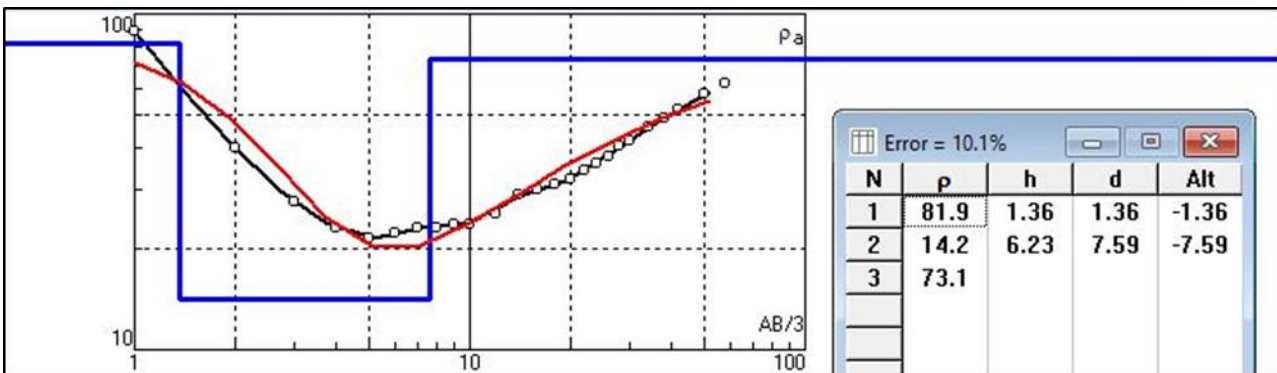


Figure 4.2-2: The VES curve of Borehole 1D7-1

However, because of variation in the lithological composition of the aquifer, a more complex VES curve can also be expected. The VES curve will then reflect layers of different resistivities such as at Borehole 2E11-1 (Figure 4.2-3), where more than one layer is contained in the middle zone of lower resistivity.

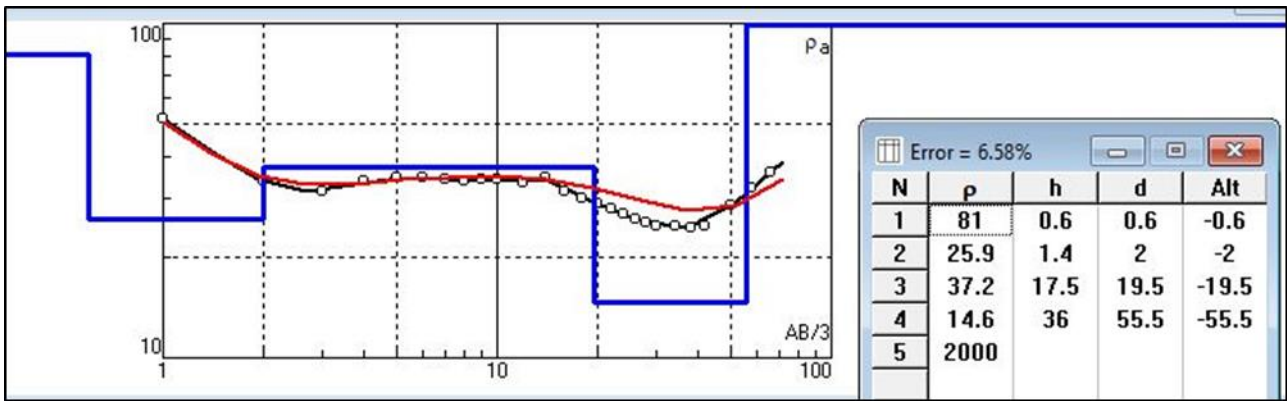


Figure 4.2-3: The VES curve of Borehole 2E11-1

The third shape of VES curve that is encountered, is one of a progressive lower resistivity with depth. This case is presented in Figure 4.2-4: *The VES curve of Borehole 1315-1*. At first the trend seems contrary to the curves with shapes as discussed in (a) and (b), but the solution still relates to the depth of the highly resistive basement. The depth of the VES investigation was simply not deep enough to reach the basement.

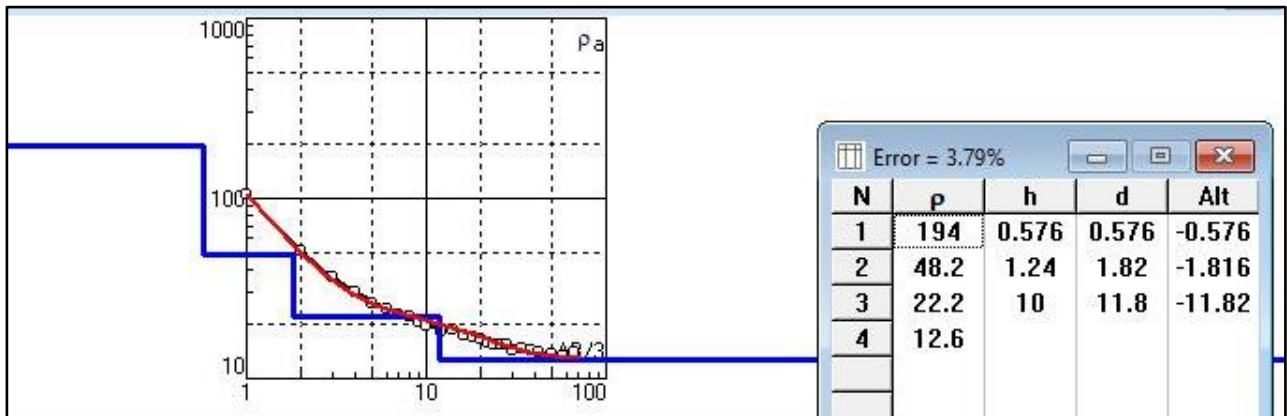


Figure 4.2-4: The VES curve of Borehole 1315-1

4.2.1.2 Correlation between geology and layer resistivities

The layer resistivities obtained through the inverse modelling process, were plotted against the logged geology of the boreholes on a normal scale to correlate the respective layers with each other. These results are presented in Appendix B. For a meaningful interpretation of the resistivity results let us first look at the variation in the geology as encountered in the boreholes.

In the south of the project area, at boreholes 1B8, 1B10 and 1D7, no shale is encountered. A succession of sand and gravel lies directly upon the lava basement. The geology of Borehole 1B10 is presented in Figure 4.2-5.

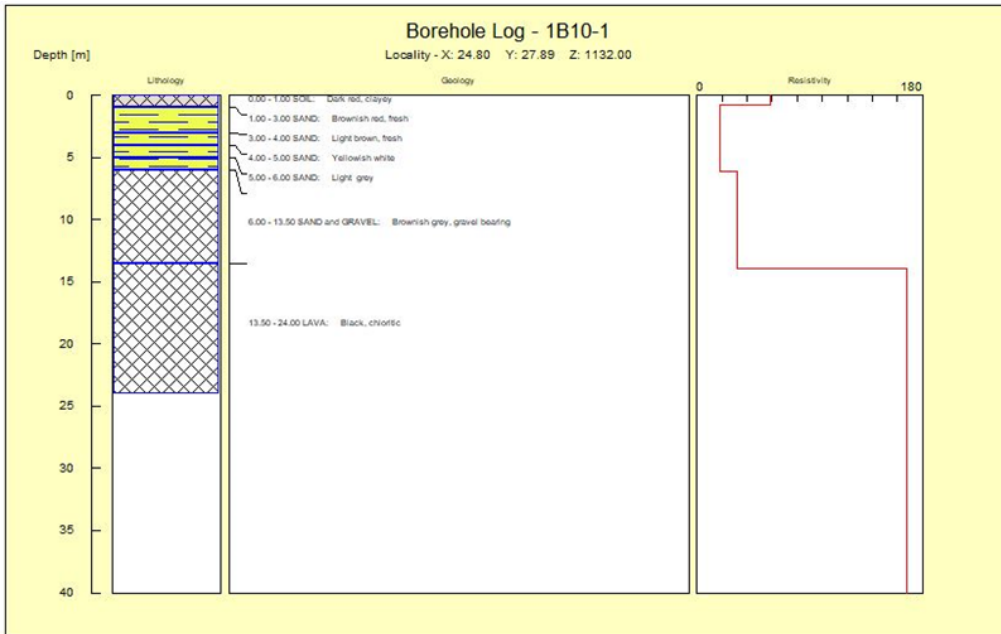


Figure 4.2-5: The comparison of the geology with resistivity of Borehole 1B10-1

In Figure 3.3-1, this geology correlates with the dolerite mapped. The thickness of the shale horizon increases towards the north, from boreholes 2E11 (shale thickness 44 m) to 1K10, where a maximum shale thickness of 82 m is encountered. In a westerly direction, from 1K10 to 6L16, the shale layer lessens to 23 m. Thus, it seems that the shale layer is at its thickest in the vicinity of 1K10. At 2J5 (Figure 4.2-6), sand and gravel, possibly weathered tillite, was intersected underneath the shale.

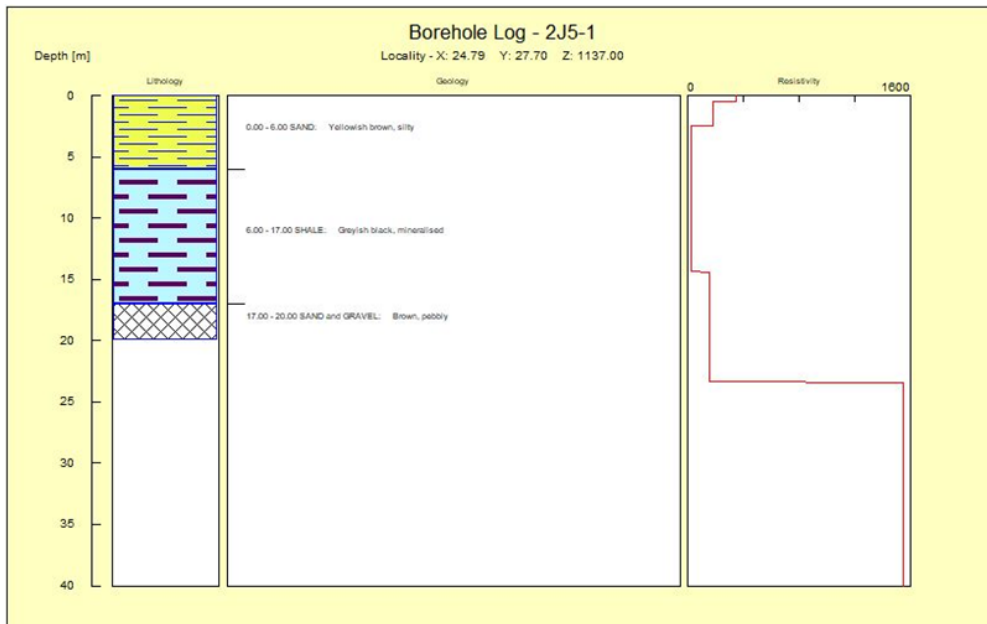


Figure 4.2-6: The comparison of the geology with resistivity of Borehole 2J5-1

The sand and gravel horizons that are encountered in 8H14 (Figure 4.2-7), are also unique from other boreholes and probably owe their origin to the depositional environment of the Phokwane River that drains towards the Harts River. A similar gravel horizon was encountered in 8L3 and are probably also fluvial deposits from stream drainage from the eastern hills.

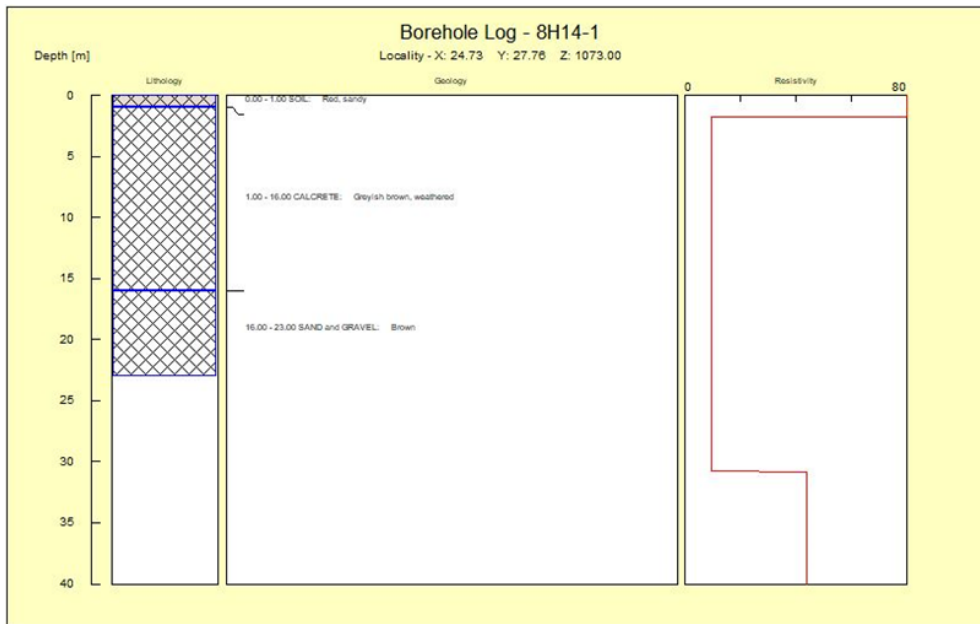


Figure 4.2-7: The comparison of the geology with resistivity of Borehole 8H14-1

When comparing the geology with the layer resistivities, four groups of layers can be distinguished:

a) The unsaturated soil horizon:

This is a layer of pronounced high resistivity encountered at the surface. The resistivities of this layer varies between 18.9 to 349 Ωm . It may be followed by a layer of lesser resistivity that might indicate a clay horizon (Figure 4.2-6), or it may have a clean break at the waterlevel (Figure 4.2-7). This unsaturated zone is expected to exhibit a complex electrical footprint because of the interaction between the degree of saturation (see Figure 2.4-1), and the physical properties of the soil, hence the wide variation in resistivity encountered.

b) The saturated alluvium horizon:

The layer resistivities of this horizon varies between 9 and 66 Ωm . It consists mainly of soil with interspersed gravel layers. The lower resistivities can be compared with soft calcrete occurrences (Boreholes 8H14 (Figure 4.2-7), 5L7, 2L7, 1L15), and resistivities of up to 66 Ωm with hard calcrete occurrences (5L7 (Figure 4.2-8), 2E11). Resistivities associated with sand and gravel show resistivities in the 16-37 Ωm range depending on the assumed clay content.

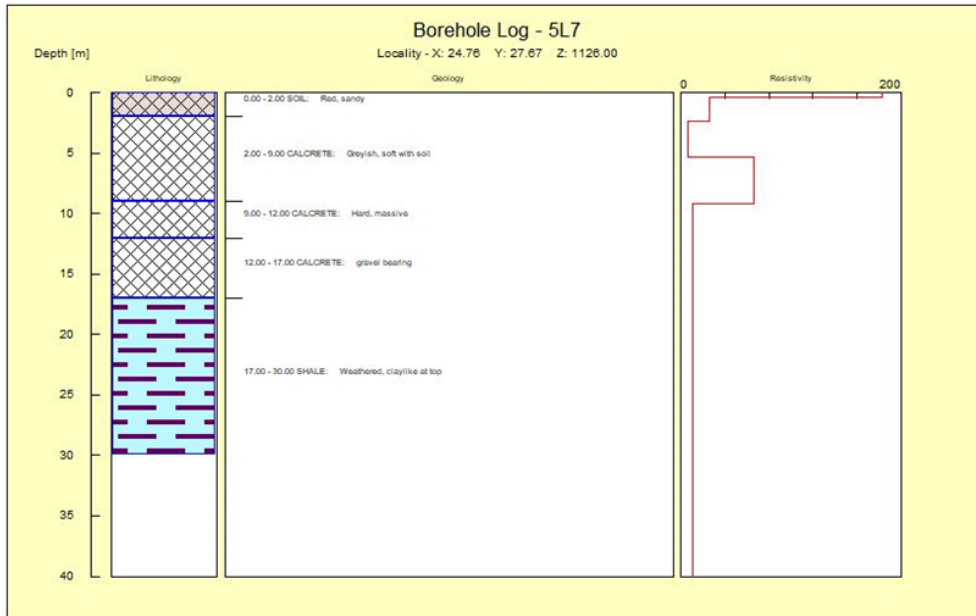


Figure 4.2-8: The comparison of the geology with resistivity of Borehole 5L7

c) The shale horizon:

The lowest resistivities recorded during the inverse modelling, are correlated with the shale horizon. Resistivities range between 6 and 18 Ωm . These are very low resistivity values if taken in consideration that the shale is not weathered. However, from borehole logs some mineralization in the shale is recorded, and this might explain this phenomenon. The layer resistivities in boreholes 2J14 and 6L16 are somewhat higher at 31.7 and 28 Ωm respectively. The fact that these boreholes lie closest to the bottom of the Harts river valley, and top of the succession, might be an indication of facies change in the lithological succession.

d) The bedrock:

At VES sites where the sounding intersected the bedrock, very high layer resistivities were obtained through the inverse modelling process ($>145 \Omega\text{m}$). This shows as a very prominent layer (Figure 4.2-5) at the bottom of the layer resistivity plot with the geology. The very high resistivity contrast with the overlying shales is responsible for this feature.

The geology was also correlated to the resistivity in resistivity profiles that were compiled. The position of these profiles are shown in Figure 4.2-1. These profiles cover the majority of the investigated boreholes, and some boreholes on the fringes were omitted for the sake of clarity. These profiles are to present the correlation of the geology and resistivity. The continuation and variation of the layers is evident.

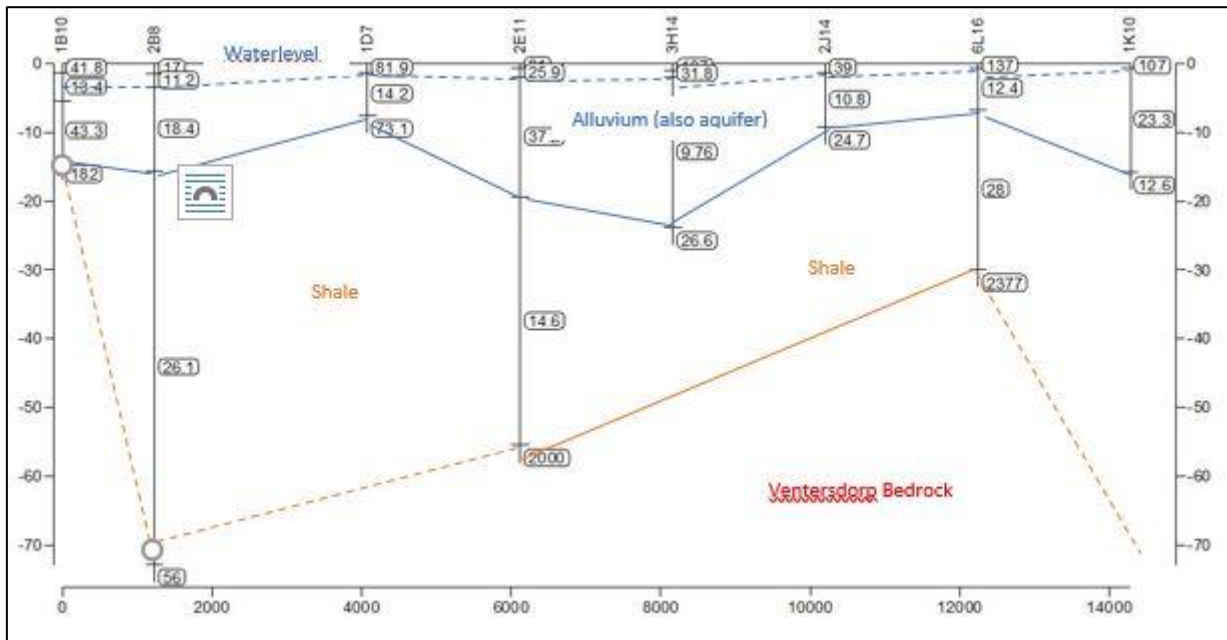


Figure 4.2-9: Profile A; The continuation of geology and resistivity layers; Boreholes 1B10 to 1K10

In Figure 4.2-9, the thickness and resistivities of the alluvium layer in relation to the underlying geological layers is shown. This profile covers the southern end of the project area. Both the alluvium layer and shale layers are highly conductive and meaningful inverse modelling of the resistivity layers could only be done with the borehole geology as measure. No prominent layering in the alluvium profile could be discerned. The shale contact with the Ventersdorp bedrock is interpreted as not all boreholes intersected this boundary.

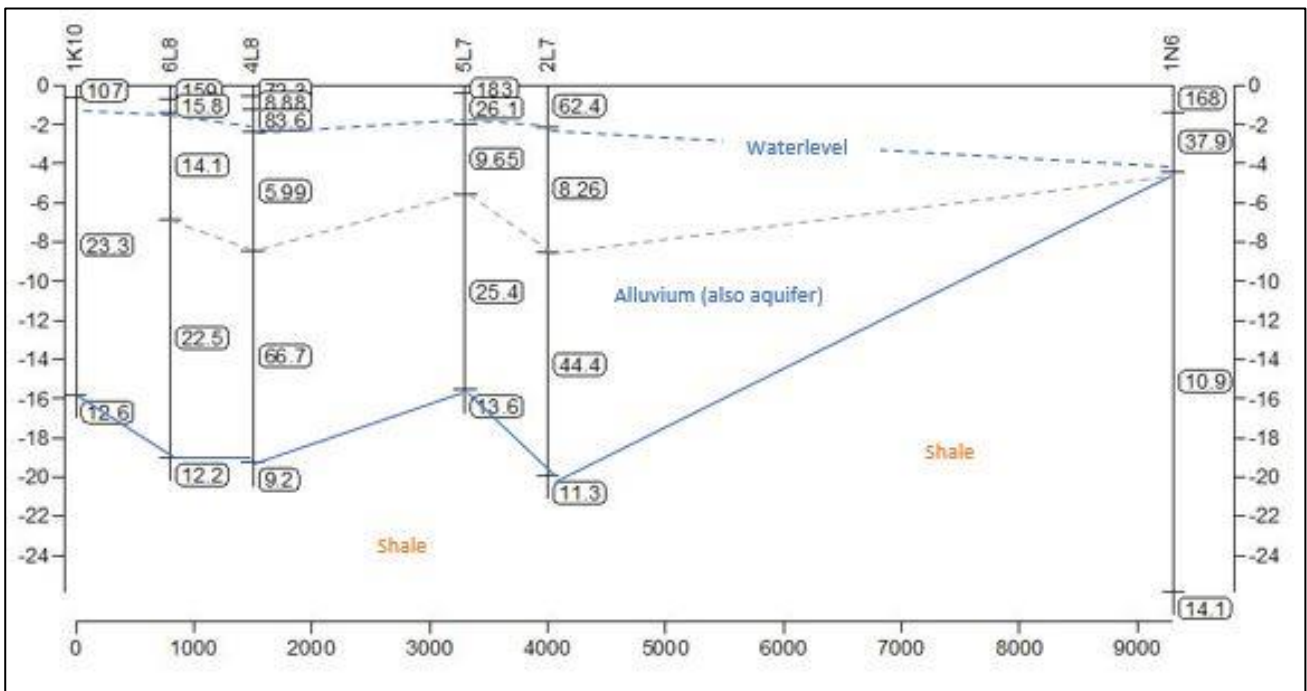


Figure 4.2-10: Profile B; The continuation of the geology and resistivity layers; Boreholes 1K10 to 1N6

Profile B (Figure 4.2-10), is a South-North continuation of Profile A. This section displays prominent layering of the alluvium layer as defined by geology and confirmed by the modelled resistivity layers.

The top layer is defined by low resistivity values (6-14 $\Omega.m$), while the bottom where more gravel and solid calcrete is encountered, by higher resistivity values (22-44 $\Omega.m$). It also shows the discontinuation of the alluvium layer to the eastern boundary of the project area. The resistivities of the shale layer show very low values of between 9 and 12 $\Omega.m$. No Ventersdorp contact zone is modelled in this profile. The aquifer layer will then be defined by the sum of the Dar Zarrouk parameters of the two layers.

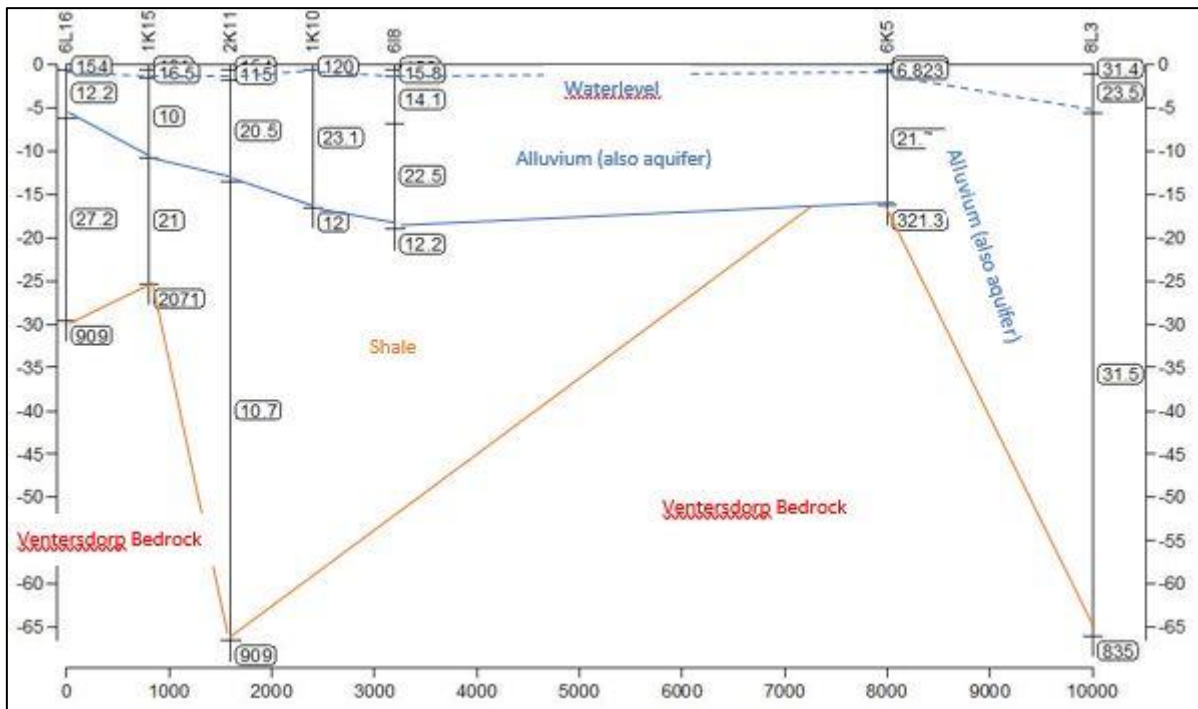


Figure 4.2-11: Profile C; The continuation of geological and resistivity layers; Boreholes 6L16 to 8L3

Profile C (Figure 4.2-11), covers the project area in a West to East direction and crosses Profiles A and B at Borehole 1K10. Although also present in Profile B, Borehole 6L8 is included due to its close proximity to this profile. It is evident through the geology that the alluvium layer thins towards the bottom of the valley at Borehole 6L16. Higher resistivity values (21-31 $\Omega.m$) in the alluvium layer correlates with those of the gravel and solid calcrete layers in Profile B. The low resistivity values of the shale layer correlate with those of Profiles A and B. A rise in resistivity towards Borehole 6L16 indicates the hypothesised facies change. The depth of the Ventersdorp bedrock as indicated in Profile C is an inferred contact due to lack of sufficient geological data.

In Profile C the geology of three boreholes was interpreted. 1K15 and 2K11 are boreholes where pump testing for this project was done, while borehole 6K5 is an accessible borehole where a VES sounding was done. The inverse modelling to obtain the layer resistivities for these locations was constrained by using interpolation of geological information of boreholes either side of them.

4.2.2 ERT Profile

As a definite facies change in the Dwyka geology, from tillite to shale, is observed in outcrops, an ERT profile was done across the project area to detect possible boundaries of such change. The ERT electrode spacing of 5m was chosen to obtain a continuous resistivity profile of relatively good resolution and depth. The results of the profile are presented in Figure 4.2-12. This profile is analogous to Profile C (Figure 4.2-11), and the shale layer according to borehole geology was plotted. As both the alluvium and shale layer exhibit very low resistivities of overlapping range, it is very difficult to distinguish the contact between the two layers. The resistivity contrast on the contact with the Ventersdorp bedrock however, is very clear. On the eastern side the slope at the location of borehole 8L3, the Ventersdorp is evident as the bedrock with a steeply dipping slope. This is replaced by the very conductive shale layer to the west. This shale layer thin out towards the west and the lower valley, and highly resistive bedrock is encountered at shallower depths. The contact with this highly resistive bedrock is not a flat floor as expected, but seems to be of an undulating nature. No obvious facies changes reflected in the resistivity profile could be interpreted.

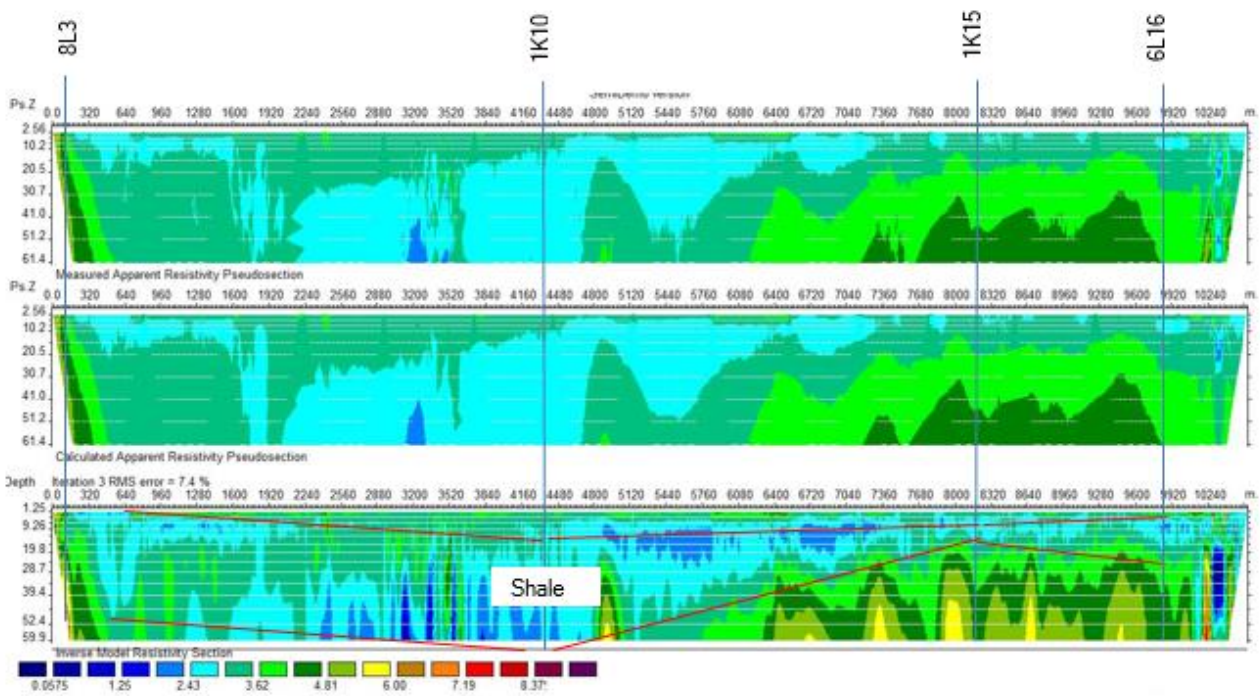


Figure 4.2-12: The ERT profile from east to west

4.3 PUMPING TESTS

During the course of this study, the opportunity presented itself to gather data from four pumping tests. The tests were commissioned by a local farmer to test the yield of newly drilled and existing boreholes. Two boreholes were freshly drilled, and a geological log could be compiled from borehole samples. Several limitations were experienced during the pumping tests. These were:

- The pumping test contractor did not apply a scientific approach to conducting the pumping tests.
- Drawdown during the pumping tests was difficult to measure due to cascading in the borehole.
- Borehole construction (casing depth) information are not available.
- The pump was not equipped with a foot valve which enables the water in the rising pipe to flow back into the borehole at cessation of pumping.

Despite these limitations, accurate measurements during the recovery period could be taken.

4.3.1 The pumping test method

A very short version of the constant rate pumping test was applied on all four boreholes.

The contractor's modus operandus entailed the initial pumping of the boreholes at a high rate to exceed the yield of the borehole. As soon as air gushing is observed, the engine was throttled back to about two thirds of the initial revolution rate (rpm). This stage occurred during the first five minutes of the pumping test period.

The constant rate pumping period followed for about one hour. The pumping rate was monitored using the bucket and stopwatch method every fifteen minutes. Minor adjustments were made to the engine rpm to maintain a constant pumping rate.

After pumping for an hour, the pump was stopped, and the recovery period commenced. It was only during this period that accurate water levels could be measured. The recovering in water level was monitored to about +/- 20 cm of the rest water level.

4.3.2 Interpretation of the pumping tests

Using the Theis method (Section 5.2.3.1), the recovery data were plotted on semi-log paper. The results are attached in Appendix C.

Three of the boreholes exhibited the same three stage recovery pattern as shown by borehole 5L7 (Figure 4.3-1). The odd one out, borehole 2K11, will be discussed separately.

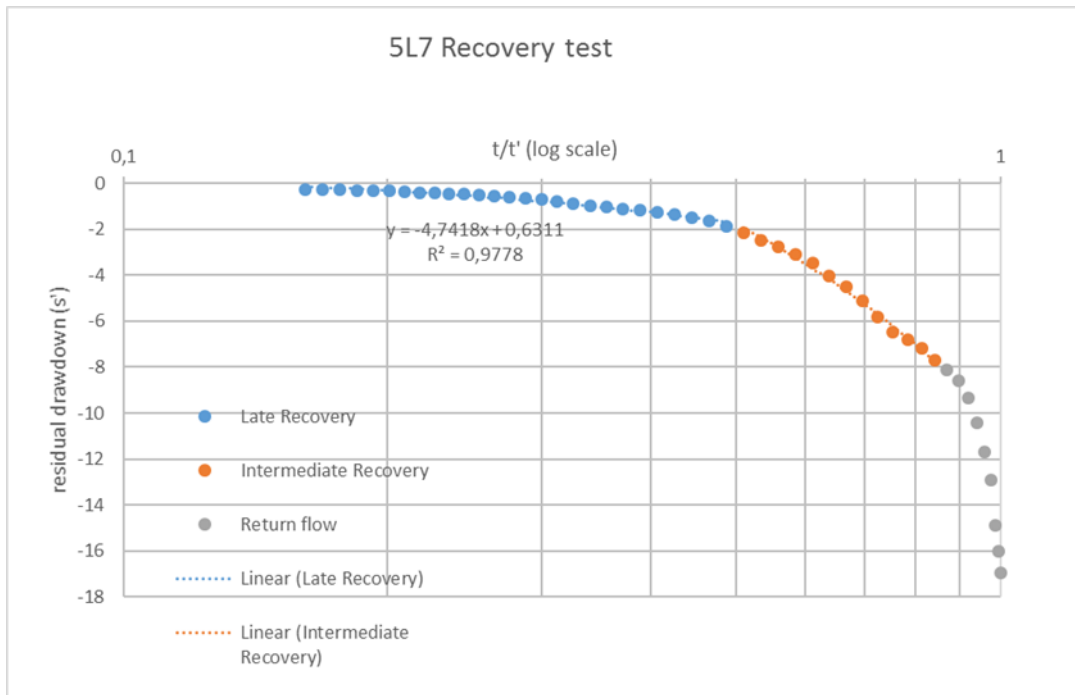


Figure 4.3-1: Theis curve of recovery data 5L7

In Figure 4.3-1 it is evident that the first stage of recovery is dominated by a quick rise in water level. This is due to the return flow of water in the rising pipe of the pump after the pump has stopped.

The second stage exhibits a linear pattern, indicating a constant recovery. This stage is representative of the intermediate stage present during the drawdown in an unconfined aquifer. The assumptions of the Theis equation is not valid and the equation cannot be applied (see also Section 2.5.1.2).

The third stage is the late recovery period during which the recovery slowed significantly but at a constant rate as suggested by the fitted trend line. The assumptions of the Theis equation is valid and can therefore be applied.

The recovery data of Borehole 2K11 (Figure 4.3-2), displays a more rapid transition between the initial return flow stage and the late recovery stage. The intermediate recovery stage could not be clearly identified. The normal recovery curve is inclined to recover to the origin of the graph where time and drawdown is zero. In the case of Borehole 2K11, the recovery curve will intersect the time axis way before the origin is reached, indicating a recharge to the borehole in addition to the normal flow (Also see Figure 2.5-10). It must be noted that this borehole is situated within ten metres of an irrigation reservoir which can explain this occurrence. The hydraulic parameters calculated will probably be influenced by the additional recharge.

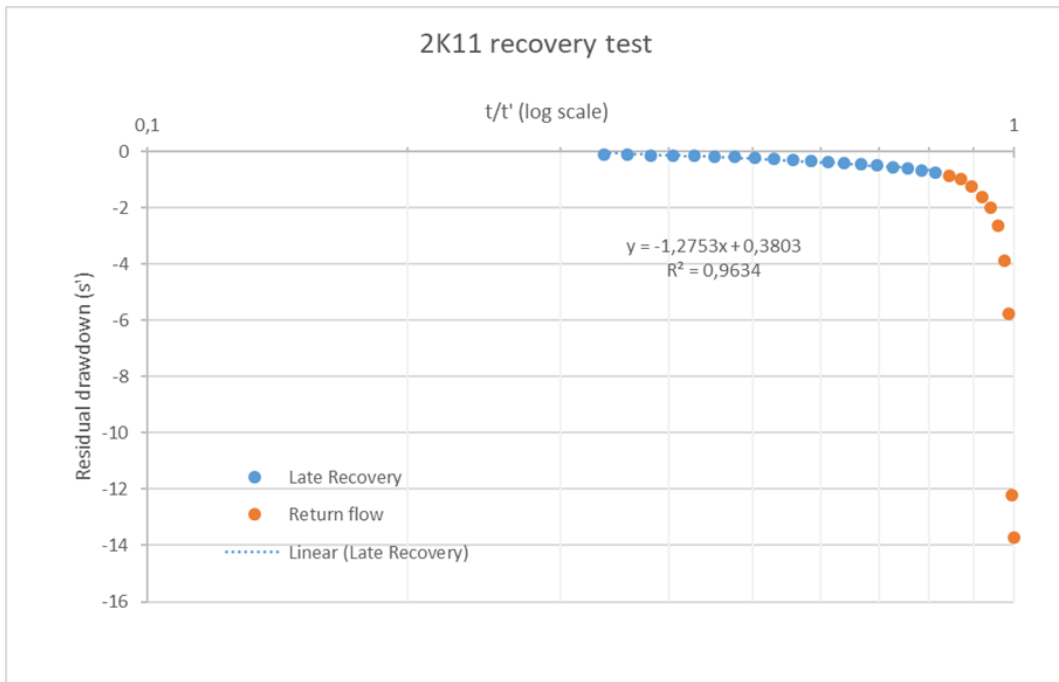


Figure 4.3-2: This curve of recovery data; 2K11

Using the equation $\Delta s = \frac{2.30Q}{4\pi KD}$ and Δs the slope of the linear regression line from the graphs, the transmissivities and hydraulic conductivities of the boreholes were calculated. This is presented in Table 4.3-1.

Table 4.3-1: Transmissivity and Hydraulic conductivity calculated from pumping test

	Transmissivity (KD) m ² /d	Thickness of aquifer (D) m	Hydraulic conductivity (K) m/d
1K15	158,19	30	5,27
2L7	106,71	25	4,27
5L7	13,34	25	0,53
2K11	117,78	31	3,80
		1K15 & 2K11 conductivities calculated from b/hole depths	

CHAPTER 5: RELATIONSHIP BETWEEN THE GEOHYDROLOGICAL, GEOPHYSICAL AND PHYSICAL PARAMETERS

The complexity of the Vaalharts Aquifer became evident as the investigation progressed. From the resistivity, geological and geohydrological data gathered, an attempt can now be made to establish the relationships between the different parameters. These relationships can ultimately be used to estimate the hydraulic and physical parameters through the application of electrical methods. (Batayneh, 2009; Coetsee, 1994; Kazakis *et al.*, 2016; Niwas *et al.*, 2011)

The interconnection between the measured and estimated data of this study, can be visualised in the flowchart presented in Figure 4.3-1.

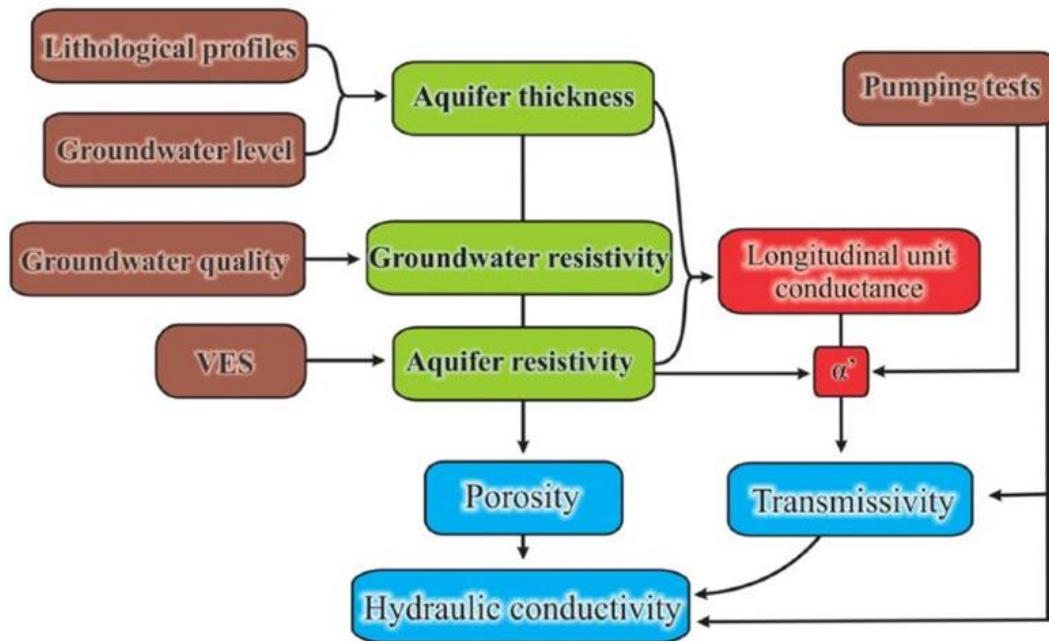


Figure 4.3-1: Flowchart showing the interconnection between the measured and estimated data of this study (after Kazakis *et al.*, 2016)

The compiled data set is presented in Table 4.3-1. From this data set the regression relationships will be discussed in order to establish an empirical relationship between the hydrogeophysical parameters. This discussion will describe the factors that govern groundwater and electrical flow in the aquifer, and ultimately establish the parameters of the conceptual aquifer.

Borehole /VES no.	B/H depth (m)	Thickness of aquifer inverse modelled (d) in (m)	Aquifer resistivity modelled (Ω.m)	Historical EC (mS/cm)	Water EC (mS/cm)	Water resistivity (Ω.m)	Formation factor ρ_a/ρ_w	T pumptested (m ² /day)	K pumptested (m/day)	R Transverse Resistance (hp)	C Longitudinal Conductance (h/p)	T' calculated (m ² /day)	K' calculated (m/day)
1B8-1	41	24,74	17,81		1,22	8,20	2,17			440,530	1,4158	163,2538	6,5988
1B10-1	24	12,84	33,86		1,36	7,35	4,61			434,800	0,0506	-80,1454	-6,2419
1D7-1	20	6,23	14,20	2,25	2	5,00	2,84	194	9,7	88,470	0,4387	43,5424	6,9891
2E11-1	70	17,5	37,02	1,49	1,52	6,58	5,63			647,850	0,4727	46,9153	2,6809
1315-1	20	11,24	25,07		0,78	12,82	1,96			281,770	0,4762	47,2586	4,2045
8H14-1	23	23,9	8,98	1,90	1,49	6,71	1,34	1,2	0,05	214,720	2,2541	223,7102	9,3603
2J5-1	20	20,82	78,92	1,74	2	5,00	15,78	123	6,15	1643,200	0,5881	58,3668	2,8034
2J14-1	27	8	10,80	2,18	1,76	5,68	1,90	58	2,15	86,400	0,7407	73,5156	9,1894
1K10-1	101	15	23,61	1,20	1,2	8,33	2,83	31,6	0,3	354,160	0,6524	64,7442	4,3163
2K11	31	13,7	18,09		1,63	6,13	2,95	117	3,8	247,800	0,5619	55,7668	4,0706
1K15	30	14,8	8,85		1,9	5,26	1,68	158	5,27	130,950	1,3918	138,1259	9,3328
8L3		60,5	31,90		2,11	4,74	6,73			1929,950	1,8966	188,2252	3,1112
2L7	30	17,85	31,34		2,29	4,37	7,18	106	4,27	559,437	1,0376	102,9805	5,7692
5L7	28	13,55	21,25		2,99	3,34	6,35	13	0,53	287,943	0,7629	75,7109	5,5875
4L8	65	18,07	46,31		1,82	5,49	8,43			836,759	1,1933	118,4269	6,5538
6L8	45	17,61	19,92		1,8	5,56	3,59			350,781	0,9259	91,8927	5,2182
6L16	36	6,41	11,88	2,59	1,73	5,78	2,05	4,2	0,1	76,136	0,4952	49,1428	7,6666
1N6-1	20	3,04	38,27	2,17	1,23	8,13	4,71			116,353	0,0810	8,0392	2,6445
												wayward values not used	

Table 4.3-1: Compiled data set with actual and estimated values of K and T

5.1 FORMATION FACTOR

The formation factor (FF), is a factor of proportionality as presented by Archie (1942) in Worthington (1982). It is also known as the tortuosity factor that presupposes that the electrical current follows the same paths as the water. This is discussed in Section 2.4.1.1:

$$FF = \frac{\rho}{\rho_w} = a\phi^{-m} \tag{Equation 5.1-1}$$

According to Worthington (1982), the formation factor of a reservoir rock is an intrinsic quantity which does not vary with the salinity of the saturating electrolyte. A direct relationship between the aquifer resistivity and the water resistivity will indicate a constant of the product of $a\phi^{-m}$.

The plot of apparent resistivities against the water resistivities is presented in Figure 5.1-1. It is evident that no correlation exists. As the factors of a and m are considered to be constant, porosity will be the varying factor. This is consistent with the heterogeneous conditions within the alluvium of the Vaalharts Aquifer of layers of gravel, silt calcrete and clay. Thus, the formation factor is of little consequence in this environment.

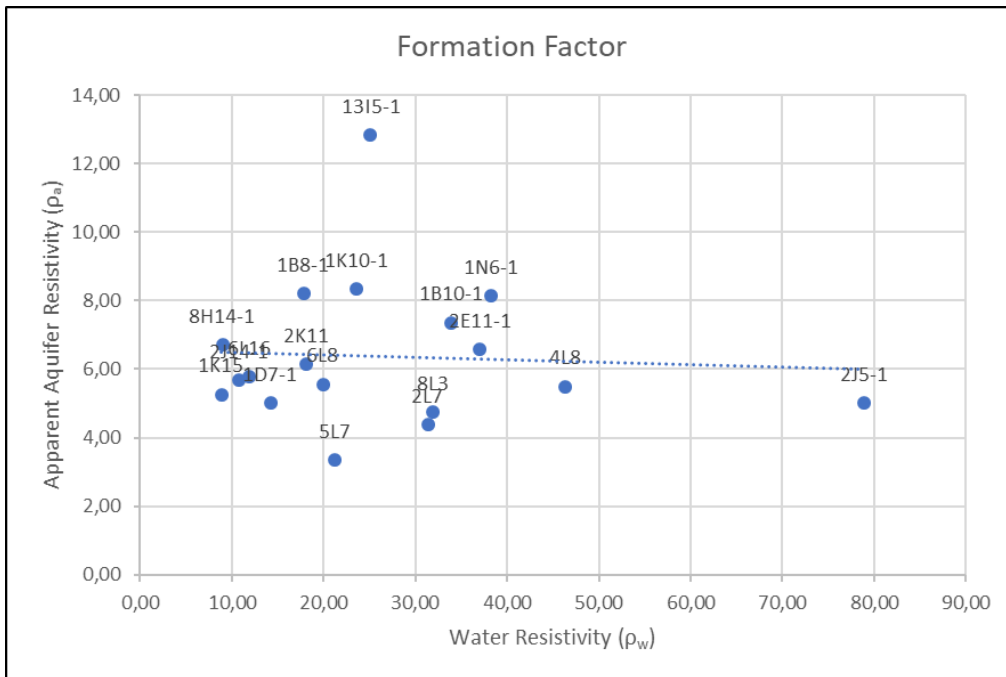


Figure 5.1-1: Formation Factor of the Vaalharts Aquifer

5.2 REGRESSION RELATIONSHIPS WITH K AND T

Using the Dar Zarrouk parameters, transverse resistance (R) and longitudinal conductance (C), of the aquifer layers, the relationship with the transmissivity and hydraulic conductivity values are investigated.

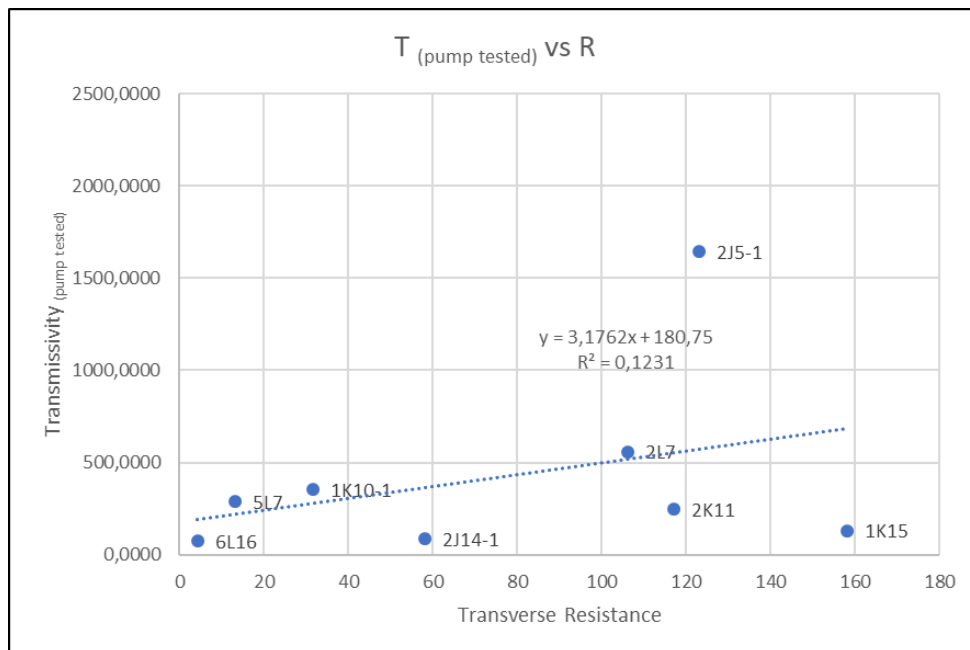


Figure 5.2-1: Correlation of Transmissivity with Transverse Resistance

In Figure 5.2-1, the transverse resistance (R) is correlated with the actual transmissivity values (T) obtained through pumping tests. No correlation between T and R exists. It is also not unexpected as

the form of the VES curves (no highly conductive layer beneath resistive layer), does not support this relationship.

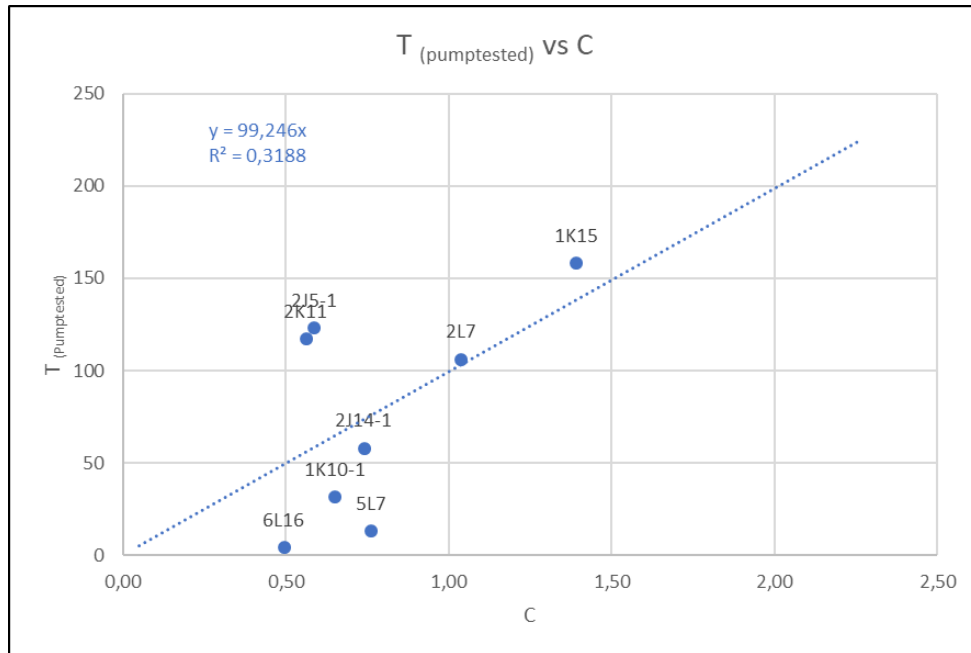


Figure 5.2-2: Correlation of Transmissivity (pump tested) with Longitudinal Conductance

The correlation of T with the longitudinal conductance (C) is presented in Figure 5.2-2. A very weak correlation ($R^2 = 0.3188$) is found. It must be noted that two points, those of 1D7 and 8H14 is not included because of abnormal wayward values. The weak correlation may be the result of the small sample size available. An important consideration is the fact that the regression line passes through the origin of the graph, supporting the validity of the factor β as used in the equation of Niwas *et al.* (2011):

$$T = \beta C; \quad \beta = K/\rho \quad \text{Equation 5.2-1}$$

From Figure 5.2-2, the value of β is found to be 99.246. Using the above equation, the T -values of the VES points were calculated using the longitudinal conductance (Table 4.3-1). The calculated T -values were then correlated with the pumping tested T (Figure 5.2-3) to test the calculation. A weak correlation of about the same order that exists between T and C were found. The reason being the same - the small sample size available.

The correlation between T and C is supported by the findings in Mazac *et al.*, (1985) and Niwas and de Lima, (2003). That is, that the correlation between T and C will exist when a layer of lesser resistivity is underlain by a layer of high resistivity. Because of the relative thick layer of low resistivity, this characteristic is enhanced.

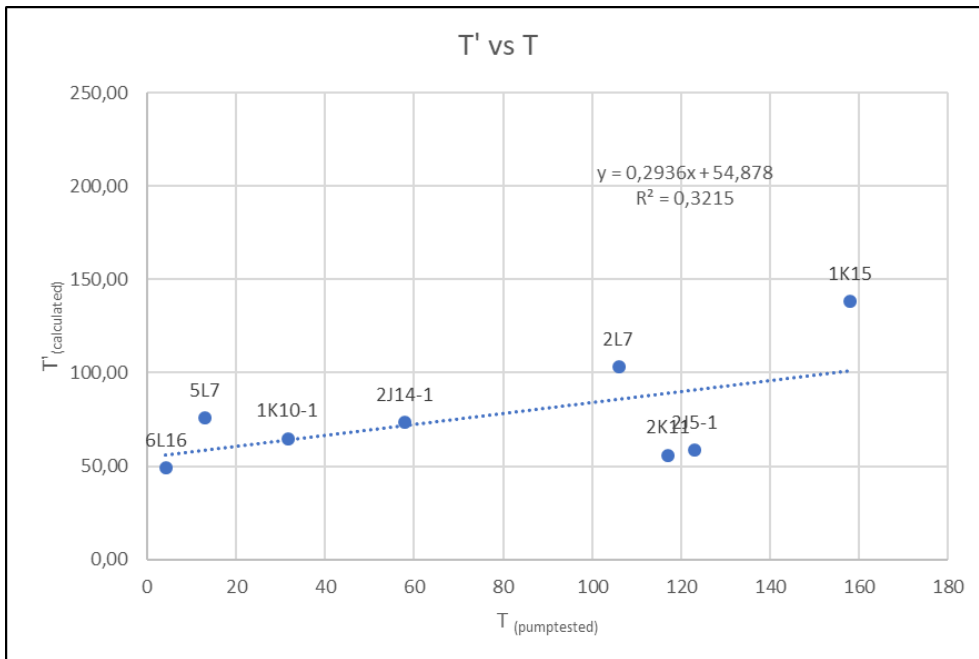


Figure 5.2-3: The correlation of transmissivity (calculated) with transmissivity (pumptested)

Following the correlation of the transmissivity with the longitudinal conductance, the relationship between the hydraulic conductivity and longitudinal conductance might also be of importance. This correlation is presented in Figure 5.2-4. No correlation is evident.

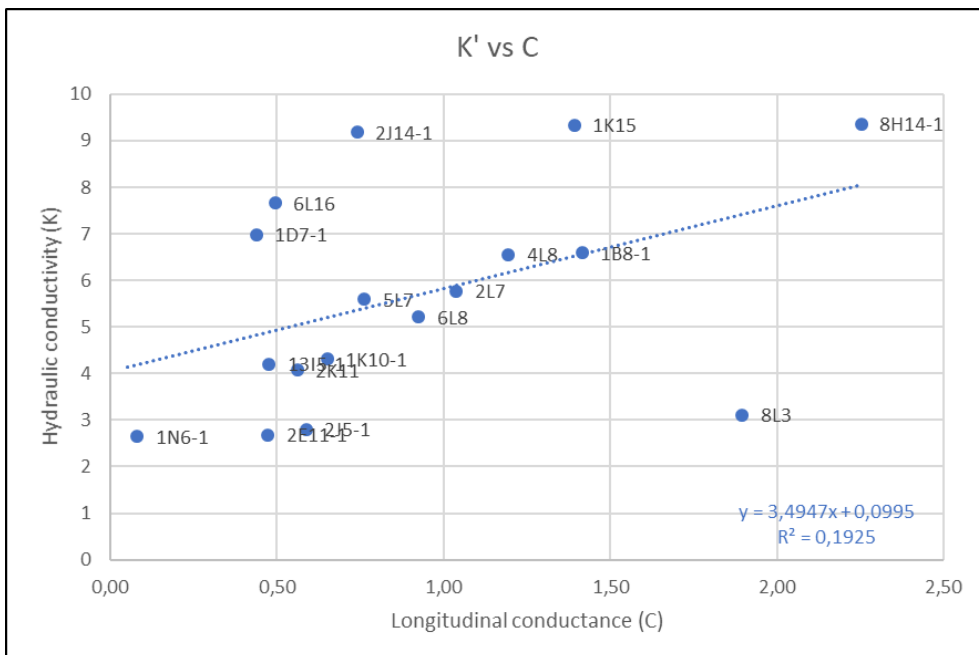


Figure 5.2-4: Correlation of hydraulic conductivity with longitudinal conductance

From Equation 2.5-25, the constant of proportionality β , is dependent on the ratio of K and ρ_a . Thus the correlation between the two is explored in Figure 5.2-5. A negative correlation can be seen ($R^2 = 0.4338$). This is about the same order of the correlation as between T and C .

The negative correlation that exists, is normal of resistivity variation within a lithological unit, (for instance clay or silt or gravel (Figure 2.5-13)), with a positive correlation between lithological units (from clay to silt to gravel - Mazac *et al.*, 1985). Although the negative correlation predominates, a case may be made for a positive correlation between points 6L8, 5L7, 2L7 and 4L8. The scatter evident in the graph, may be due to different mixes of clay, silt and gravel. The reason for this scatter also apply to the formation factor ($FF=\rho^a/\rho_w$), and a correlation between K and FF will produce an even more scattered picture with no correlation. This relationship between K and FF is then not considered.

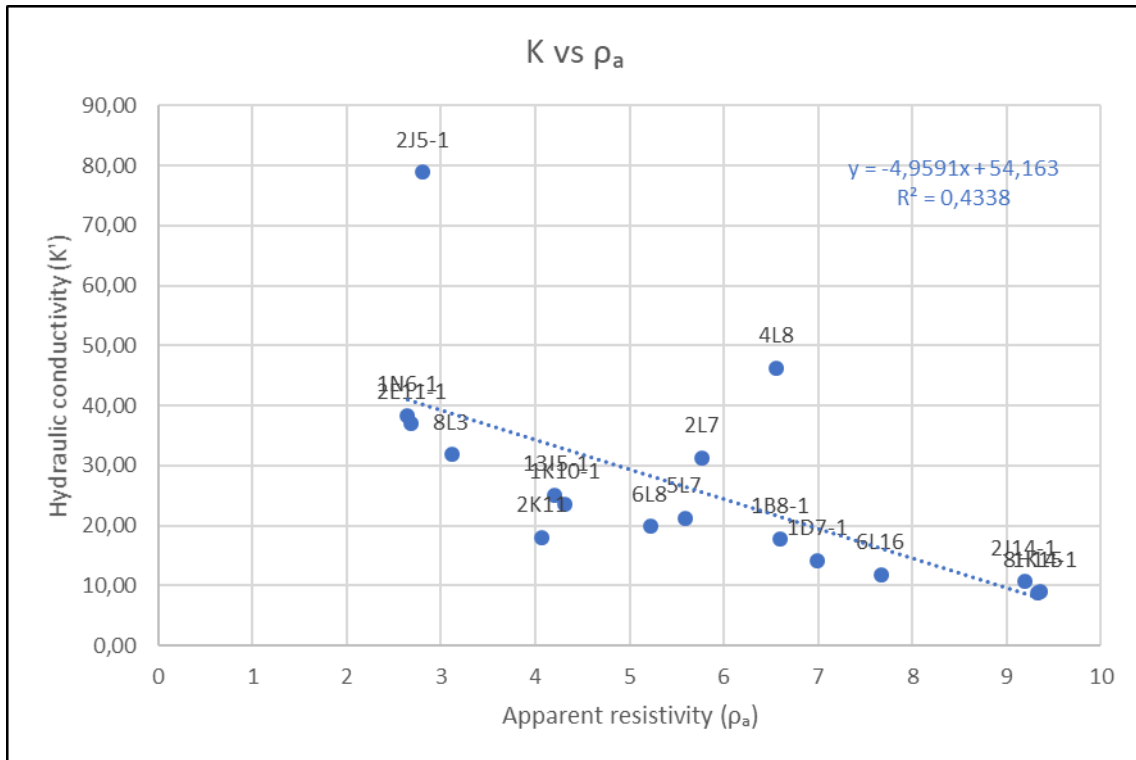


Figure 5.2-5: Correlation of Hydraulic Conductivity with Apparent Resistivity

5.3 NOTES ON THE CALCULATION OF POROSITY

The formation factor (FF) is used to determine if the characteristics of a lithological unit can be described by Archie's Law. Although Archie's Law can be used to calculate the porosity of non-conforming units where the rock matrix is not perfectly insulating, Worthington, (1982) advise against this as interpreted values of porosity and water saturation may be grossly in error.

According to the finding in Section 5.1 regarding the FF , Archie's Law in its pure form cannot be used to determine porosity of this aquifer.

5.4 NOTES ON THE EC, TDS AND DETECTION OF SALINATION USING GEOPHYSICAL METHODS.

With reference to Table 5.1-1, the water EC measured in the boreholes during this study, is generally lower than the “historical EC” that was recorded during previous investigations. Although seasonal variations do occur (Ellington *et al.*, 2004; Verwey, 2009), the forecasted increase in salination seems not to have taken place. The recent EC measurements also fluctuate no more than 20 mS/m from the historical measurements.

The EC of a saline solution is dependent on the concentration of cations and anions dissolved in water (Section 2.4.1.3). The EC can be calculated from a chemical analysis of a water sample, or the TDS obtained from a gravimetric analysis. Estimating the TDS from an EC measurement is also done using a predetermined conversion factor (C) in the formula:

$$\text{TDS}=\text{C}*\text{EC}$$

This factor has been established in the studies of Ellington (2004) (factor = 7.62) and Verwey (2009) (factor 7.699+5.4) and is unique to the Vaalharts Irrigation Scheme.

Regarding the detection of a variation of EC in the Vaalharts aquifer by means of geophysical investigations, a change bigger than the background variation must take place. If the expected increase in EC of the irrigation water of 20 mS/m (Du Preez, 2000) occurs, against background values of 120 to 299 mS/m, the increase might be masked by seasonal variations, and not be detected as such.

5.5 SYNTHESIS OF THE RESULTS - THE CONCEPTUAL AQUIFER

With the results of the preceding regression analysis, the characteristics of the Vaalharts Aquifer can be conceptualised.

From this investigation, the shale layer can be regarded as the aquiclude to the aquifer. It can at best act as an aquitard as hydrological- and electrical parameters are positively correlated to the alluvium layer. High transmissivities reported by Ellington (2004) through pump testing and attributed to fracturing in shale, seems to be rather because of high transmissivities encountered in the alluvium. This supports the high variability of the hydraulic parameters due to the depositional history of the alluvium.

That the aquifer is very heterogeneous in nature as confirmed by geology and depositional environment, is also reflected by the absence of a formation factor as electrical parameter.

From the regression analysis, it can be concluded that the longitudinal conductance is the more representative electrical parameter describing electrical flow in the aquifer. The low resistivity (presumed clay content) in the alluvium, the very low resistivity of the shales and the resistivity contrast with the bedrock, are thought to be responsible for this characteristic.

The constant of proportionality (β) that is derived from Figure 5.2-2, can be used to estimate T and K from an electrical investigation, greatly enhancing the practical application of the electrical method. The practical application is evident in that calculated values of T and K from VES points is used to compile the contour maps presented in the following Figures 5.1-8 to 5.1-10. Although these maps are produced with very sparse and widely dispersed data, it gives a reference point for future investigations. Any data added to the database in future will enhance the accuracy of these maps and the estimation of geohydrological parameters.

As transmissivity and hydraulic conductivity is directly related, it stands to reason that the contour maps (Figures 5.1-8 and 5.1-9) will mirror this relationship. It can be seen that higher transmissivity and hydraulic conductivity values are both found in the west towards the lower elevation of the Harts River valley.

Because the hydraulic conductivity is calculated from the transmissivity by dividing by the thickness of the aquifer, an inverse relationship will exist. This is evident in Figure 5.1-10 where the higher thickness of the aquifer corresponds to lower transmissivity and hydraulic conductivity values. The areas of probable thicker river gravels such as at Borehole 8H14 may be anomalous from the surroundings by having high hydraulic conductivity as well as high thickness of the aquifer.

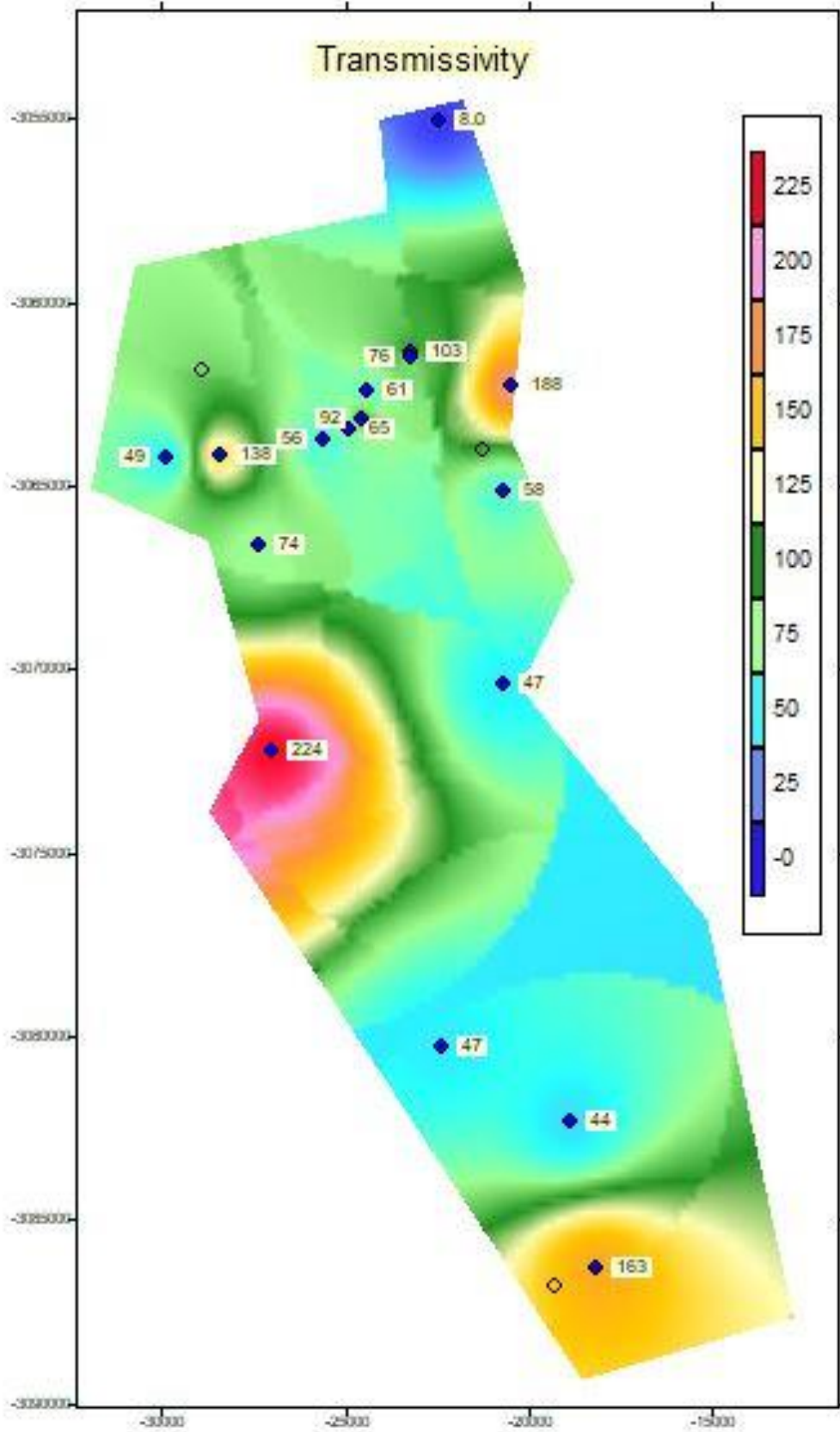


Figure 5.5-1: Contour map of Transmissivity encountered in the Vaalharts Aquifer

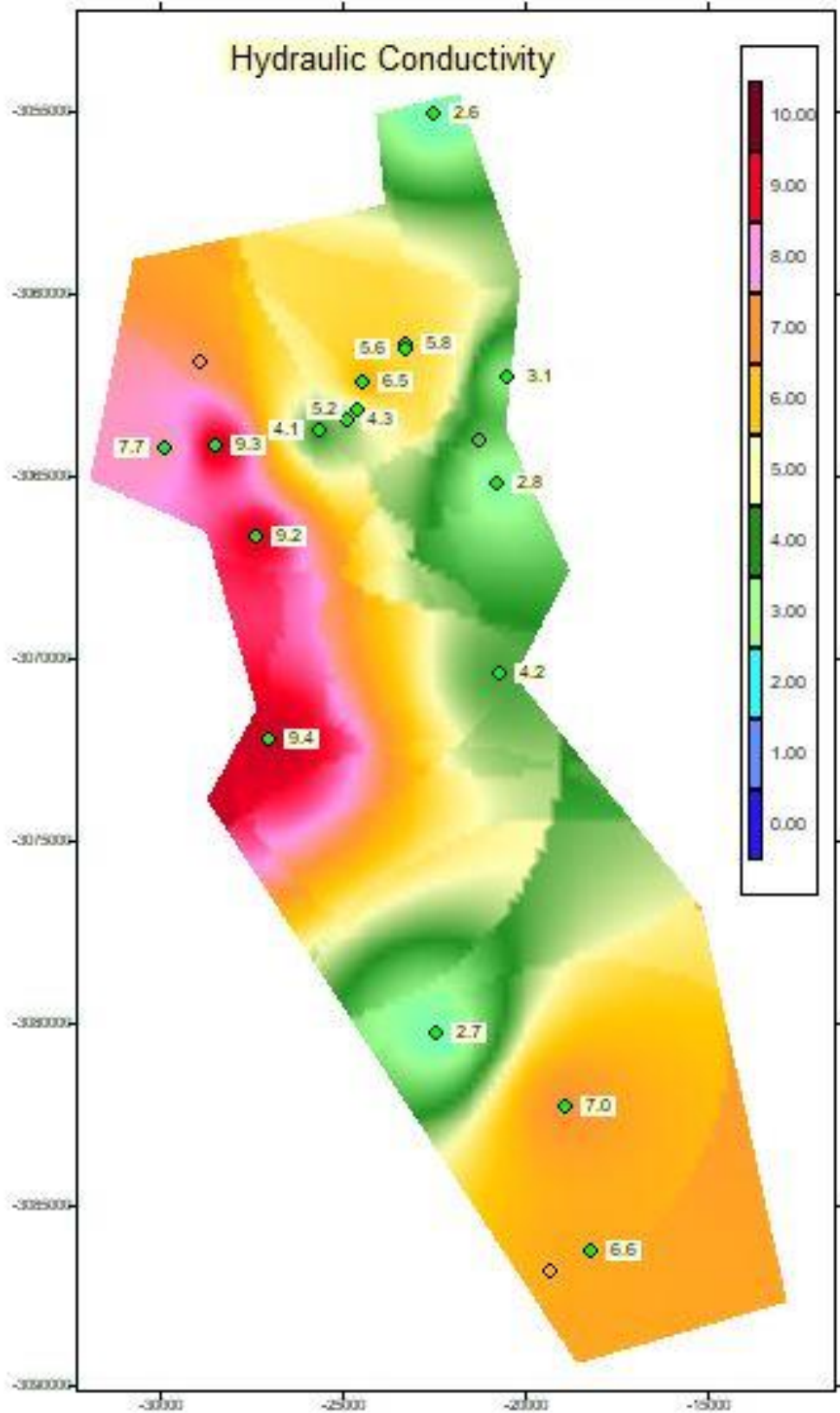


Figure 5.5-2: Contour map of Hydraulic Conductivities encountered in the Vaalharts Aquifer

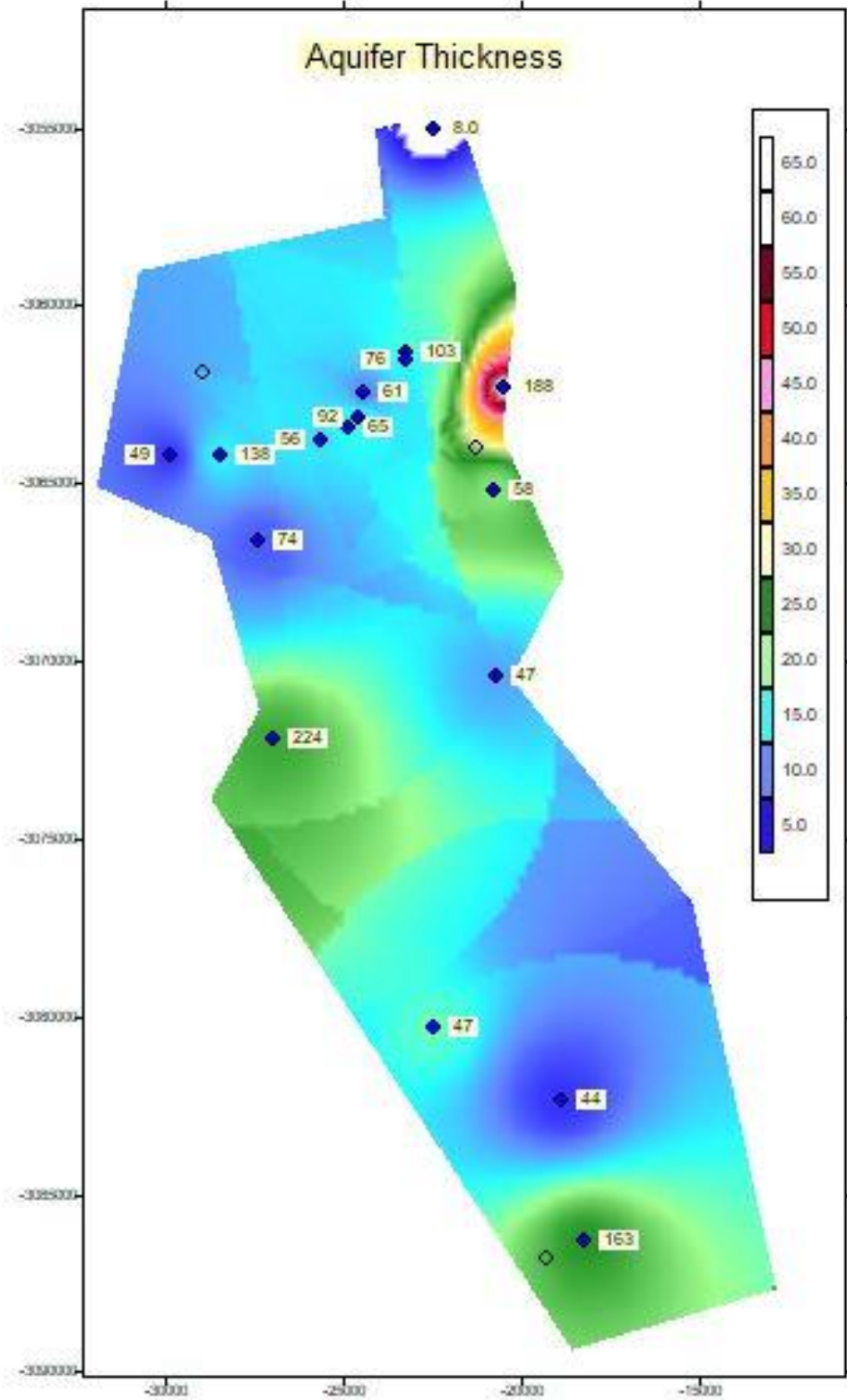


Figure 5.5-3: The modelled aquifer thickness in the Vaalharts Aquifer

CHAPTER 6: CONCLUSIONS AND RECOMMENDATIONS

6.1 CONCLUSIONS

No record of any geophysical surveys in the Vaalharts area could be found during the literature study. In fact, no literature of any similar ventures such as this project was found anywhere in South Africa. The only exception was the thesis of Coetsee (1994) on the geohydrophysical relationships of the Atlantis Aquifer. Since 1994, work done by Niwas and de Lima (2003), Niwas *et al.* (2011), and Niwas and Celik (2012), led to a clearer understanding of the geohydrophysical relationships and the application thereof.

Applying their methods to this project, the relationship between the geohydrological, geophysical and physical parameters of the Vaalharts Aquifer could be established. Although resting on relatively weak correlations, the conclusion could be made that a definite relationship between transmissivity and the longitudinal conductance exists for the Vaalharts Aquifer. This relationship is based on the factor of proportionality (β) that was calculated during this investigation.

It is also concluded that a relationship between hydraulic conductivity and the apparent resistivity exists. The negative nature of this relationship indicates variation of resistivity within a lithological unit with a rise in hydrological conductivity as lower resistivities are measured. However, positive relationships occurring in smaller areas should not be ruled out.

Because of the complex nature the aquifer, the porosity could not be calculated using Archie's Law because a formation factor for the porous medium could not be determined. Other empirical formulas such as those of Waxman and Smits (1968) and later authors might be used to compensate for the presence of clay, but is expected to be only of value in very localised areas of the Vaalharts Aquifer.

The lateral and vertical extent of the aquifer can be determined using electrical methods. The importance of using borehole geology in constraining the inverse modelling of the layer resistivities is again underlined in this investigation. Because of the absence of a resistivity contrast between the aquifer and shale layer, the effects of equivalence and suppression make the partition of these layers nearly impossible without the correlation with known geology. The resistivity contrast between the shale and the Ventersdorp bedrock, however, is very high but still needs to be correlated to known geology.

6.2 RECOMMENDATIONS

As this project has by no means exhausted all the aspects of the relationship between the geohydrological, geophysical and physical parameters of the Vaalharts Aquifer, recommendations for further study might include the following:

- Studies to investigate the isotropy/anisotropy of the aquifer.
- Gravimetric analyses of physical borehole samples to obtain grain size distributions. This will quantify the influence of clay in electrical investigations and will provide the basis in porosity calculations.
- Studies to investigate the influence of an increase in the salt load of the aquifer and the resulting effect on the EC and electrical investigations.

Apart from the above recommendations, it is recommended that additional resistivity surveys be done to further characterise the Vaalharts Aquifer. These surveys could be done using smaller electrode spacings to specifically focus on the shallower materials representing the aquifer. The methodology followed in this dissertation should then be used to increase the confidence in the relationships between the different geophysical, physical and geohydrological parameters.

In addition, the resistivity surveys could be extended to other parts of the Vaalharts Aquifer not included in the current study. This will not only increase the understanding of the aquifer and its relation to the geophysical parameters, but could also be important to allow future studies of the salination of the aquifer. The resistivity dataset recorded could be used as background data against which the results of future surveys can be compared to detect changes in the subsurface resistivities and to evaluate the degree to which salination of the aquifer has occurred.

Point injection tests, in conjunction with time-lapse ERT surveys, should also be considered as a method to obtain further insight into the geohydrological parameters affecting flow through the Vaalharts Aquifer. Such injection tests could introduce brines to the aquifer at specific positions, while the temporal changes in the subsurface conductivities could be used to monitor brine migration. From the brine migration rates, information on the aquifer hydraulic parameters may be derived.

If funding can be obtained, the drilling of investigative boreholes will further contribute to the understanding of the Vaalharts Aquifer and its physical properties. Such boreholes will allow insight into the subsurface geological and geohydrological conditions and will allow access to the aquifer for groundwater sampling and hydraulic tests. The boreholes will furthermore allow calibration of the results of VES surveys conducted in the vicinities of the boreholes, which could in turn improve the delineation of the aquifer at positions where no boreholes are present if VES surveys are done at such positions.

REFERENCES

- Barnard, J.; 2013. On-Farm Management of Salinity associated with Irrigation for the Orange Riet and Vaalharts Schemes, Bloemfontein: Ph.D. Thesis, OFS.
- Batayneh, A. T., 2009. *A Hydrogeophysical Model of the Relationship between Geoelectric and Hydraulic Parameters, Central Jordan.* [Online] Available at: <http://www.scirp.org/journal/jwarp> [Accessed November 2017].
- Bear, J., 1979. *Hydraulics of Groundwater.* 1st ed. s.l.:McGraw-Hill Inc..
- Coetsee, V. d. A., 1994. *Hidrogeologiese Verwantskappe vir Akwifere Parameter Identifikasie.* Bloemfontein: Ph.D. Tesis, Dept. van Geohidrologie, Universiteit van die Oranje Vrystaat..
- De Bruyn, W., 2016. *Northern Cape Department of Agriculture* [Interview] 2016.
- Driscoll, F., 1986. *Groundwater and Wells.* Second ed. St.Paul,MN: Johnson Filtration Systems Inc..
- Du Preez, CC; Strydom, MG; Le Roux, PAL; Pretorius, JP; Van Rensburg, LD; Bennie, ATP, 2000. *Effect of Water Quality on Irrigation Farming along the Lower Vaal River: The influence on Soils and Crops.*, Pretoria: WRC Report.740/1/00.
- Ellington, R., 2003. *Quantification of the Impact of Irrigation on the Aquifer underlying the Vaalharts Irrigation Scheme.* Bloemfontein: Institute for Groundwater Studies.
- Ellington, R., Usher, B, Van Tonder, G., 2004. *Quantification of the impact of irrigation on the groundwater resource in the Vaalharts Irrigation Scheme,* Pretoria: WRC Report 1322/2/04.
- Fitzpatrick, R., Thomas, M., Davies, P. & Williams, B., December 2003. *Dry saline land: An investigation using ground-based geophysics, soil survey and spatial methods near Jamestown, South Australia.*; CSIRO Technical Report 55/03.
- Fourie, F.D. (2010). *Investigating flow rates through the fly ash at Sasol's Secunda Plant.* Orpheus Hydrogeophysics. Report No. OHGP2010/08/SSAF.3.
- Frohlich, K. and Kelly, W., 1985. The relation between hydraulic transmissivity and transverse resistance in a complicated aquifer of glacial outwash deposits.. *Journal of Hydrology*, 79(3-4), pp. 215-229.
- Frohlich, R. and Kelly, W., 1988. Estimates of specific yield with the geoelectric resistivity method in glacial aquifers.. *Journal of Hydrology*, 97(1-2), pp. 33-44.
- Glover, P., Hole, M. & Pous, J., 2000. A modified Archie's law for two conducting phases. *Earth and Planetary Science Letters*, Volume 180, pp. 369-383.
- Gombar, O. and Erasmus, C., 1976. *Vaalharts Ontwaterings Projek*, Pretoria:
- Grandjean, G; Cousin, I; Seger, M; Thiesson, J; Lambot, S; Van Wesemael, B; Stevens, A; Samyn, K; Bitri, A; Bernardie, S, 2009. *From geophysical parameters to soil characteristics.*, s.l.: Report No:BRGM/FP7-DIGISOIL-D2.1.
- Haarbron, J., 2015. *Vaalharts Water* [Interview] (June 2015).
- Herman, R., 2001. An introduction to electrical resistivity in geophysics.. *American Journal of Physics*, 69(9), pp. 943-952.
- Herold, A. and Bailey, C., 1996. *Long term salt balance of the Vaalharts Irrigation Scheme,* Pretoria: WRC Report 420/1/96.
- ICRC, 2011. *Technical Review: Practical guidelines for test pumping in water wells.* Geneva, Switzerland: International Committee of the Red Cross.
- Kazakis, N., Vargemezis, G., Voudouris, K., 2016. Estimation of hydraulic parameters in a complex porous aquifer system using geoelectrical methods.. *Science of the Total Environment*, Volume 550, pp. 742-750.

- Keller, G. and Frischknecht, F., 1996. *Electrical methods in geophysical prospecting*. Oxford: Pergamon Press.
- Kent, L. and De Grys, A., 1980. *The Stratigraphy of South Africa. Handbook 8. Part 1: Lithostratigraphy of the Republic of South Africa, South West Africa/Namibia, and the Republics of Bophuthatswana, Transkei, and Venda*. Pretoria: Geological Survey, Dept of Mineral and Energy Affairs, South Africa.
- Kruseman, G. and De Ridder, N., 2000. *Evaluation and Analysis of Pumping Test Data*. Second ed. Netherlands: International Institute for Land Reclamation and Improvement (ILRI Publication 47).
- Loke, M., 2000. *Electrical imaging surveys for environmental and engineering studies: A practical guide to 2-D and 3-D surveys*. [Online] Available at: <http://www.heritagegeophysics.com/images/lokenote.pdf> [Accessed 22 Nov 2017].
- Macdonald, A., Davies, J., Calow, R. and Chilton, J., 2005. *Developing Groundwater: A Guide to Rural Water Supply*. Bourton on Dunsmore: Practical Action Publishing.
- Maillet, R., 1947. The fundamental equations of electrical prospecting.. *Geophysics*, Issue 12, pp. 529-556.
- Mazac, O., Kelly, W. and Landa, I., 1985. A hydrogeophysical model for relations between electrical and hydraulic properties of aquifers. *Journal of Hydrology*, 79(1-2), pp. 1-19.
- McNeill, J., 1980a. *Electrical conductivity of soils and rocks. TN5*, ON, Canada: Geonics Limited.
- McNeill, J., 1980b. *Electromagnetic terrain conductivity measurement at low induction numbers. TN6*, ON, Canada: Geonics Limited.
- McNeill, J., 1996. *Why doesn't Geonics Limited build a multifrequency EM31 or EM38? TN30*, Ontario, Canada.: Geonics Limited.
- Miyamoto, S., Henggeler, J. and Benton Storey, J., 1995. Water Management in Irrigated Pecan Orchards in the South Western United States.. *HortTechnology*, July/Sept, 5(3), pp. 214-218.
- Negi, J. & Saraf, P., 1989. *Anisotropy in geoelectromagnetism*., Elsevier.
- Niwas, S. & Celik, M., 2012. Equation estimation of porosity and hydraulic conductivity of Ruhrtal aquifer in Germany using near surface geophysics.. *Journal of Applied Geophysics*, Volume 84, pp. 77-85.
- Niwas, S. and de Lima, O., 2003. Aquifer Parameter Estimation from Surface Resistivity Data.. *Groundwater*, 41(1), pp. 94-99.
- Niwas, S., Tezkan, B. and Israil, M., 2011. Aquifer hydraulic conductivity estimation from surface geoelectrical measurements for Krauthausen test site, Germany.. *Hydrogeology Journal*, Volume 19, pp. 307-315.
- Nosetto, M.D.; Acosta, A.M.; Jayawickreme, D.H.; Ballesteros, S.I.; Jackson, R.B.; Jobbágy, E.G., 2013. Land-use and topography shape soil and groundwater salinity in central Argentina.. *Agricultural Water Management*, 129(1), pp. 120-129.
- Parasnis, D., 1997. *Principles of Applied Geophysics*.. 5th ed. New York: Chapman & Hall, London.
- Rhoades, J., Raats, P. and Prather, R., 1976. Effects of Liquid-phase Electrical Conductivity, Water Content, and Surface Conductivity on Bulk Soil Electrical Conductivity. *Soil Science Society of America Journal*, Volume 40, pp. 651-665.
- Rhoades, JD; Shouse, PJ; Alves, WJ; Manteghi, NA; Lesch, SM, 1990. Determining Soil Salinity from Soil Electrical Conductivity using different Models and Estimates.. *Soil Sci. Soc. Am.* , Volume 54, pp. 46-54.
- Rudolph, D. and Hough, J., 2003. *Vaalharts Groundwater Protocol for onsite Sanitation*., Bloemfontein: GHT Consulting.

- Salem, H., 1999. Determination of fluid transmissivity and electric transverse resistance for shallow aquifers and deep reservoirs from surface and well log electric measurements.. *Hydrology and Earth System Sciences*, 3(3), pp. 421-427.
- Samouëlian, A; Cousin, I; Tabbagh, A; Bruand, A; Richard, G, 2005. Electrical resistivity survey in soil science: A review.. *Soil and Tillage Research*, Volume 83, pp. 173 - 193.
- Sinha, R., Israil, M. & Singhal, D., 2009. *A hydrogeophysical model of the relationship between geoelectric and hydraulic parameters of anisotropic aquifers*. [Online]Available at: [DOI 10.1007/s10040-008-0424-9](https://doi.org/10.1007/s10040-008-0424-9) [Accessed July 2016].
- Turton, A., Meissner, R., Mampane, P. & Seremo, O., 2004. *Hydropolitical history of South Africa's river basins*, Pretoria: WRC 1220/1/04.
- Utom, A., Benard, I. and Okoro, A., 2012. Estimation of Aquifer Transmissivity using Dar Zarrouk Parameters derived from Surface Resistivity Measurements: A Case History from parts of Enugu Town (Nigeria).. *Journal of Water Resource and Protection*, Volume 4, pp. 993-1000.
- Van Rensburg, Lj; Barnard, JH; Bennie, ATP; Sparrow, JB; Du Preez, CC, 2012. *Managing Salinity associated with Irrigation at Orange-Riet and Vaalharts Irrigation Schemes.*, s.l.: Water Research Commission Reportno: 1647/1/12.
- Van Vuuren, L., 2010. Vaalharts - a Garden in the Desert. *Water Wheel*, January/February, 9(1), pp. 20-24.
- Van Zijl, J., 1977. *A Practical Manual on the Resistivity Method*, Pretoria, South Africa: Geophysics Division, CSIR.
- Verwey, P., 2009. *The Impact of Irrigation on the Groundwater of the Vaalharts Irrigation Scheme*. M.Sc thesis, University of the Free State, Bloemfontein: Institute for Groundwater Studies.
- Verwey, P. and Vermeulen, P., 2011. Influence of irrigation on the level, salinity and flow of groundwater at the Vaalharts Irrigation Scheme. *Water SA*, 2 April, 37(2), pp. 155-164.
- Waxman, M. and Smits, L., 1968. Electrical Conductivities in Oil-bearing Shaly sands.. *Society of Petroleum Engineers*, 8(2), pp. 107-122.
- Worthington, P., 1982. The influence of shale effects upon the electrical resistivity of reservoir rocks.. *Geophysical Prospecting*, Volume 30, pp. 673-687.
- Zohdy, A., 1974. *Use of Dar Zarrouk curves in the interpretation of vertical electrical sounding data.*, s.l.: U.S. Geol. Surv. Bull. 1313-E,39.
- Zohdy, A., Eaton, G. and Mabey, D., 1974. *Application of surface geophysics to groundwater investigations.*, s.l.: U.S. Geol. Surv. Book 2, Chap D1.

ABSTRACT

As with any human intervention, the balances of nature are impacted when applying irrigation water. The biggest changes usually manifest as a rise in the groundwater level, as well as a build-up of salts in the soils and groundwater. The impact of irrigation on the natural balances, however, can be controlled to a certain extent through farming and irrigation practices, and scientific methods for fast and efficient monitoring are continually evolving.

In the Vaalharts Irrigation Scheme, a very shallow water level (± 2 m) of the underlying aquifer, interacts with the irrigated soil zone. Because of this interaction, the build-up of the salt load in the deeper aquifer cannot be ruled out. This may have a direct impact on the cultivation of perennial crops, especially pecan nuts, which are not very salt tolerant. With a shortage of irrigation water in times of drought and with climate change a very real scenario, farmers are starting to exploit groundwater to augment surface water. Unfortunately, the groundwater is much more saline than the surface water due to the local geology that constitutes the aquifer adding to the problem of salinization. In the short-term, exploitation of the Vaalharts Aquifer may provide a solution, but eventually it must impact on the broader hydrological system as it has a direct influence on the environmental balances that currently exist.

Thus, the aims and objectives of this study was to apply electrical geophysical methods to determine the lateral and vertical extent of the Vaalharts Aquifer, to determine any lateral homogeneity/inhomogeneity in the underlying geology and to investigate the relationship between the geohydrological, geophysical- and physical parameters of the aquifer.

Field investigations included pumping testing and VES soundings at locations of known geology and the measuring of the electrical conductivity of groundwater samples. An ERT traverse provided insights to the lateral variation in geology. Inverse modelling of the electrical data was constrained to the geological layers and the layer resistivities determined. The Dar Zarrouk parameters were correlated with known hydrological parameters (T and K) to establish a relationship.

A linear relationship was found between transmissivity (T) and longitudinal conductance (C) with the determination of the factor of proportionality (β). This factor was used to calculate T and K values at VES stations where no geohydrological data were available. Although the data points were few and far between, the calculated data enabled the compilation of contour maps that gives an indication of the lateral distribution of the hydrological parameters in the Vaalharts area.

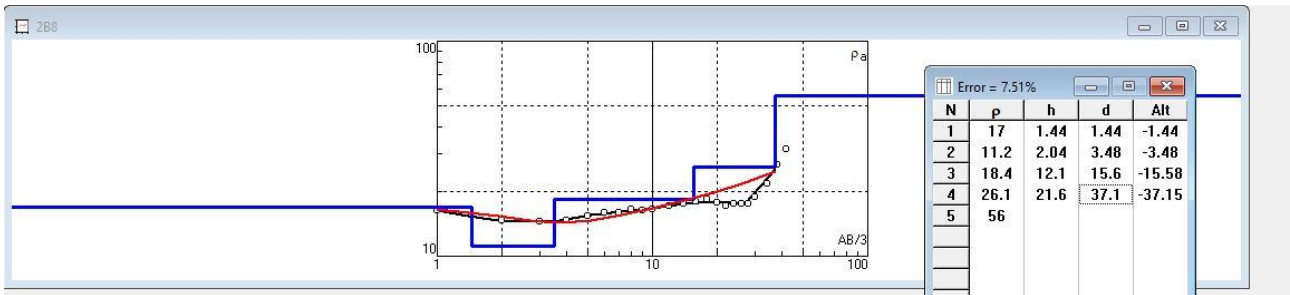
This project thus established a method for use in evaluating the aquifer for groundwater exploitation, that may be extended to the monitoring of salinization in the aquifer.

Appendix A

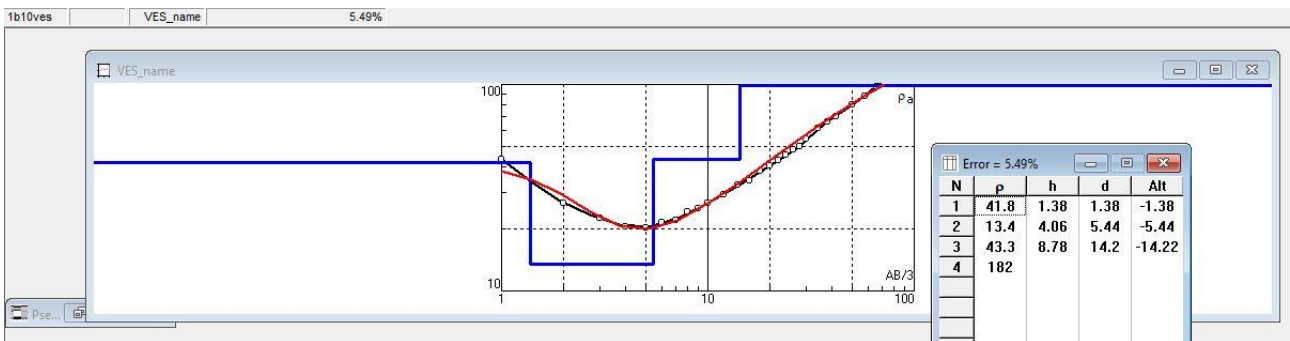
VES Field Curves with inverse modelled layers

VES Fieldcurves with inverse modelled layers using IPI2WIN.

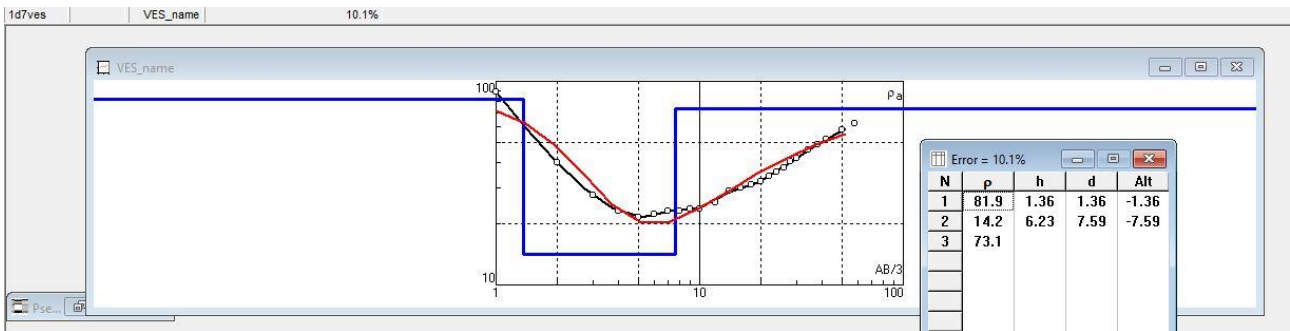
1. Borehole 1B8-1



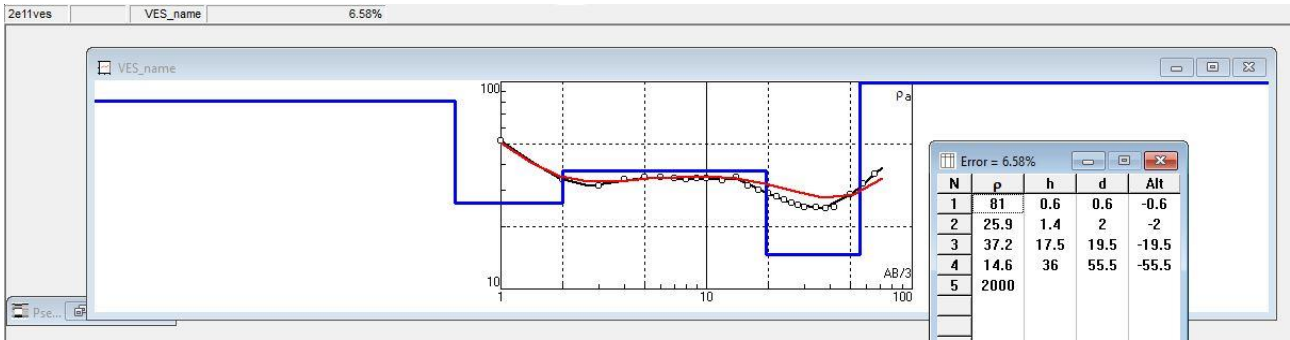
2. Borehole 1B10-1



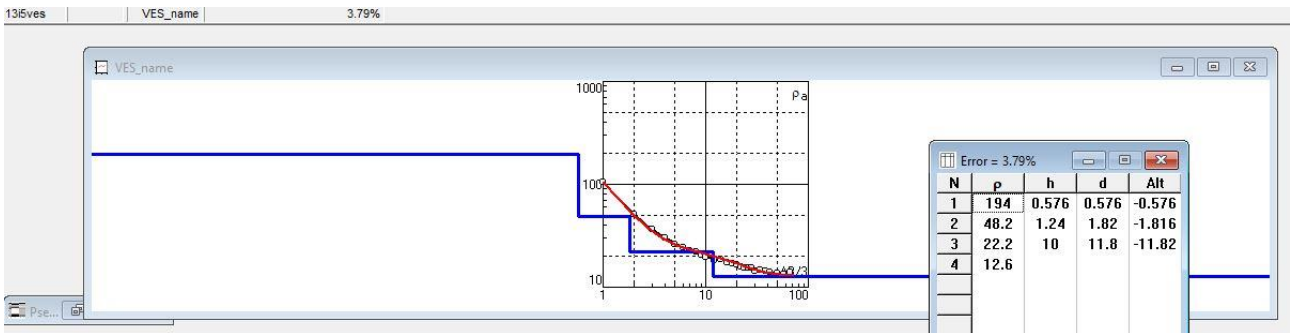
3. Borehole 1D7-1



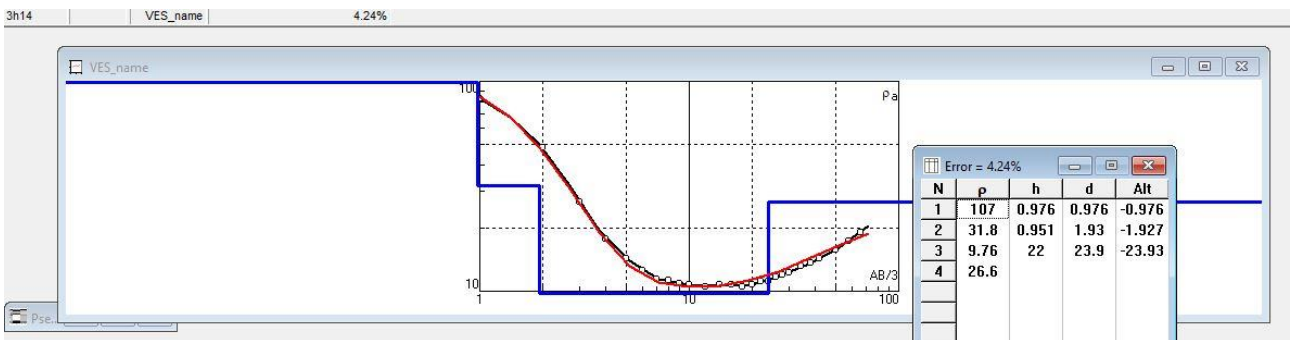
4. Borehole 2E11-1



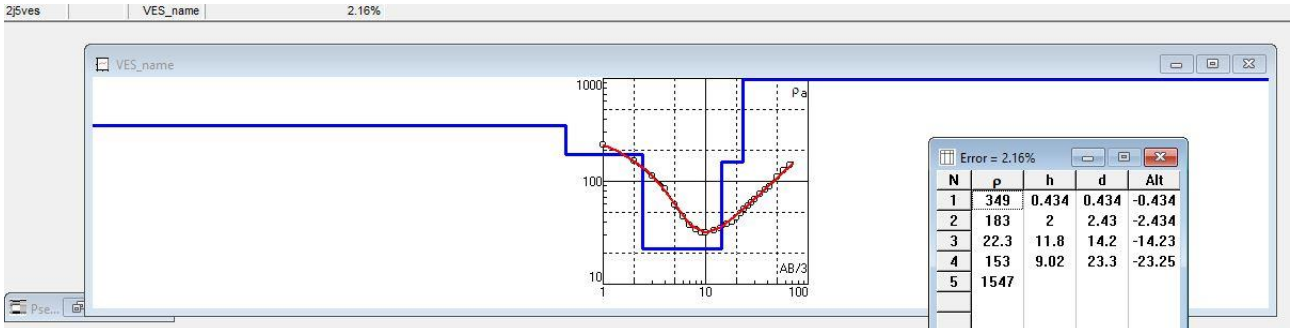
5. Borehole 13I5-1



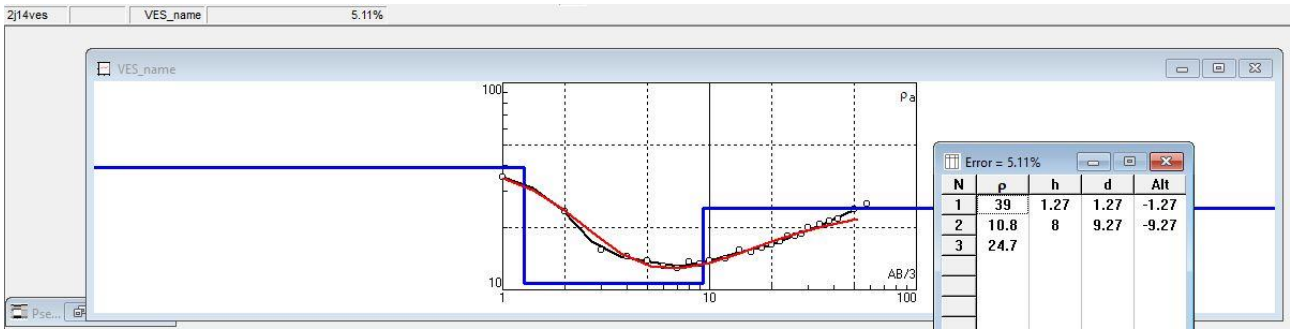
6. Borehole 8H14-1



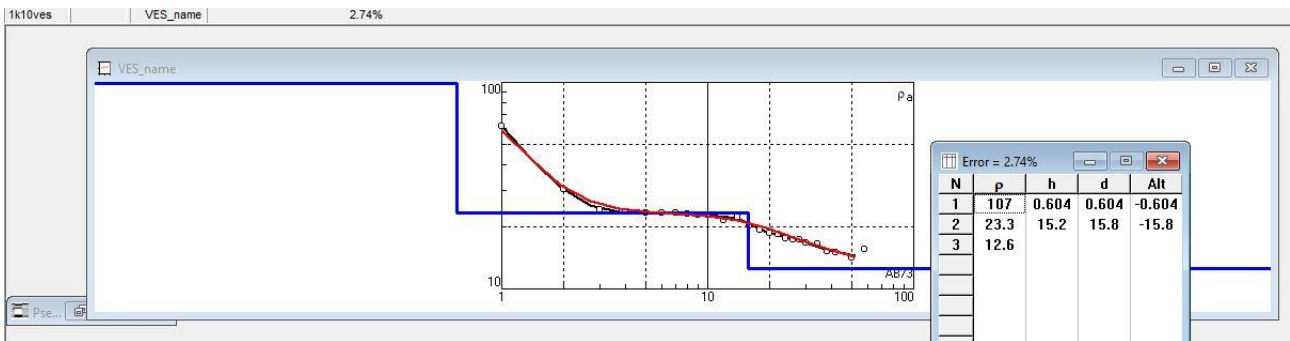
7. Borehole 2J5-1



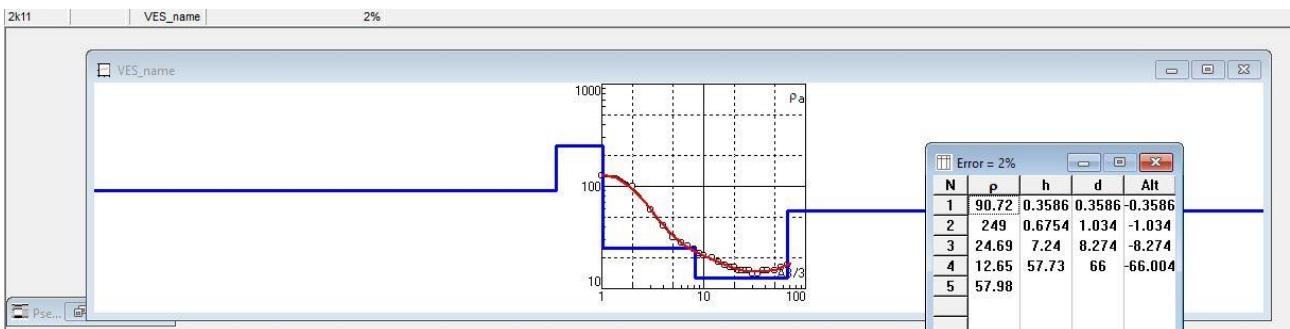
8. Borehole 2J14-1



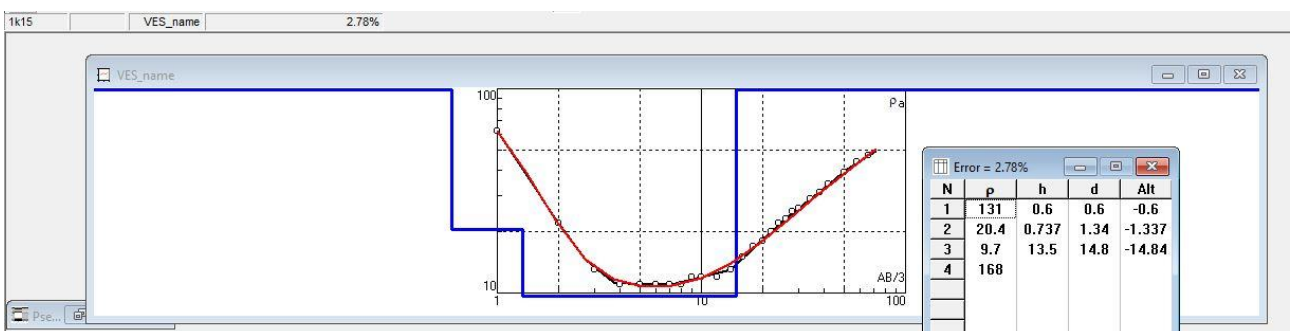
9. Borehole 1K10-1



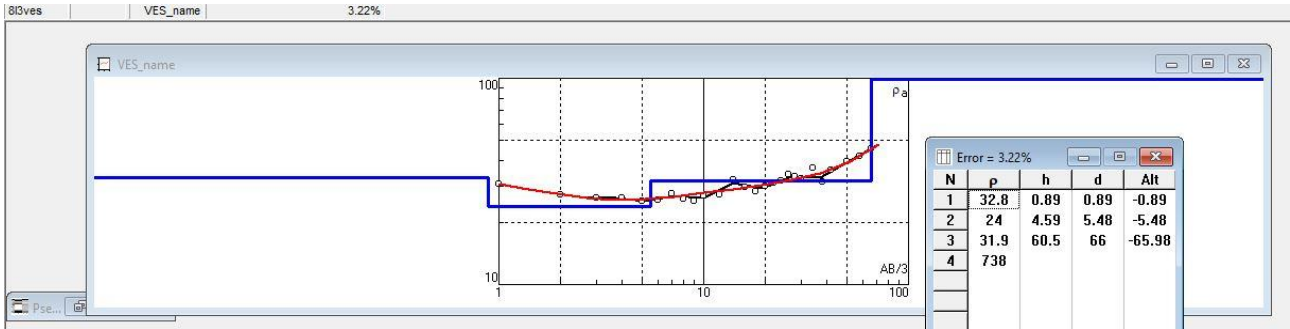
10. Borehole 2K11



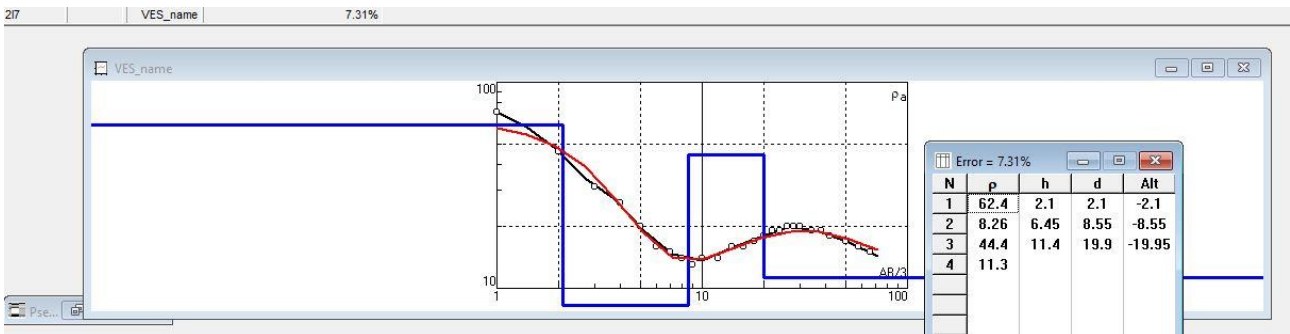
11. Borehole 1K15



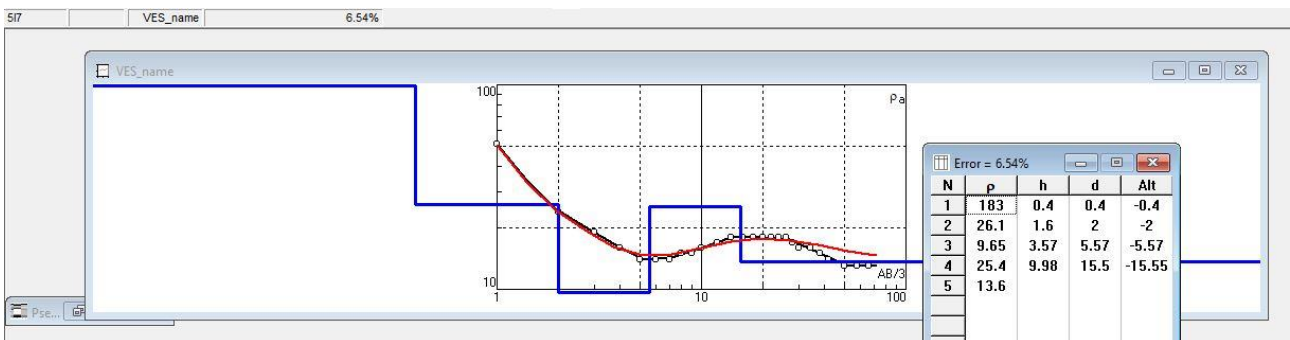
12. Borehole 8L3



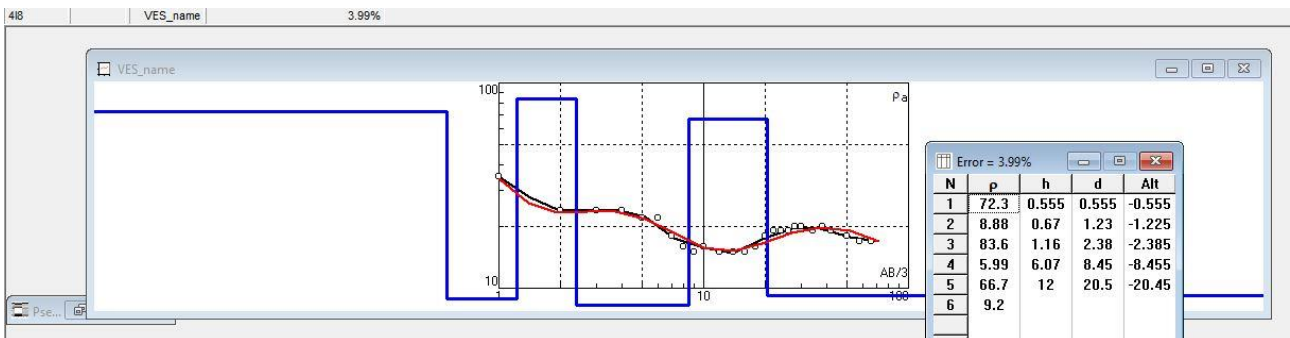
13. Borehole 2L7



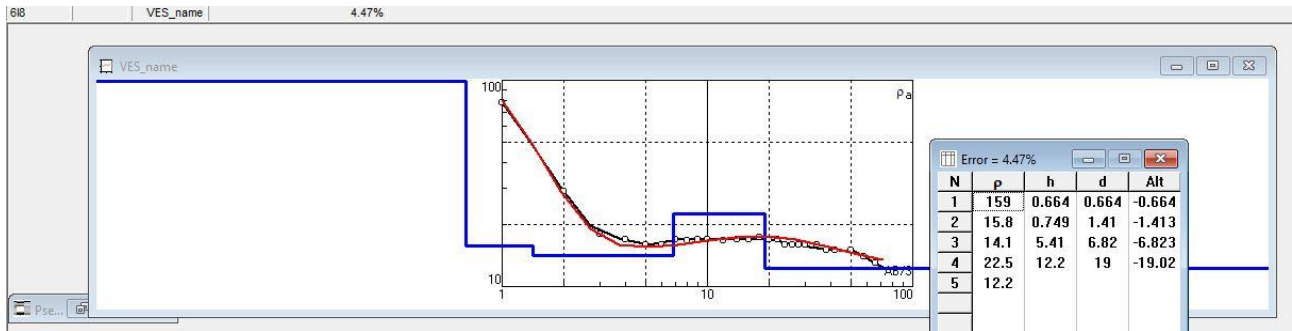
14. Borehole 5L7



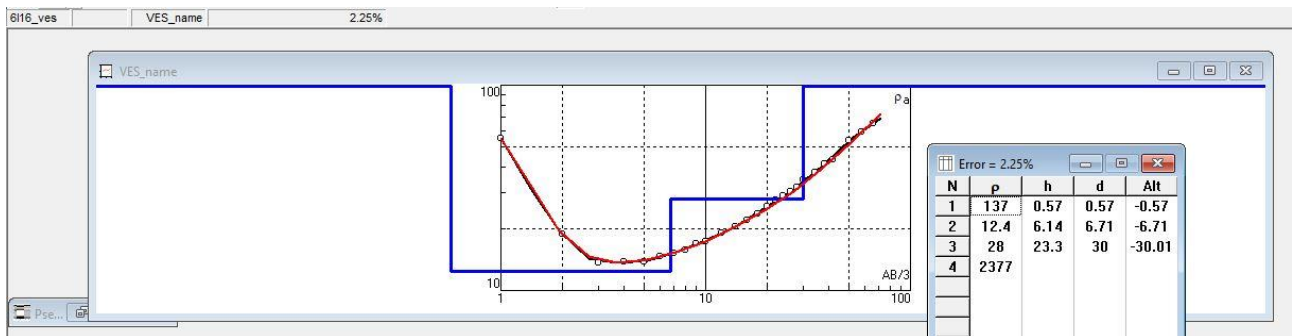
15. Borehole 4L8



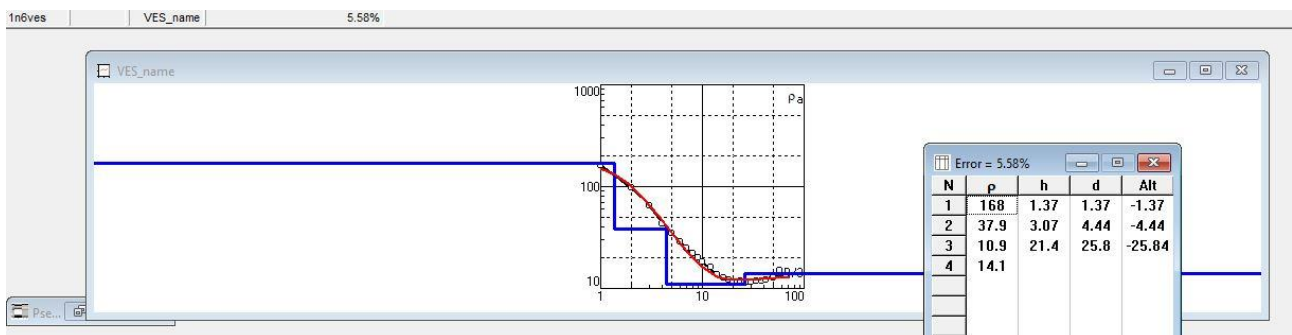
16. Borehole 6L8



17. Borehole 6L16-1



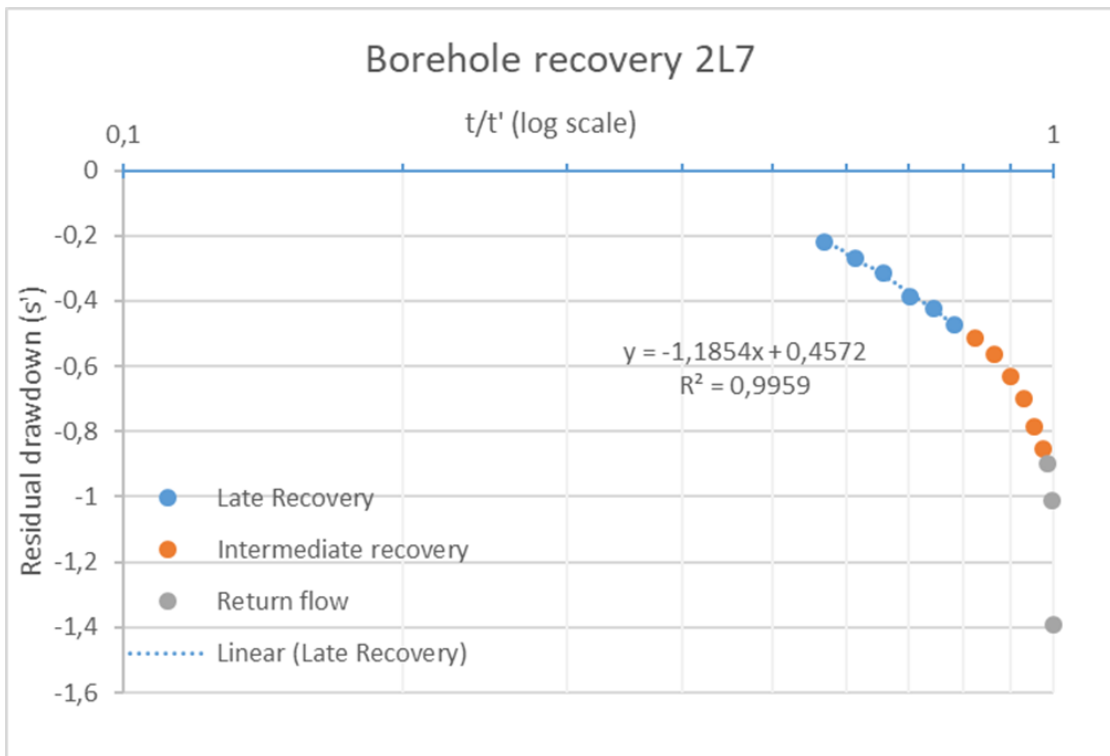
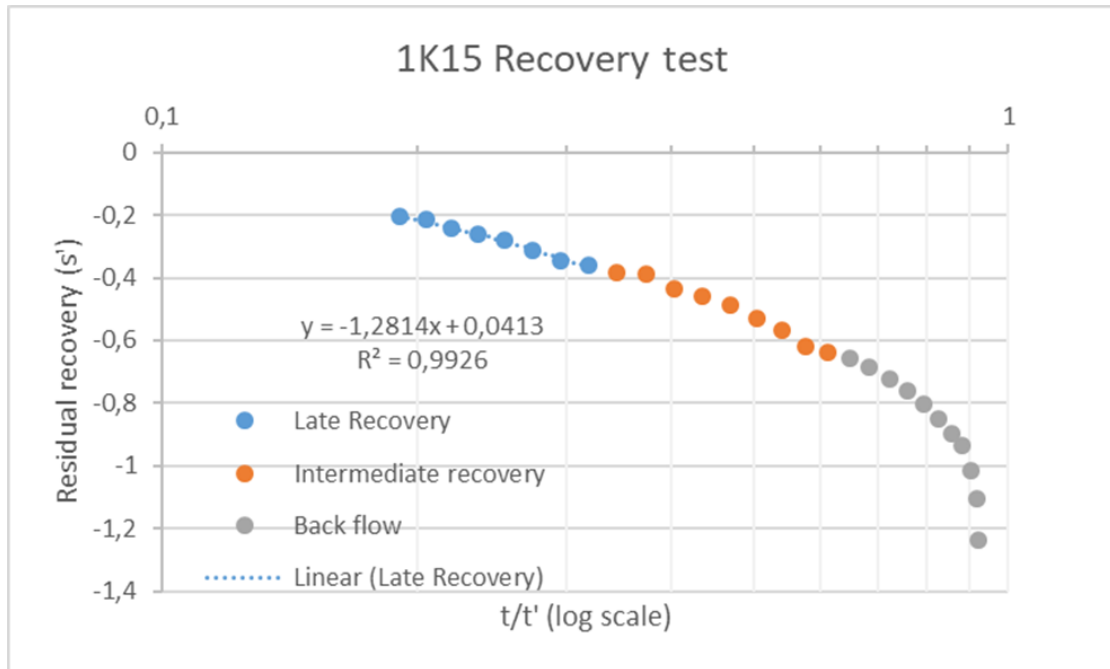
18. Borehole 1N6-1

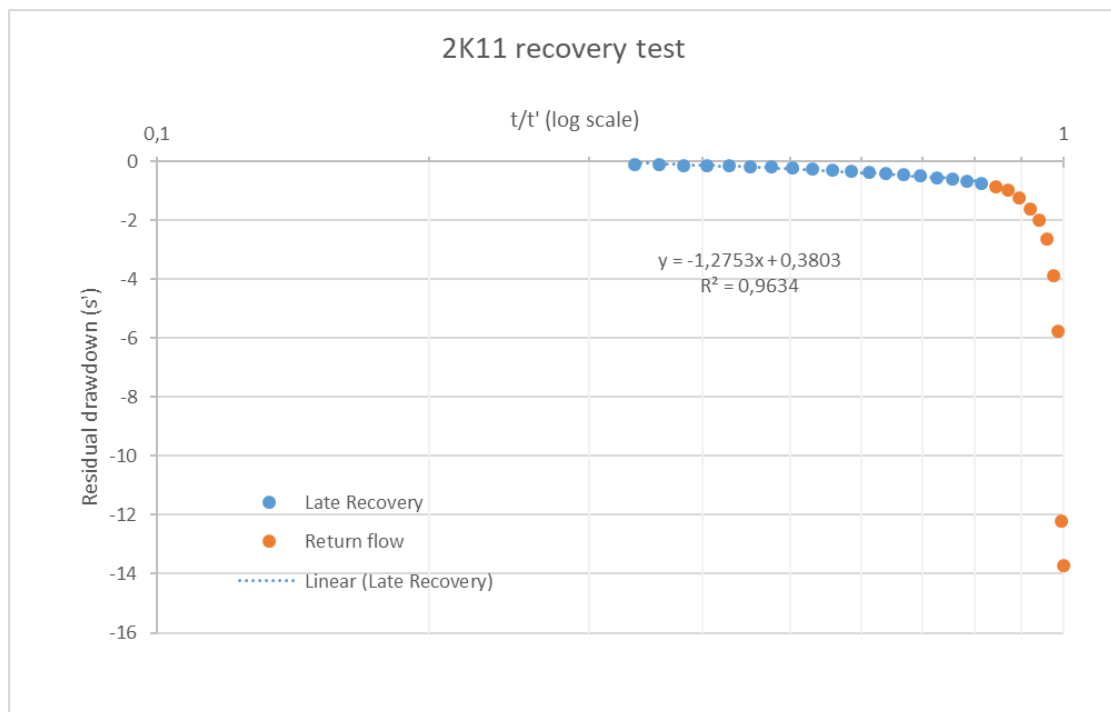
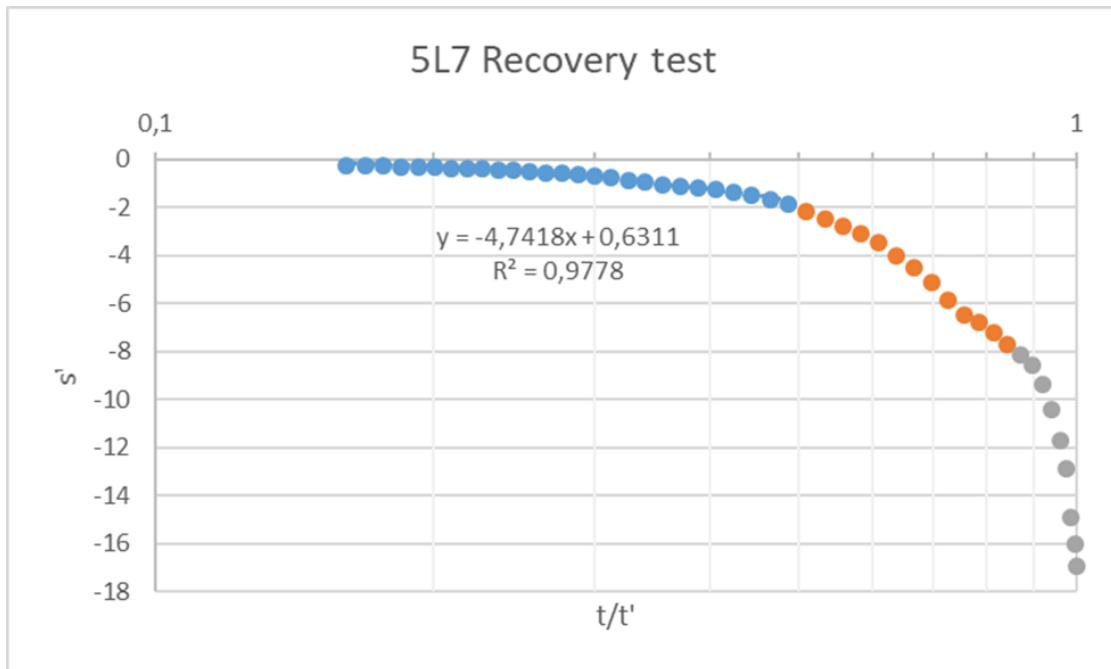


Appendix B

Pumping test curves

Pumping test curves





Appendix C

**Table of VES data and
modelled Dar Zarrouk
parameters**

IPI2WIN inverse modelling of Wenner VES data - WLevel and geology constrained												
	N	Modelling of apparent ρ				Error %	Dar Zarrouk Parameters				Aquifer R and S	
		ρ	h	d			hp	R	h/ ρ	S	R	S
1B8-1	1	17	1,44	1,44	6,17	24,48	24,48	0,084706	0,084706			
1B8-1	2	11,2	2,04	3,48		22,848	47,328	0,182143	0,266849	440,528	1,415839	
1B8-1	3	18,4	22,7	26,2		417,68	465,008	1,233696	1,500544			
1B8-1	4	26,1	18,4	44,6		480,24	945,248	0,704981	2,205525			
1B8-1	5	56										
1B10-1	1	41,8	1,38	1,38	5,49	57,684	57,684	0,033014	0,033014			
1B10-1	2	13,4	4,06	5,44		54,404	112,088	0,302985	0,335999	434,578	0,505756	
1B10-1	3	43,3	8,78	14,2		380,174	492,262	0,202771	0,538771			
1B10-1	4	182										
1D7-1	1	81,9	1,36	1,36	10,1	111,384	111,384	0,016606	0,016606			
1D7-1	2	14,2	6,23	7,59		88,466	199,85	0,438732	0,455338	88,466	0,438732	
1D7-1	3	73,1										
2E11-1	1	81	0,6	0,6	6,58	48,6	48,6	0,007407	0,007407			
2E11-1	2	25,9	1,4	2		36,26	84,86	0,054054	0,061461			
2E11-1	3	37,02	17,5	19,5		647,85	732,71	0,472717	0,534179	647,85	0,472717	
2E11-1	4	14,6	36	55,5		525,6	1258,31	2,465753	2,999932			
2E11-1	5	2000										
13I5-1	1	194	0,576	0,576	3,79	111,744	111,744	0,002969	0,002969			
13I5-1	2	48,2	1,24	1,82		59,768	171,512	0,025726	0,028695	281,768	0,476177	
13I5-1	3	22,2	10	11,8		222	393,512	0,45045	0,479146			
13I5-1	4	12,6										
4H18-1	1	107	0,976	0,976	2,59	104,432	104,432	0,009121	0,009121			
4H18-1	2	31,8	0,951	1,93		30,2418	134,6738	0,029906	0,039027			
4H18-1	3	9,76	22	23,9		214,72		2,254098		214,72	2,254098	
	4	26,6										
2J5-1	1	349	0,434	0,434	2,16	151,466	151,466	0,001244	0,001244			
2J5-1	2	183	2	2,43		366	517,466	0,010929	0,012173			
2J5-1	3	22,3	11,8	14,2		263,14	780,606	0,529148	0,54132	1643,2	0,588102	
2J5-1	4	153	9,02	23,3		1380,06	2160,666	0,058954	0,600275			
2J5-1	5	1547										
2J14-1	1	39	1,27	1,27	5,11	49,53	49,53	0,032564	0,032564			
2J14-1	2	10,8	8	9,27		86,4	135,93	0,740741	0,773305	86,4	0,740741	
2J14-1	3	24,7										
1K10-1	1	107	0,604	0,604	2,74	64,628	64,628	0,005645	0,005645			
1K10-1	2	23,3	15,2	15,8		354,16	418,788	0,652361	0,658005	354,16	0,652361	
1K10-1	3	12,6										

2K11	1	154	0,562	0,562	2	86,548	86,548	0,003649	0,003649		
2K11	2	115	1,3	1,87		149,5	236,048	0,011304	0,014954		
2K11	3	21	11,8	13,7		247,8	483,848	0,561905	0,576858	247,8	0,561905
2K11	4	9,76	42,6	56,2		415,776	899,624	4,364754	4,941613		
2K11	5	909									
1K15	1	131	0,6	0,6	2,78	78,6	78,6	0,00458	0,00458		
1K15	2	20,4	0,737	1,34		15,0348	93,6348	0,036127	0,040708		
1K15	3	9,7	13,5	14,8		130,95	224,5848	1,391753	1,43246	130,95	1,391753
1K15	4	168									
8L3	1	32,8	0,89	0,89	3,22	29,192	29,192	0,027134	0,027134		
8L3	2	24	4,56	5,48		109,44	138,632	0,19	0,217134		
8L3	3	31,9	60,5	66		1929,95	2068,582	1,896552	2,113686	1929,95	1,896552
8L3	4	738									
2L7	1	62,4	2,1	2,1	7,31	131,04	131,04	0,033654	0,033654		
2L7	2	8,26	6,45	8,55		53,277	184,317	0,780872	0,814526	559,437	1,037628
2L7	3	44,4	11,4	19,9		506,16	690,477	0,256757	1,071282		
2L7	4	11,3									
5L7	1	183	0,4	0,4	6,54	73,2	73,2	0,002186	0,002186		
5L7	2	26,1	1,6	2		41,76	114,96	0,061303	0,063488		
5L7	3	9,65	3,57	5,57		34,4505	149,4105	0,369948	0,433437	287,9425	0,762862
5L7	4	25,4	9,98	15,5		253,492	402,9025	0,392913	0,82635		
5L7	5	13,6									
4L8	1	72,3	0,56	0,56	3,99	40,488	40,488	0,007746	0,007746		
4L8	2	8,88	0,67	1,23		5,9496	46,4376	0,07545	0,083196		
4L8	3	83,6	1,16	2,38		96,976	143,4136	0,013876	0,097072		
4L8	4	5,99	6,07	8,45		36,3593	179,7729	1,013356	1,110427	836,7593	1,193266
4L8	5	66,7	12	20,5		800,4	980,1729	0,17991	1,290337		
4L8	6	9,2									
6L8	1	159	0,66	0,66	4,47	104,94	104,94	0,004151	0,004151		
6L8	2	15,8	0,75	0,41		11,85	116,79	0,047468	0,051619		
6L8	3	14,1	5,41	6,82		76,281	193,071	0,383688	0,435307	350,781	0,92591
6L8	4	22,5	12,2	19		274,5	467,571	0,542222	0,977529		
6L8	5	12,2									
6L16-1	1	137	0,57	0,57	2,25	78,09	78,09	0,004161	0,004161		
6L16-1	2	12,4	6,14	6,71		76,136	154,226	0,495161	0,499322	76,136	0,495161
6L16-1	3	28	23,3	30		652,4	806,626	0,832143	1,331465		
6L16-1	4	2377									
1N6	1	168	1,37	1,37	5,58	230,16	230,16	0,008155	0,008155		
1N6	2	37,9	3,07	4,44		116,353	346,513	0,081003	0,089157	116,353	0,081003
1N6	3	10,9	21,4	25,8		233,26	579,773	1,963303	2,05246		
1N6	4	14,1									
											= aquifer